ORTHONORMAL-BASIS PARTITIONING AND TIME-FREQUENCY REPRESENTATION OF NON-STATIONARY SIGNALS

by

Benhur Aysin

B.S. in E.E., Istanbul Technical University, Istanbul, Turkey, 1991

M.S. in E.E., University of Pittsburgh, Pittsburgh, PA, 1995

Submitted to the Graduate Faculty of

the School of Engineering in partial fulfillment

of the requirements for the degree of

Doctor of Philosophy

University of Pittsburgh

2002

UNIVERSITY OF PITTSBURGH

SCHOOL OF ENGINEERING

This dissertation was presented

by

Benhur Aysin

It was defended on

November 26, 2002

and approved by

Dr. J. Robert Boston, Professor, Department of Electrical Engineering

Dr. Ching-Chung Li, Professor, Department of Electrical Engineering

Dr. Amro A. El-Jaroudi, Professor, Department of Electrical Engineering

Dr. Delma J. Hebert, Professor, Department of Mathematics

Dissertation Co-director: Dr. Vladimir Shusterman, Professor, Department of Medicine

Dissertation Director: Dr. Luis F. Chaparro, Professor, Department of Electrical Engineering

ABSTRACT

ORTHONORMAL-BASIS PARTITIONING AND TIME-FREQUENCY REPRESENTATION OF NON-STATIONARY SIGNALS

Benhur Aysin, Ph.D.

University of Pittsburgh, 2002

Spectral analysis is important in many fields, such as speech, radar and biomedicine. Many signals encountered in these areas possess time-varying spectral characteristics. The power spectrum indicates what frequencies exist in the signal but it does not show when those frequencies occur. Time-frequency analysis provides this missing information. A time-frequency representation of the signal shows the intensities of the frequencies in the signal at the times they occur, and thus reveals if and how the frequencies of a signal are changing over time.

Time-dependent spectral analysis of beat-to-beat variations of cardiac rhythm, or heart rate variability (HRV), represents a major challenge due to the structure of the signal. A number of time-frequency representations have been proposed for the estimation of the time-dependent spectra. However, time-frequency analysis of multicomponent physiological signals such as cardiac rhythm is complicated by the presence of numerous, ill-structured frequency elements. We sought to develop a simple method for 1) detecting changes in the structure of the HRV signal, 2) segmenting the signal into pseudo-stationary portions, and 3) exposing characteristic patterns of the changes in the time-frequency plane. The method, referred to as Orthonormal-Basis Partitioning and Time-Frequency Representation (OPTR), is validated on simulated signals and HRV data. Unlike the traditional time-frequency HRV representations, which are usually applied to short segments of signals recorded

in controlled conditions, OPTR can be applied to long and "content-rich" ambulatory signals to obtain the signal representation along with its time-varying spectrum. Thus, the proposed approach extends the scope of applications of the time-frequency analysis to all types of HRV signals and to other physiological data.

DESCRIPTORS

Discrete Evolutionary Transform
Heart Rate Variability
Non-stationary signal Analysis
Signal Segmentation
Eigenvalue
Karhunen-Loeve Expansion
Signal Reconstruction
Time-Frequency Representation

ACKNOWLEDGEMENTS

I am very thankful to my advisors, Dr. Luis F. Chaparro and Dr. Vladimir Shusterman, for their guidance, encouragement and patience during this research. I would also like to thank Dr. Ilan Gravè for his useful feedback and suggestions. Special thanks goes to Dr. J. R. Boston, Dr. C. C. Li, Dr. A. El-Jaroudi and Dr. D. J. Hebert for serving in my Ph.D. committee and for their helpful comments.

I would also like to thank to Turkish Government for their financial support.

Finally, I want to thank my parents, Ismail and Sabiha Aysin, for their unconditional support and encouragement during all my studies. I dedicate this thesis to them.

TABLE OF CONTENTS

LIST OF FIGURES

NOMENCLATURE

$x(n)$	A signal
$x_i(n)$	A signal of ith partition
c_{ij}	KL expansion coefficients
$\phi_{ij}(t)$	KL basis functions
$R_i(t,s)$	Correlation function of a signal
λ_{ik}	Eigenvalues of a correlation matrix
$\mathrm{w}_i(n)$	A window of ith partition
H	Hermitian operator
$E\{.\}$	Expected value operator
E_j	90% of the total energy in jth segment
E_j^{tot}	Total energy in jth segment
N_j	Number of the eigenvalues corresponding to 90% of the energy
E_j^{lw}	Lower threshold for energy
E_j^{up}	Upper threshold for energy
$N_j^{s,u}$	Upper threshold for the number of eigenvalues
$\delta(t)$	Dirac delta function
$S(n,k)$	Evolutionary spectrum
$u_{ik}(n)$	Orthonormal basis functions in ith partition
$X(n,k)$	Evolutionary kernel

ABBREVIATIONS

ANS	Autonomic Nervous System
ECG	Electrocardiogram
EP	Evolutionary periodogram
GKL	Global Karhunen-Loeve Expansion
HRV	Heart Rate Variability
KL	Karhunen-Loeve Expansion
LTCA	Life Threatening Cardiac Arrhythmias
NN	Normal-to-Normal
OPTR	Orthonomal-Basis Partitioning and Time-Frequency Representation
PSD	Power Spectral Density
PVC	Premature Ventricular Complexes
STFT	Short Time Fourier Trasformation

1.0 INTRODUCTION

1.1 Motivation

Most of the signals in life such as speech, radar, biomedical and communication are non-stationary. Standard frequency analysis techniques will not be enough to analyze those signals. The power spectrum indicates what frequencies exist in the signal but it does not show when those frequencies occur. Recently, there has been an interest in time-frequency representation of non-stationary signals [1–3]*. Time-frequency representation gives energy distribution of the signal along the time.

Time-frequency representations of biological signals especially of heart rate variability (HRV) signals have been of great interest recently. Beat-to-beat variations of cardiac rhythm, referred to as the HRV, provide a noninvasive probe of the autonomic nervous system regulation, which is widely used in cardiovascular research[4]. Analysis of these variations in the frequency domain revealed three major periodic components in the low-frequency (0.04 Hz), mid-frequency (0.12 Hz), and high-frequency (0.25 Hz) parts of the power spectrum [5]. Pharmacological tests have shown that the high frequency component is modulated by parasympathetic branch of the autonomic nervous system (ANS), whereas the low-frequency component is modulated by combined sympathetic and parasympathetic effects.

Standard spectral analysis techniques require signals to be stationary which is not the case with most of the biological signals. Processing of these signals during transition phases of experiments such as moment of tilt or the instant of fainting, is not possible with standard techniques. Standard spectral analysis smears the time variations of the spectral component over the entire duration. Therefore, to overcome the stationarity and analyze the signal even during transition periods, researchers have

*Bracketed references placed superior to the line of text refer to the bibliography.

tried to utilize new techniques [6, 7]. All these lead to time-frequency distributions which show the spectral components as a function of time.

A number of time-frequency representations, including the Wigner distribution [8] and the evolutionary spectrum [9], have been proposed for the estimation of time-dependent spectrum of the nonstationary signals [1]. These methods provide the tools for tracking the changes in relatively simple signals. However, time-frequency analysis of multicomponent physiological signals as cardiac rhythm is complicated by the presence of numerous, ill-structured frequency elements.

We sought to develop a simple method for 1) detecting changes in the structure of the HRV signal, 2) segmenting the signal into pseudo-stationary portions, and 3) exposing characteristic patterns of the changes in the time-frequency plane. We show how an orthogonal decomposition can be used first, for compressing the information and selecting the sections of interest and second, for tracking time-dependent changes in the spectral energy distribution. We also obtained a representation of a non-stationary signal to which a time-dependent spectrum can be associated. In developing a representation for non-stationary signals, it is important to select appropriate basis to represent signal and its time-frequency representation. The method, referred to as Orthonormal-Basis Partitioning and Time-Frequency Representation (OPTR), was validated on simulated signals and HRV data obtained in humans undergoing physiological tests.

1.2 Background

1.2.1 Heart Rate Variability

Heart rate variability (HRV) refers to the beat-to-beat alterations in heart rate. Under resting conditions, the electrocardiogram (ECG) of healthy individuals exhibits periodic variation in R-R intervals. Heart rate changes in response to physiological manipulations or circumstances has been known since man has been able to express himself. However, the ability to study these relationships has been limited by our ability to quantify physiological data. The study of heart rate changes in

response to psychological demands is the focus of research. Additional information can be obtained by describing the variability of heart rate. The measurements of HRV provides important information regarding both metabolic and central nervous system activity.

Interest in monitoring cardiac variables has changed historically. Early studies focused on the use of these variables as indicator of viability. Cessation of heart beat has been used in clinical definitions of death. Furthermore, medical evaluation of health have always emphasized the quality of the rhythm of the heart beat. Recent studies have focused on the neural control of the cardiac responses, how the neural system interacts with cardiac responses and how these variables are influenced by mental states, physiological stress, health status and drugs. Clinical monitoring of heart rate and respiration variables have been used in critical settings to evaluate both health status and response to various medical treatments [10]. The clinical relevance of HRV was first appreciated in 1965 when Hon and Lee [11] noted that fetal distress was preceded by alterations in interbeat intervals before any important change occurred in heart rate itself [12]. More than two decades ago, Sayers [13] and others[14–16] focused attention on the existence of physiological rhythms imbedded in the beat-to-beat heart rate signal. In 1981, Akselrod et al [4] introduced power spectral analysis of heart rate variations to quantitatively evaluate beat-to-beat cardiovascular control. Frequency domain analysis helped to understand autonomic nervous system activity on RR interval fluctuations [17]. The clinical importance of HRV became clear when it was shown that HRV was a strong and independent predictor of mortality. With the availability of current technology such as 24 hour digital multichannel ECG recorders, HRV has the potential to provide additional insight into physiological and pathological conditions.

1.2.2 Neural Control of the Heart

Since heart rate is neurally mediated, it has been proposed that the monitoring of heart rate will provide a good indicator of central nervous system status. Many studies have suggested that the

neurally mediated oscillations in the heart rate pattern reflect a variety of mental states such as stress, emotion, alertness and attention. Therefore, the measurement of heart rate patterns may provide a tool to understand brain activities and may be used as an index of general central nervous system status. Autonomic response systems are regulated by complex feedback. Feedback loops produce a rhythmic pattern characterized by increase and decrease in neural efferent output to organs such as the heart. In the case of the heart, there are numerous feedback influences and, thus, the response is composed of the sum of numerous rhythmic components [18]. In many physiological systems, efficient neural control is manifested as rhythmic physiological variability. Within normal parameters, greater amplitude of oscillation is associated with health.

Heart rate in the healthy adult is not constant. The pattern of heart rate reflects the continuous feedback between the central nervous system and autonomic receptors. The feedback system between the central control of autonomic processes and the heart produces phasic increase and decrease in neural efferent output via vagus. The higher the range of increases and decreases, the healthier the individual.

The vagal tone index is one measure of the nervous system modulation of heart rate activity via vagus. Heart rate patterns are dependent on the status of the nervous system and quality of the neural feedback. Therefore, measures of cardiac vagal tone provide an important window into central control of autonomic processes. Vagal tone is reflected in the amplitude of a heart rate rhythm associated with frequency of spontaneous breathing.

1.2.3 Quantification of Heart Rate

HRV is a complex and ambiguous process. It has had many definitions as well as quantification methods. The beat-to-beat pattern is continuously affected by the changing neural influence from the brainstem to the heart. Although slow shifts in heart rate may be influenced by sympathetic systems, the rapid oscillations reflecting direct neural feedback from the respiratory system are mediated via

direct vagal output. Thus, procedures to quantify HRV are critical in both extracting physiological meaningful components and in building a biopsychological model relating individual differences in physiological activity to behavior [12, 18].

1.2.3.1 Time Domain Methods. The variations in the heart rate can be evaluated by many methods. The simplest to perform can be the time domain measures. In these methods, either the heart rate or the intervals between successive normal beats are determined. In a continuous ECG record, each QRS complex is detected, and normal-to-normal (NN) intervals (all intervals between adjacent QRS complexes) or the instantaneous heart rate is determined. Time intervals between abnormal beats are not included. Simple time domain variables that can be calculated include the mean NN interval, the mean heart rate, the difference between the longest and shortest NN interval, the difference between night and day and so forth. These differences can be described as either differences in heart or cycle length.

1.2.3.2 Statistical Methods. From a series of instantaneous heart rates or cycle intervals, especially those recorded over longer periods, such as 24 hours, more complex statistical time domain measures can be calculated. These may be divided into two classes: (1) those derived from direct measurements of the NN intervals or instantaneous heart rate (2) those derived from the differences between NN intervals. These variables may be derived from analysis of the total ECG recording or may be calculated using smaller segments of the recording period. The simplest variable to calculate is the standard deviation of the NN intervals (SDNN). In many studies SDNN is calculated over a 24-hour period. Other frequently used statistical variables calculated from segments of the total monitoring period include SDANN, the standard deviation of the average NN intervals calculated over short periods, usually 5 minutes, which is an estimate of the changes in heart rate due to cycles longer than 5 minutes. The most commonly used measures derived from interval differences

include RMSSD, the square root of the mean squared differences of successive NN intervals, NN50, the number of interval differences of successive NN intervals greater than 50 ms.

1.2.3.3 Frequency Domain Methods. Many spectral methods for the analysis of the HRV have been applied since the late 1960s. Power spectral density (PSD) analysis provides the basic information of how power distributes as a function of frequency. Independent of the method used, only an estimate of the true PSD of the signal can be obtained by proper mathematical algorithms. Methods for calculation of PSD may be generally classified as nonparametric and parametric. In most cases, both methods provide comparable results. The advantages of nonparametric methods are (1) the simplicity of the algorithm used (fast Fourier transform (FFT) in most of the cases) and (2) the high processing speed, while the advantages of parametric methods are (1) smoother spectral components (2) easy postprocessing of the spectrum with an automatic calculation of low-and-high-frequency power components with an easy identification of the central frequency of each component, and (3) an accurate estimation of PSD even on a small number of samples. The basic disadvantage of parametric methods is the need of verification of the suitability of the chosen model and its order. These frequency analysis techniques show what frequencies exist in the signal at a certain time but not over a period of time.

1.3 Organization of Thesis

In Chapter 2, we discuss the Karhunen-Loeve (KL) expansion and its two important properties which are minimum representation error and minimum entropy. The expansion is described for two cases: 1) Global KL (GKL) expansion, 2) Local KL expansion.

In Chapter 3, we show how local and global KL expansion can be used for partitioning nonstationary signals. Two orthogonal-basis partitioning techniques are introduced: 1) a computation-

ally efficient low-resolution partitioning for long signals, and 2) a high resolution, computationally intensive partitioning for short signals.

In Chapter 4, a new time-frequency representation which employs the segmentation algorithm introduced in the Chapter 3 is described. The algorithm exposes characteristic patterns of the changes in the time-frequency plane. It provides the signal representation, along with its time-varying spectrum.

Application to HRV signals follows in Chapter 5. First, it is shown how GKL expansion and its coefficients can be used for the prediction of life threatening cardiac arrhythmias, then time-frequency representation is applied to HRV signal obtained during several physical experiments and compared with other techniques. Conclusions is given in Chapter 6. Appendix A and Appendix B conclude the thesis. Appendix A reviews the orthonormality of the basis functions used in orthonormal expansion of the partitioned signal. Appendix B gives a brief explanation about why we used 90% energy threshold for signal segmentation.

2.0 KARHUNEN-LOEVE EXPANSION

Stationary and nonstationary random processes can be represented by general orthogonal expansions as proposed by Priestley [19]. This general orthogonal expansion representation provides different ways to represent random processes. If the random signal is stationary, Fourier basis $\{e^{j\omega t}\}$ are valid. But if the signal is nonstationary, exponential functions can no longer be used. One choice can be $A_t(\omega)e^{j\omega t}$ for a nonstationary signal.

The Fourier transform is the ideal method for analyzing stationary signal. It represents the signal as linear combinations of exponentials. However actual signals are mostly nonstationary and we need a different approach to deal with the nonstationarities. There is always the question of which basis functions should be used. Which one represent the signal best? The answer usually is that it depends on the signal features.

In here we will focus on representing the process with Karhunen-Loeve (KL) bases which are completely obtained from the signal. No specification of the basis functions is needed. The KL expansion is a well known method [20–26] which employs weighted combination of several basis functions to represent a stochastic process. Basis functions of the KL expansion is signal dependent while other orthogonal transformations use fixed basis functions. Advantage of using signal dependent basis functions is that we can represent the process with fewer number of the basis functions. These basis functions reflect the signal features better than any other bases. The KL expansion has been mostly used in pattern recognition, feature extraction. [27–29]. It has two important features:

- It minimizes the mean-square error when only a finite number of basis functions are used in the expansion,
- It minimizes the entropy function defined in terms of the averaged squared coefficients used in the expansion, i.e., it carries more information regarding the discrimination of different classes.

The first property is important because it guarantees that no other expansion will yield a lower approximation error in mean square sense. The significance of the second property is that it associates with the coefficients of the expansion a measure of minimum entropy or dispersion [20].

Although the KL expansion is the best orthogonal representation to represent the signals with a limited number of bases functions, it has a drawback which is the computational cost. Correlation matrix of the signal has to be estimated to obtain basis functions. The KL bases have no specific mathematical structure that leads to 'fast' implementations. The KL expansion in this study is used for signal representation, signal compression and feature extraction. Another application of the expansion is denoising of noisy signals which was explained in one of our previous study [30]. In this chapter, we will describe the basic principles of the KL expansion.

2.1 Local Karhunen-Loeve Expansion

A nonstationary stochastic process $x_i(t)$ in an interval $[a, b]$ can be represented as [20]

$$x_i(t) = \sum_{j=1}^{\infty} c_{ij}\phi_{ij}(t) \tag{2-1}$$

where $\{c_{ij}\}$ are uncorrelated random coefficients which can be real or complex and $\{\phi_{ij}\}$ are a set of orthonormal functions on $[a, b]$, namely,

$$\int_a^b \phi_{ij}(t)\phi_{il}^*(t)dt = \begin{cases} 1 & \text{if } j = l \quad \text{(2-2a)} \\ 0 & \text{if } j \neq l \quad \text{(2-2b)} \end{cases}$$

where $*$ stands for complex conjugate. Equation (2-1) is an orthogonal expansion of the random process $x(t)$ in the given interval. For a stationary process, $\phi_j(t)$s are exponentials and $\{c_{ij}\}$s are the Fourier coefficients.

In general, basis functions $\phi_{ij}(t)$ and the coefficients c_{ij} can be obtained as follows. The correlation function of $x_i(t)$ is given by

$$R_i(t, s) = E\left\{x_i(t)x_i^*(s)\right\} \tag{2-3}$$

then by replacing Equation (2-1) into the last equation, we get

$$\begin{aligned} R_i(t,s) &= E\left\{\sum_j c_{ij}\phi_{ij}(t)\sum_l c_{il}^*\phi_{il}^*(s)\right\} \\ &= E\left\{\sum_j\sum_l c_{ij}c_{il}^*\phi_{ij}(t)\phi_{il}^*(s)\right\} \end{aligned} \tag{2-4}$$

Since expansion coefficients are uncorrelated, i.e.,

$$E\{c_{ij}c_{il}^*\} = \begin{cases} \lambda_i & \text{if } j = l \quad \text{(2-5a)} \\ 0 & \text{if } j \neq l \quad \text{(2-5b)} \end{cases}$$

Equation (2-4) becomes

$$R_i(t,s) = \sum_j \lambda_i\phi_{ij}(t)\phi_{ij}^*(s) \tag{2-6}$$

Using Equation (2-6), we have

$$\begin{aligned} \int_a^b R_i(t,s)\phi_{il}(s)ds &= \int_a^b \sum_j \lambda_i\phi_{ij}(t)\phi_{ij}^*(s)\phi_{il}(s)ds \\ &= \sum_j \lambda_i\phi_{ij}(t)\int_a^b \phi_{ij}^*(s)\phi_{il}(s)ds \end{aligned} \tag{2-7}$$

Because of Equation (2-2), the last equation reduces to

$$\int_a^b R_i(t,s)\phi_{il}(s)ds = |c_{il}|^2\phi_{il}(t) \tag{2-8}$$

Determination of c_{il} and $\phi_{il}(t)$ requires the solution of this integral equation. From this integral equation, we conclude that λ_i are the eigenvalues and $\phi_{il}(t)$ are the eigenvectors of $R_i(t,s)$. Then, the basis functions of the KL expansion are actually the eigenvectors of $R_i(t,s)$.

The expansion coefficients c_{il} are obtained as follows. By multiplying both sides of Equation (2-1) by $\phi_{il}^*(t)$ we get

$$x(t)\phi_{il}^*(t) = \sum_j c_{ij}\phi_{ij}(t)\phi_{il}^*(t) \tag{2-9}$$

Taking the integral of the both sides over interval $[a, b]$ in Equation (2-9) results in

$$\begin{aligned} \int_a^b x(t)\phi_{il}^*(t)dt &= \int_a^b \sum_j c_{ij}\phi_{ij}(t)\phi_{il}^*(t)dt \\ &= \sum_j c_{ij} \int_a^b \phi_{ij}(t)\phi_{il}^*(t)dt \end{aligned} \tag{2-10}$$

Considering Equation (2-2), the last equation can be written as

$$\int_a^b x(t)\phi_{il}^*(t)dt = c_{il} \tag{2-11}$$

2.1.1 The Discrete Case

The discrete equivalent of the KL expansion is given by

$$x_i(n) = \sum_{j=1}^{\infty} c_{ij}\phi_{ij}(n) \qquad 0 < n \leq N-1 \tag{2-12}$$

where c_{ij} are random coefficients and $\{\phi_{ij}(n\}$'s are orthonormal basis functions which are the eigenvectors of the correlation matrix $R(n, m) = E\{x(n)x^*(m)\}$. The expansion coefficients c_{ij} are given by

$$c_{ij} = \sum_{n=0}^{N-1} x(n)\phi_{ij}(n) \tag{2-13}$$

2.2 Global Karhunen-Loeve Expansion

The KL expansion is also applied to an array of functions derived from random processes [20, 27]. This is usually the case in pattern recognition applications where the functions are the observations from different pattern classes. Chien and Fu [25] called the expansion a generalized KL expansion. We will describe the expansion for the discrete case where the functions are vectors and call it the global KL expansion. Although the expansion is not applied to pattern recognition problem directly, we will use the same concept to analyze non-stationary signals. The expansion is described as follows.

Suppose we have the functions $x_i(t)$, $0 \leq i \leq M-1$, defined on a time interval $T_i \leq t \leq T_{i+1}$ ($T_{i+1} - T_i$ is the same for every i). Each function can be written as a linear combination of basis

functions $\{\phi_k(t)\}$ as follows: [20]

$$x_i(t) = \sum_{k=1}^{\infty} c_{ik}\phi_k(t) \qquad T_i \leq t \leq T_{i+1} \qquad 0 \leq i \leq M-1 \tag{2-14}$$

where $\{c_{ik}\}$ are random uncorrelated coefficients and $\{\phi_k(t)\}$ are orthonormal functions. An average autocorrelation function over all observations $x_i(t)$ is defined as [20]

$$R(t,s) = \sum_{i=1}^{M} p_i E\{x_i(t)x_i^*(s)\} \tag{2-15}$$

where $*$ stands for complex conjugate and p_i is the probability of the occurrence of $x_i(t)$. Note that the autocorrelation function is defined over all functions $x_i(t)$. It means that we will have only one covariance function for all the functions and therefore there will be only one set of basis functions $\{\phi_k(t)\}$. The term "global" emphasizes the point that a single set of basis functions is used to represent each of the functions $x_i(t)$. These basis functions $\{\phi_k(t)\}$ are different from the ones used in local KL expansion. Local basis functions reflect the properties of the local signal. However, global basis functions carry information about all $x_i(t)$s. On the other hand, the GKL coefficients will be unique for each function $x_i(t)$; i.e., the projection of the corresponding function onto the global basis functions.

Substituting Equation (2-14) into Equation (2-15) yields

$$\begin{aligned} R(t,s) &= \sum_{i=1}^{M} p_i E\left\{\sum_{k=1}^{\infty} c_{ik}\phi_k(t) \sum_{l=1}^{\infty} c_{il}^*\phi_l^*(s)\right\} \\ &= \sum_{k=1}^{\infty}\sum_{l=1}^{\infty} \phi_k(t)\phi_l^*(s) \sum_{i=1}^{M} p_i E\{c_{ik}c_{il}^*\} \end{aligned} \tag{2-16}$$

Since the random coefficients are uncorrelated, we have

$$\sum_{i=1}^{M} p_i E\{c_{ik}c_{il}^*\} = \begin{cases} \lambda_k & \text{if } k = l \qquad \text{(2-17a)} \\ 0 & \text{if } k \neq l \qquad \text{(2-17b)} \end{cases}$$

then Equation (2-16) becomes

$$R(t,s) = \sum_{k=1}^{\infty} \lambda_k \phi_k(t)\phi_k^*(s) \tag{2-18}$$

Multiplying both sides of Equation (2-18) by $\phi_k(s)$ and integrating over the time interval $[T_i, T_{i+1}]$, we get

$$\begin{aligned}\int_{T_i}^{T_{i+1}} R(t,s)\phi_k(s)ds &= \int_{T_i}^{T_{i+1}} \sum_{l=1}^{\infty} \lambda_l \phi_l(t)\phi_l^*(s)\phi_k(s)ds \\ &= \sum_{l=1}^{\infty} \lambda_l \phi_l(t) \int_{T_i}^{T_{i+1}} \phi_l^*(s)\phi_k(s)ds \end{aligned} \tag{2-19}$$

Since the basis functions are orthonormal

$$\int_{T_i}^{T_{i+1}} R(t,s)\phi_k(s)ds = \lambda_k \phi_k(t) \tag{2-20}$$

From this integral equation, one can conclude that the basis functions $\phi_k(t)$ are the eigenvectors and λ_k's are the eigenvalues.

2.2.1 The Discrete Case

Suppose we have an array of vectors $\{x_i\}$ where every vector is non-periodic random process, given by

$$x_i = \begin{bmatrix} x_i(0) \\ x_i(1) \\ \vdots \\ x_i(L-1) \end{bmatrix} \qquad 1 \leq i \leq M \tag{2-21}$$

where L is the length of the vector. Then, the GKL expansion of the vector x_i is given by

$$x_i = \sum_{j=1}^{L} c_{ij}\phi_j \tag{2-22}$$

where c_{ij} are uncorrelated random coefficients and ϕ_j is the basis vector

$$\phi_j = \begin{bmatrix} \phi_j(0) \\ \phi_j(1) \\ \vdots \\ \phi_j(L-1) \end{bmatrix} \tag{2-23}$$

Equation (2-22) can be represented in matrix notation

$$x_i = \Phi c_i \tag{2-24}$$

where Φ is the matrix whose columns are basis vectors

$$\Phi = \begin{pmatrix} \phi_1 & \phi_2 & \cdots & \phi_L \end{pmatrix} \tag{2-25}$$

and

$$c_i = \begin{bmatrix} c_{i1} \\ c_{i2} \\ \vdots \\ c_{iL} \end{bmatrix} \tag{2-26}$$

The discrete case of the covariance function of Equation (2-15) is the covariance matrix,

$$R = \sum_{i=1}^{M} E\{x_i x_i^H\} \tag{2-27}$$

Replacing Equation (2-24) in Equation (2-27) for x_i results in

$$\begin{aligned} R &= \sum_{i=1}^{M} E\{\Phi c_i c_i^H \Phi^H\} \\ &= \Phi \left(\sum_{i=1}^{M} E\{c_i c_i^H\} \right) \Phi^H \end{aligned} \tag{2-28}$$

Since coefficients are uncorrelated, we have

$$\sum_{i=1}^{M} E\{c_i c_i^H\} = D_\lambda \tag{2-29}$$

where D_λ is a diagonal matrix

$$D_\lambda = \begin{bmatrix} \lambda_1 & 0 & \cdots & 0 \\ 0 & \lambda_2 & \cdots & 0 \\ \vdots & \vdots & \ddots & \vdots \\ 0 & 0 & \cdots & \lambda_L \end{bmatrix} \tag{2-30}$$

Then Equation (2-28) can be written as

$$R = \Phi D_\lambda \Phi^H \tag{2-31}$$

Post-multiplying above equation by the matrix Φ yields

$$\begin{aligned} R\Phi &= \Phi D_\lambda \Phi^H \Phi \\ &= \Phi D_\lambda \end{aligned} \tag{2-32}$$

since $\Phi\Phi^H = I$, i.e., the basis vectors composing Φ are orthonormal.

By looking at the Equation (2-32), we have that

$$R\phi_j = \lambda_j \phi_j \tag{2-33}$$

Above equation is the discrete analog of Equation (2-20). From the Equation (2-33) and the definition of eigenvalues and eigenvectors, we see that the jth basis vector used in the expansion given in Equation (2-22) is simply the eigenvector of the covariance matrix corresponding to the eigenvalue λ_j [20]. Because the covariance matrix is a symmetric, the eigenvalues of a positive definite matrix are positive and its eigenvectors, consequently the basis vectors, are orthonormal.

$$\phi_j^H \phi_k = \begin{cases} 1 & \text{if } i = k \quad \text{(2-34a)} \\ 0 & \text{if } i \neq k \quad \text{(2-34b)} \end{cases}$$

The expansion coefficients are obtained as follow: Pre-multiplying Equation (2-24) by Φ^H we have

$$\begin{aligned} \Phi^H x_i &= \Phi^H \Phi c_i \qquad \text{(2-35)} \\ &= c_i \end{aligned}$$

2.3 Properties of KL Expansion

2.3.1 Minimum Representation Error Property

The KL expansion minimizes the mean-square error in representing the signal due to the use of a finite number of basis functions in the expansion given in Equation (2-1), i.e., a minimum number of basis functions is needed to obtain a fixed reconstruction error as compared to any other orthogonal expansion. The reason for this is that the basis functions are derived from the statistics of the signal. Sub-optimal expansions such as Fourier or Walsh use fixed-form basis functions. For the Fourier expansions, basis functions are sinusoidal. For the Walsh expansion, the basis functions are square

waves. To get the same residual error in the case of Walsh or Fourier expansions, a larger number of basis functions are required.

A theoretical derivation of the property is as follows [25, 27]:

Let $\{\varphi_k(t)\}$ be a set of arbitrary orthonormal functions and let Equation (2-1) be written as

$$x(t) = \sum_{k=1}^{N} c_k \varphi_k(t) + e_N(t) \tag{2-36}$$

where $e_N(t)$ is the residual error when the expansion uses any N basis functions. Let us consider the expected value of the magnitude square of residual error $E\{|e_N(t)|^2\}$. We want to get orthonormal functions which give the best approximation of the random process $x(t)$. From Equation (2-36), $E\{|e_N(t)|^2\}$ can be written as

$$\begin{aligned}
E\{|e_N(t)|^2\} &= E\left\{\left[x(t) - \sum_{k=1}^{N} c_k\varphi_k(t)\right]\left[x^*(t) - \sum_{k=1}^{N} c_k^*\varphi_k^*(t)\right]\right\} \\
&= E\left\{x(t)x^*(t) - x(t)\sum_{k=1}^{N} c_k^*\varphi_k^*(t) - \sum_{k=1}^{N} c_k\varphi_k(t)x^*(t)\right\} \\
&\quad + E\left\{\sum_{k=1}^{N} c_k\varphi_k(t)\sum_{k=1}^{N} c_k^*\varphi_k^*(t)\right\} \\
&= E\{|x(t)|^2\} - \sum_{k=1}^{N} E\{x(t)c_k^*\}\varphi_k^*(t) + \sum_{k=1}^{N} E\{x^*(t)c_k\}\varphi_k(t) \\
&\quad + \sum_{k=1}^{N}\sum_{l=1}^{N} E\{c_k c_l^*\}\varphi_k(t)\varphi_l^*(t)
\end{aligned} \tag{2-37}$$

KL expansion of $x(t)$ is given by $x(t) = \sum_{l=1}^{\infty} c_l^{\phi(}{}_l t)$, then $E\{x^*(t)c_k\}$ can be written as

$$\begin{aligned}
E\{x^*(t)c_k\} &= E\left\{\sum_{l=1}^{\infty} c_l^*\phi_l^*(t)c_k\right\} \\
&= \sum_{l=1}^{\infty} E\{c_l^* c_k\}\phi_l^*(t) \\
&= |c_k|^2\phi_k^*
\end{aligned} \tag{2-38}$$

Similarly,

$$E\{x(t)c_k^*\} = |c_k|^2\phi_k^* \tag{2-39}$$

Then replacing Equation (2-38) and (2-39) in Equation (2-37), we have

$$E\{|e_N(t)|^2\} = E\{|x(t)|^2\} + \sum_{k=1}^{N}\sum_{l=1}^{N} E\{c_k c_l^*\}\varphi_k(t)\varphi_l^*(t)$$

$$+\sum_{k=1}^{N}|c_k|^2\{|\varphi_k(t)|^2-\varphi_k(t)\phi_k^*(t)-\varphi_k^*(t)\phi_k(t)\} \tag{2-40}$$

The last equation can also be written in the following form

$$\begin{aligned} E\{|e_N(t)|^2\} &= E\{|x(t)|^2\}+\sum_{k=1}^{N}\sum_{l=1}^{N}E\{c_kc_l^*\}\varphi_k(t)\varphi_l^*(t) \\ &\quad -\sum_{k=1}^{N}|c_k|^2|\phi_k(t)|^2+\sum_{k=1}^{N}|c_k|^2|\varphi_k(t)-\phi_k(t)|^2 \end{aligned} \tag{2-41}$$

From Equation (2-41), we can realize that the minimum is achieved at $\varphi_k(t)=\phi_k(t)$ where $\phi_k(t)$ is a basis function of the KL expansion given in Equation (2-1).

2.3.2 Minimum Entropy Property

The KL expansion minimizes the entropy function defined in terms of average squared coefficients used in the expansion. The significance of this property is that it associates with the coefficients of the expansion a measure of minimum entropy. A theoretical proof of the property can be found in [25, 27]. Let $x_i(t)$ be square integrable and normalized so that

$$\int_{T_i}^{T_{i+1}}|x_i(t)|^2dt=1 \tag{2-42}$$

Then,

$$\begin{aligned} |x_i(t)|^2 &= x_i(t)x_i^*(t) \\ &= \sum_{k=1}^{\infty}c_{ik}\phi_k(t)\sum_{l=1}^{\infty}c_{il}^*\phi_l^*(t) \\ &= \sum_{k=1}^{\infty}\sum_{l=1}^{\infty}c_{ik}c_{il}^*\phi_k(t)\phi_l^*(t) \end{aligned} \tag{2-43}$$

By integrating both sides of Equation (2-43) in the interval $[T_i, T_{i+1}]$, we get

$$\int_{T_i}^{T_{i+1}}|x_i(t)|^2dt=\sum_{k=1}^{\infty}\sum_{l=1}^{\infty}c_{ik}c_{il}^*\int_{T_i}^{T_{i+1}}\phi_k(t)\phi_l^*(t)dt \tag{2-44}$$

Since basis functions $\phi_k(t)$ are orthonormal, the last equation becomes

$$\begin{aligned}\int_{T_i}^{T_{i+1}} |x_i(t)|^2 dt &= \sum_{k=1}^{\infty} |c_{ik}|^2 \\ &= 1\end{aligned}$$

Define $\rho_k = \sum_{i=1}^{M} p_i E(|c_{ik}|^2)$ $1 \leq k < \infty$, where p_i is the probability that $x_i(t)$ occurs and $\sum_{i=1}^{M} p_i = 1$. Note that the ρ_k's are the eigenvalues of the integral equation (2-20). Since $\rho_k \geq 0$ and

$$\begin{aligned}\sum_{k=1}^{\infty} \rho_k &= \sum_{k=1}^{\infty} \sum_{i=1}^{M} p_i E\{|c_{ik}|^2\} \\ &= \sum_{i=1}^{M} p_i \sum_{k=1}^{\infty} E\{|c_{ik}|^2\} \\ &= \sum_{i=1}^{\infty} p_i \\ &= 1\end{aligned}$$

Therefore, ρ_k $1 \leq k < \infty$ form a probability distribution on the KL coordinate functions $\{\phi_k(t)\}$. Define an entropy function for the ρ_k's of the $\{\phi_k(t)\}$

$$H(\{\phi_k(t)\}) = -\sum_{k=1}^{\infty} \rho_k \log \rho_k \tag{2-45}$$

If ρ_k's are ordered such that

$$\rho_1 \geq \rho_2 \geq ... \geq \rho_k \geq \rho_{k+1}$$

then for any other γ_k's associated with any other set of coordinate functions $\{\varphi_k\}$ we have

$$\sum_{k=1}^{n} \rho_k \geq \sum_{k=1}^{n} \gamma_k \tag{2-46}$$

Hence

$$-\sum_{k=1}^{\infty} \rho_k \log \rho_k \leq -\sum_{k=1}^{\infty} \gamma_k \log \gamma_k \tag{2-47}$$

and

$$H(\{\phi_k(t)\}) = \min H(\{\varphi_k(t)\}) \tag{2-48}$$

The proof from Equation (2-45) through (2-47) is given in Watanabe [26].

Although the KL expansion is considered as the most efficient way to represent signals, it has a few drawbacks. First, its computational cost since it is a solution to an eigenvalue problem. Cost can be reduced if we deal with shorter signals rather than the long ones since in this case, we will need to estimate smaller covariance matrices. Then partitioning of the large signal can be useful for reducing computational cost. Second, it is difficult to capture signal features localized in the time-frequency plane due to the global eigenvectors [31]. Therefore to be able to get the localized features of a signal we need to establish "localized KL bases". To get localized KL bases, the signal first needs to be partitioned into almost stationary segments. Although segments can be considered almost stationary we will still assume non-stationarity in the calculations as shown in the following chapters. Getting these segments will be explained in the next section.

3.0 ORTHONORMAL-BASIS PARTITIONING OF NONSTATIONARY SIGNALS

Detection of changes in a non-stationary signal is an important problem that has been studied by many researchers [32–40]. The problem of partitioning a non-stationary signal into non-overlapping semi-stationary ones arises in many areas such as speech, communication and biomedical signal analysis. Partitioning the signal into almost stationary segments makes it easier to deal with it since data in segments will be shorter and less non-stationary. Lovell and Boashash partitioned the signal into near stationary segments using a modified Appel and Brandit algorithm [35]. Their algorithm uses two spectral distance measures and is insensitive to the changes in the energy of the signal. An entropy based algorithm [37, 38] is proposed by Coiffman and Wickerhauser for optimal segmentation. Their method looks for the most significant coefficients of the Malvar expansion to achieve the most parsimonious representation possible. But the algorithm does not consider other important signal characteristics such as frequencies of the signal and the number of sinusoidal components. For example this algorithm does not give an acceptable segmentation for signals composed of multiple, superimposed gated sinusoids.

Because accurate time-dependent analysis of multicomponent nonstationary signals requires segmentation [35], in this section, we consider methods for partitioning nonstationary signals into segments that approximately behave as stationary signals. We introduce two orthogonal-basis partitioning techniques: 1) a computationally efficient low-resolution partitioning for long signals, and 2) a high-resolution partitioning for short signals or segments of particular interest [41].

The low resolution partitioning is based on the projection of consecutive time segments onto a small set of global basis vectors, compressing the information into a few projection coefficients. Since these basis vectors are fixed for all the time segments, the time series formed by the projection coefficients represents the gross structure of the signal. Changes in this series could be used for

tracking major changes in the signal and for selecting the segments of interest [42, 43], which can be subsequently analyzed in-depth using high-resolution partitioning and time-frequency representation.

In the high-resolution partitioning, the basis vectors are segment-specific or local. Changes in frequency content that occur between two consecutive time segments may be detected by comparing the number of eigenvalues and the local energy in two overlapping windows of different lengths. Although this technique is computationally demanding, it has a low sensitivity to artifacts which is desirable for accurate partitioning. The idea of using eigenvalues for segmentation of a nonstationary, multidimensional signal is not new. Basseville et al. [44] analyzed changes in the eigenvalues and eigenvectors of the state transition matrix to detect small changes in the characteristics of a vibrating mechanical system. The proposed method can be considered a simplified implementation of a more general eigenstructure analysis that allows partitioning nonstationary, multidimensional signals into pseudo-stationary segments. A combined application of a long-term and a short-term window, corresponding to the periods before and after a possible change, has been described in [45].

3.1 Low Resolution Partitioning

Detection of transients in a long non-stationary signal is a challenging problem. In this section, we propose to partition such a signal into arbitrarily small segments and obtain a global orthogonal representation by projecting each segment onto a fixed set of basis vectors. Then we use a much more parsimonious time series, formed by the coefficients of the orthogonal representation, to characterize the gross structure of the signal. Changes in this time series relate to transients, which can be marked for further study. The Karhunen-Loeve (KL) orthogonal representation has long been used in pattern recognition applications for feature selection and ordering [20] . An extended version of the KL representation, which we call the Global Karhunen-Loeve (GKL) expansion, will be used here as an efficient way of finding where transients occur. The GKL expansion is applied to an array of random vectors $y_i = [y(iL)\ y(1+iL)\ ...\ y(L-1+iL)]^T$, $i = 0, 1, ..., M-1$, obtained from dividing

a long non-stationary signal $y(n)$ into short non-overlapping segments of equal length L. Then the GKL expansion of a vector y_i is given by

$$y_i = \sum_{j=1}^{L} c_{ij}\phi_j^g, \tag{3-1}$$

where c_{ij} are the GKL coefficients and $\{\phi_j^g\}$ are the global basis vectors or the eigenvectors [20] of the correlation matrix

$$R_y = \frac{1}{M}\sum_{i=0}^{M-1} y_i y_i^T. \tag{3-2}$$

The existence of one LxL covariance matrix, and one set of basis vectors used for representing $\{y_i\}$ explains the "global" nature of the GKL expansion. The GKL coefficients are unique for each time segment and given by

$$c_i = \Phi^H y_i, \tag{3-3}$$

where $c_i = [c_{i1}\ c_{i2}\ ...\ c_{iL}]^T$, $i = 0, 1, ..., M-1$, and Φ is a LxL matrix whose columns are the eigenvectors ϕ_j^g of the covariance matrix R_y. Thus, changes in the signal $y(n)$ that occur from one segment y_i to another y_{i+1} are reflected in these coefficients. Constructing time series of the most significant GKL coefficients (for example, the time series of the first GKL coefficients is given by $T_1 = [c_{01}\ c_{11}....\ c_{M-1,1}]$) and tracking the changes in their amplitudes and local variances allows detection of the segments in which the transients occur [42, 43]. In such segments, we perform further in-depth analysis as described in the next section.

3.2 High Resolution Partitioning

Suppose that $x(n)$, $0 \leq n \leq N-1$, is one of the non-stationary segments identified by the low resolution segmentation and needs to be partitioned into approximately stationary segments. Initial partitioning of $x(n)$ is performed using Malvar windows [46, 47]. A typical segmentation Malvar window $\mathrm{w}_j(n)$ is shown in Figure 1. The segmentation window does not have to be Malvar window

but since we used Malvar windows in signal reconstruction (Chapter 4) we decided to use Malvar windows for segmentation to be consistent.

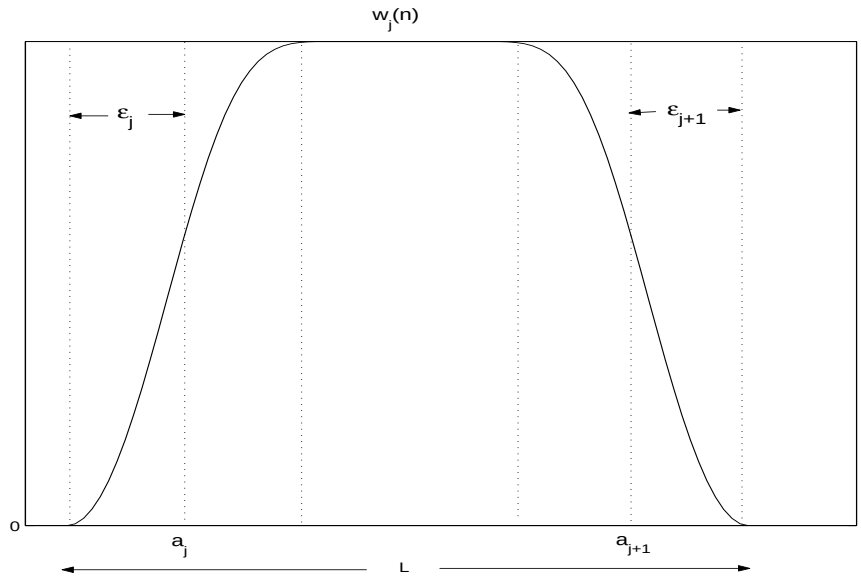

Figure 1 Segmentation window

The window displayed in Figure 1 is composed of three sections. The first one is an attack section with a duration of $2\varepsilon_j$; the next section is a stationary section with a duration of $L - \varepsilon_j - \varepsilon_{j+1}$; and a decay section with a duration of $2\varepsilon_{j+1}$.

For segmentation purposes, we are only interested in the windowed signal $x_j(n)$. The windowed signal is given by $x_j(n) = x(n)\mathrm{w}_j(n)$, $a_j - \varepsilon < n \leq a_{j+1} + \varepsilon$, and its KL expansion is

$$x_j(n) = \sum_{l=0}^{L-1} b_{jl}\theta_{jl}(n) \tag{3-4}$$

where b_{jl} are the uncorrelated random KL coefficients and $\{\theta_{jl}(n)\}$ are the orthonormal basis vectors obtained from the covariance matrix of the windowed signal $x_j(n)$ and $L = a_{j+1} - a_j + 2\varepsilon$. In fact, they are the eigenvectors of the covariance matrix. Therefore, these basis functions are signal dependent. Since the signal is non-stationary, every $\{x_j(n)\}_{j=0}^{N-L-1}$ will be different and thus $\{\theta_{jl}(n)\}$ will be different for every $\{x_j(n)\}$. They do not have a standard form that could be used for all

$\{x_j(n)\}$. Furthermore, basis functions of a windowed signal cannot be used to represent the basis functions of another windowed signal. This could be impossible to do it in some cases. All these properties come from the fact that KL basis functions do not form a complete set.

To obtain a generalized representation of the KL bases in different time windows, one can use a complete set of exponentials, so that:

$$\theta_{jl}(n) = \frac{1}{L}\sum_{k=0}^{L-1} d_{jl}(k)e^{j\omega_k n} \tag{3-5}$$

where $\omega_k = \frac{2\pi k}{L}$ and $\{d_{jl}(k)\}$ are the corresponding coefficients. By replacing equation (3-5) in Equation (3-4), we get

$$\begin{aligned} x_j(n) &= \frac{1}{L}\sum_{l=0}^{L-1} b_{jl}\sum_{k=0}^{L-1} d_{jl}(k)e^{j\omega_k n} \\ &= \frac{1}{L}\sum_{k=0}^{L-1}\sum_{l=0}^{L-1} b_{jl}d_{jl}(k)e^{j\omega_k n} \end{aligned} \tag{3-6}$$

Let us define

$$\alpha_j(k) \equiv \frac{1}{L}\sum_{l=0}^{L-1} b_{jl}d_{jl}(k) \tag{3-7}$$

then

$$x_j(n) = \sum_{k=0}^{L-1} \alpha_j(k)e^{j\omega_k n} \qquad 0 < n \leq L-1 \tag{3-8}$$

We seek to adapt the initial partition using the eigenvalues of the covariance matrix of a windowed signal and the local energy. The connection between the signal representation, eigenvalues and local energy is presented here. The eigenvalues of each segment can be obtained as follows.

Equation (3-8) can also be written in matrix form as

$$x_j = Q\alpha_j \tag{3-9}$$

where

$$x_j = \begin{bmatrix} x_j(0) \\ x_j(1) \\ \vdots \\ x_j(L-1) \end{bmatrix} = \begin{bmatrix} x(a_j+1) \\ x(a_j+2) \\ \vdots \\ x(a_j+L) \end{bmatrix} \tag{3-10}$$

and

$$Q = \begin{bmatrix} 1 & 1 & \dots & 1 \\ 1 & e^{j\omega_1 1} & \dots & e^{j\omega_{L-1} 1} \\ \vdots & \vdots & \ddots & \vdots \\ 1 & e^{j\omega_1 (L-1)} & \dots & e^{j\omega_{L-1}(L-1)} \end{bmatrix} \tag{3-11}$$

and

$$\alpha_j = \begin{bmatrix} \alpha_j(0) \\ \alpha_j(1) \\ \vdots \\ \alpha_j(L-1) \end{bmatrix} \tag{3-12}$$

Assuming non-stationarity of windowed signal $x_j(n)$, the correlation matrix is given by

$$R_{x_j} = E\{x_j x_j^H\} = \begin{bmatrix} r_{x_j}(0,0) & r_{x_j}(0,1) & \dots & r_{x_j}(0,L-1) \\ r_{x_j}(1,0) & r_{x_j}(1,1) & \dots & r_{x_j}(1,L-1) \\ \vdots & \vdots & \ddots & \vdots \\ r_{x_j}(L-1,0) & r_{x_j}(L-1,1) & \dots & r_{x_j}(L-1,L-1) \end{bmatrix} \tag{3-13}$$

where H stands for conjugate transpose. Estimation of the correlation matrix is given in the next section. By replacing equation (3-9) in the last equation we have

$$\begin{aligned} R_{x_j} &= E\{Q\alpha_j\alpha_j^H Q^H\} \\ &= QE\{\alpha_j\alpha_j^H\}Q^H \end{aligned} \tag{3-14}$$

Since Q is deterministic, it can be taken out of the expected value operator E in the last equation. $\alpha_j(k)$ is given by equation (3-7) and it can also be written in matrix form as

$$\alpha_j = \Delta_j b_j \tag{3-15}$$

where

$$\Delta_j = \begin{bmatrix} d_{j0}(0) & d_{j1}(0) & \dots & d_{j(L-1)}(0) \\ d_{j0}(1) & d_{j1}(1) & \dots & d_{j(L-1)}(1) \\ \vdots & \vdots & \ddots & \vdots \\ d_{j0}(L-1) & d_{j1}(L-1) & \dots & d_{j(L-1)}(L-1) \end{bmatrix} \tag{3-16}$$

and

$$b_j = \begin{bmatrix} b_{j0} \\ b_{j1} \\ \vdots \\ b_{j(L-1)} \end{bmatrix} \tag{3-17}$$

Then, $E\{\alpha_j^H\alpha_j^H\}$ in Equation (3-14) becomes

$$
\begin{aligned}
E\{\alpha_j \alpha_j^H\} &= E\{\Delta_j b_j b_j^H \Delta_j^H\} \\
&= \Delta_j E\{b_j b_j^H\} \Delta_j^H
\end{aligned} \tag{3-18}
$$

Then, substituting Equation (3-18) in Equation (3-14) results in

$$
R_{x_j} = Q \Delta_j E\{b_j b_j^H\} \Delta_j^H Q^H \tag{3-19}
$$

By defining $\Gamma_j \equiv Q\Delta_j$ Equation (3-19) becomes

$$
R_{x_j} = \Gamma_j E\{b_j b_j^H\} \Gamma_j^H \tag{3-20}
$$

From the description of Γ_j, one can realize that columns of Γ_j are the eigenvectors of the covariance matrix of $x_j(n)$ which is R_{x_j}. Since R_{x_j} is a symmetric and positive semidefinite matrix, its eigenvalues are positive and its eigenvectors are orthonormal [48]. Since the columns of Γ_j are the eigenvectors of R_{x_j} and they are linearly independent, R_{x_j} can be diagonalizable and $E\{b_j b_j^H\}$ is a diagonal matrix, with the eigenvalues of R_{x_j} along its diagonal [49]

However, not all matrices possess n linearly independent eigenvectors and therefore not all matrices are diagonalizable[49]. Diagonalization can fail only if there are repeated eigenvalues. If there are repeated eigenvalues, there will not be enough independent eigenvectors to construct matrix Γ_j.

Since basis functions are the columns of Γ_j in Equation (3-20) and they are orthonormal, we have that

$$
\Gamma_j^H \Gamma_j = I \tag{3-21}
$$

where I is identity matrix. Then Equation (3-20) can also be written as

$$\Gamma_j^{-1} R_{x_j} \Gamma_j = E\{b_j b_j^H\} \tag{3-22}$$

$$= \begin{bmatrix} \lambda_{j0} & 0 & \dots & 0 \\ 0 & \lambda_{j1} & \dots & 0 \\ \vdots & \vdots & \ddots & \vdots \\ 0 & 0 & \dots & \lambda_{j(L-1)} \end{bmatrix} \tag{3-23}$$

where λ_{jl} are the eigenvalues of R_{x_j} and also

$$D_{\lambda_j}(i,k) = E\{b_{ji} b_{jk}^*\} = \begin{cases} \lambda_{ji} & \text{if } i = k \quad \text{(3-24a)} \\ 0 & \text{if } i \neq k \quad \text{(3-24b)} \end{cases}$$

Diagonal matrix D_{λ_j} is a function of j and any changes along the signal in consideration will be reflected by D_{λ_j} and consequently by the eigenvalues since main diagonals of D_{λ_j} are the eigenvalues λ_{jl}. For each block we will have new set of eigenvalues and number of the eigenvalues required to capture certain amount of the energy of $x_j(n)$ will be different in each block. For each basis function there is a corresponding eigenvalue. For example for a signal of one sinusoid one will only need one eigenvector (basis function) and consequently one eigenvalue to represent the signal. But for a signal of two sinusoids one will need two basis functions and consequently two eigenvalues. So if the signal gets more complex, the number of the required basis functions will increase to represent the signal. As a consequence there will be larger number of eigenvalues corresponding to those basis functions (eigenvectors).

Another feature related to the eigenvalues is that the summation of the eigenvalues of a covariance matrix obtained from a signal equals the expected value of the energy of that signal. Proof of this property is as follows. The KL expansion of $x_j(n)$ is given by Equation (3-4). Then energy of $x_j(n)$ is

$$\sum_n x_j^2(n) = \sum_n \sum_l b_{jl}\theta_{jl}(n) \sum_k b_{jk}^* \theta_{jk}^*(n)$$

$$= \sum_l \sum_k b_{jl} b_{jk}^* \sum_n \theta_{jl}(n)\theta_{jk}^*(n) \tag{3-25}$$

Since basis functions are orthonormal, we have

$$\sum_n \theta_{jl}(n)\theta^*_{jk}(n) = \begin{cases} 1 & \text{if } l = k \quad (3\text{-}26a) \\ 0 & \text{if } l \neq k \quad (3\text{-}26b) \end{cases}$$

Then,

$$\sum_n x_j^2(n) = \sum_l b_{jl}^2 \tag{3-27}$$

Expected value of the energy is

$$E\left\{\sum_n x_j^2(n)\right\} = \sum_l E\{b_{jl}b_{jl}^*\} \tag{3-28}$$

From Equation (3-24), we have $E\{b_{jl}b_{jl}^*\} = \lambda_{jl}$. Then

$$E\left\{\sum_n x_j^2(n)\right\} = \sum_l \lambda_{jl} \tag{3-29}$$

Then energy changes between windowed segments can also be found by comparing the summation of the eigenvalues in each segment. Therefore the number of the eigenvalues and their sum can be used as tools to detect changes along a non-stationary signal and to segment it.

3.2.1 Estimation of the Autocorrelation Matrix

Due to assumption of non-stationarity of the windowed signal $x_j(n)$, the autocorrelation matrix R_{x_j} in (3-13) has entries $r_{x_j}(n,m) = E\{x_j(n)x_j^*(m)\}$ that depend on both n and m rather than on their difference. The estimation of these entries can be implemented by means of evolutionary periodogram [9, 50, 51] and it is given by

$$\hat{r}_{x_j}(n,m) = \frac{L}{M}\sum_{k=K_1}^{K_2} V_n(k)x_j(k)V_m^*(k+m-n)x_j^*(k+m-n) \tag{3-30}$$

where

$$K_1 = n-m, K_2 = L-1, \qquad if \qquad n-m \geq 0$$

$$K_1 = 0, K2 = L-1-(n-m), \qquad if \qquad n-m < 0$$

and $V_n(k)$ are the time-varying windows defined using M orthonormal functions $\{\beta_i(n)\}$ such as Legendre functions:

$$V_n(k) = \sum_{i=0}^{M-1} \beta_i^*(n)\beta_i(k) \tag{3-31}$$

The window $V_n(k)$ used in estimation is shown in the Figure 2. The resulting autocorrelation matrix is positive semi-definite Hermitian symmetric. Please note that the window $V_n(k)$ has nothing to do with segmentation window $\mathrm{w}_j(n)$. $V_n(k)$ is only used in estimation of the autocorrelation matrix.

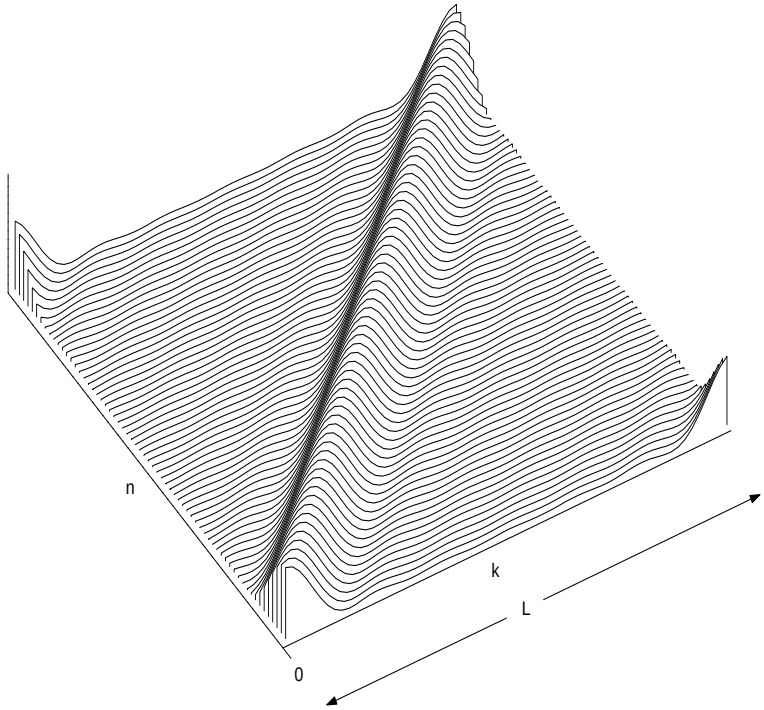

Figure 2 Windows $V_n(k)$ used in autocorrelation estimation

3.2.2 Local Segmentation Algorithm

In this section, we will describe the algorithm for high resolution partitioning. Partitioning is performed by using two short windows $\mathrm{w}_j^s(n)$ and $\mathrm{w}_{j+1}^s(n)$ of equal length L_s and a long window $\mathrm{w}_j^l(n)$ of length L_l where j is the window number, and s, l stand for short and long, respectively (Figure 3(a),(b)). The proposed algorithm first compares the eigenvalues of the covariance matrix in

the first and the second short window with those in the long window to detect any changes in the frequencies, and then analyzes energy changes between two consecutive short windows.

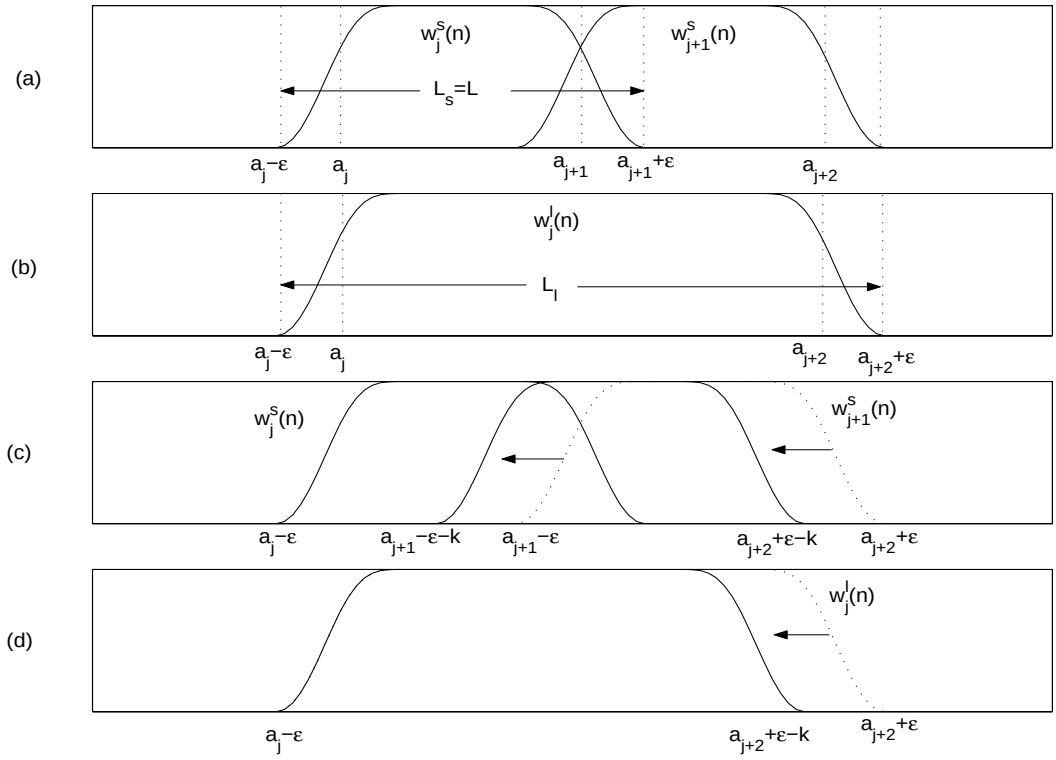

Figure 3 The Malvar windows used for the segmentation (a),(b). Boundary optimization is performed when the second criterion (c) and the first criterion (d) is satisfied in the boundary detection algorithm.

Eigenvalues of the covariance matrices of the corresponding windowed signals are used to detect frequency changes in the signal. If such a change occurs between two consecutive short windows, then the long window would display more frequencies than the first or the second short window. Thus complexity of the signal in the long window would be greater than that in each short windows ($\mathrm{w}_j^s(n)$ and $\mathrm{w}_{j+1}^s(n)$). The number of the eigenvalues required to represent a fixed proportion of energy of the signal in $\mathrm{w}_j^l(n)$ would be greater than that in $\mathrm{w}_j^s(n)$ and $\mathrm{w}_{j+1}^s(n)$. The algorithm compares the number of eigenvalues in the long window $\mathrm{w}_j^l(n)$ with the number of eigenvalues in the short windows $\mathrm{w}_j^s(n)$ and $\mathrm{w}_{j+1}^s(n)$. Note that in the algorithm below, we describe the comparison between the eigenvalues in the long window and the first short window $\mathrm{w}_j^s(n)$. Comparison between the long window and the second short window $\mathrm{w}_{j+1}^s(n)$ can be done in a similar way. Next, the energies E_j

and E_{j+1} of the windowed signals corresponding to $\mathrm{w}_j^s(n)$ and $\mathrm{w}_{j+1}^s(n)$ are computed as in (3-29) and compared.

The segmentation algorithm consists of two parts: (1) boundary detection, and (2) boundary optimization. In the first part, the location of the boundary is determined approximately. In the second part, this location is adjusted to obtain an optimal boundary.

3.2.2.1 Boundary Detection.

Step 1: Find the covariance matrix of the windowed signal $x_j^s(n) = x(n)\mathrm{w}_j^s(n)$ $a_j - \varepsilon \leq n \leq a_{j+1} + \varepsilon$ (see Figure 3(a)) by using Equation (3-30), calculate the eigenvalues of the covariance matrix $R_{x_j}^s$ and order them so that $\lambda_{j0} > \lambda_{j1} > ..... > \lambda_{j(L_s-1)}$. Next, determine the number of eigenvalues N_j^s that contain 90% of the total energy of $x_j^s(n)$. (The 90% energy threshold has been found to be appropriate experimentally. See Appendix B for a brief explanation). Find the total energy E_j of the signal $x_j^s(n)$.

Estimate the following threshold values:

$N_j^{up} = (1 + \alpha_1)N_j^s$: Upper threshold for the number of the eigenvalues

$E_j^{lw} = (1 - \alpha_2)E_j$: Lower threshold for the energy

$E_j^{up} = (1 + \alpha_3)E_j$: Upper threshold for the energy

where constants $0 < \alpha_1, \alpha_2, \alpha_3 \leq 1$ are defined a-priori.

Step 2: Repeat step 1 for the windowed signal $x_j^l(n) = x(n)\mathrm{w}_j^l(n)$, $a_j - \varepsilon \leq n \leq a_{j+2} + \varepsilon$ (see Figure 3(b)) to find the number of eigenvalues N_j^l required for representing 90% of the energy of the signal $x_j^l(n)$. Next, find the total energy E_{j+1} of the signal $x_{j+1}^s(n) = x(n)\mathrm{w}_{j+1}^s(n)$, $a_{j+1} - \varepsilon \leq n \leq a_{j+2} + \varepsilon$. Then compare the number of the eigenvalues and energy according to the following criteria:

1. If $N_j^l > N_j^{up}$, then there is a change in the frequencies of the signal, do the boundary optimization, otherwise check condition 2,

2. If $E_{j+1} < E_j^{lw}$ or $E_{j+1} > E_j^{up}$, then there is a change in the energy of the signal, do the boundary optimization,

If none of the above criteria is met, then $x_j^s(n)$ and $x_j^l(n)$ are approximately the same, and there is no need for partitioning or boundary optimization. In this case, move all segmentation windows by the length of the short window and repeat the first two steps.

If either criterion is met, $x_j^s(n)$ and $x_j^l(n)$ are different, in other words, a change in frequencies (criterion 1) and/or energy (criterion 2) occurred between a_{j+1} and a_{j+2} (see Figure 3). Then, we perform the boundary optimization.

3.2.2.2 <u>Boundary Optimization</u>. By using boundary detection we have already determined that a change from $x_j^s(n)$ to $x_j^l(n)$ has occurred at some point between a_{j+1} and a_{j+2}. Now, we would like to find the exact location of this point of the change as described below:

(a) If the first criterion in boundary detection is met:

Shrink the long window $\mathrm{w}_j^l(n)$ by reducing its length as shown in Figure 3(d). We will denote this new window by $\tilde{\mathrm{w}}_k^l(n)$, the windowed signal is given by $\tilde{x}_k^l(n) = \tilde{\mathrm{w}}_k^l(n)x(n)$, $a_j - \varepsilon \leq n \leq a_{j+2} + \varepsilon - k$, where $k = 1, 2, .., L - \varepsilon$. Find the covariance matrix of $\tilde{x}_k^l(n)$ and calculate the number of eigenvalues $\tilde{N}_k$ required for representing 90% of the energy of $\tilde{x}_k^l(n)$ as described previously in the boundary detection section. Then check the condition $\tilde{N}_k \leq N_j^s$ for $k = 1, 2, ..L - \varepsilon$. If the condition is satisfied for $k = p$, then the location of the boundary is $a_{j+2} - p$ and stop.

(b) If the second criterion in boundary detection is met:

Shift the second short window $\mathrm{w}_{j+1}^s(n)$ backwards by one point as shown in Figure 3(c). We will denote this new window by $\tilde{\mathrm{w}}_k^s(n)$ and the windowed signal is given by $\tilde{x}_k^s(n) = \tilde{\mathrm{w}}_k^s(n)x(n)$, $a_{j+1} - \varepsilon - k \leq n \leq a_{j+2} + \varepsilon - k$ where $k = 1, 2, .., L - \varepsilon$. Calculate the energy $\tilde{E}_k$ of $\tilde{x}_k^s(n)$. Then check the condition $E_j^{lw} < \tilde{E}_k < E_j^{up}$ for $k = 1, 2, ..L - \varepsilon$. If the condition is satisfied for $k = p$, then

the location of the boundary is $a_{j+2} - p$ and stop. Once we find the optimal boundary location, we repeat the procedure starting from that point.

The performance of the local segmentation algorithm will be tested on simulated signals as shown in the examples below. Signals in examples 1 and 2 are very simple since the purpose of those examples is to demonstrate how the local energy and the number of the eigenvalues change according to signal features. The algorithm is also tested on noisy signals and compared with another segmentation algorithm.

Example 1: The signal shown in Figure 4(a) is a sinusoid with a time-varying amplitude. It is given by

$$x(n) = \begin{cases} \sin(\omega_0 n) & 0 \leq n < 113 \\ \\ 3\sin(\omega_0 n) & 113 \leq n < 225 \end{cases}$$

where $\omega_0 = 2\pi f_0$ and $f_0 = .12$ Hz. The signal used here is very simple and it is used to show the use of eigenvalues and energy for segmentation. Normalized energy in first and second short windows are shown in Figure 4(b) and (c) respectively. It is clear that in the first part of the signal energy in both windows are the same but when signal amplitude changes, the energy in windows also change (6th sample on the x axis of Figure 4(b) and (c) corresponds to the location of the change in the signal). Not only the energy but also the number of eigenvalues changed as seen from Figure 4(d) and (e). Figure 4(d) corresponds to number of the eigenvalues required from the short window and Figure 4(e) corresponds to number of the eigenvalues required from long window. (Long window used in segmentation is shown in Figure 3(b)). Since amount of changes in the energy or number of the eigenvalues exceeded a pre-selected threshold, the windows were separated and final segments are given in Figure 4(f).

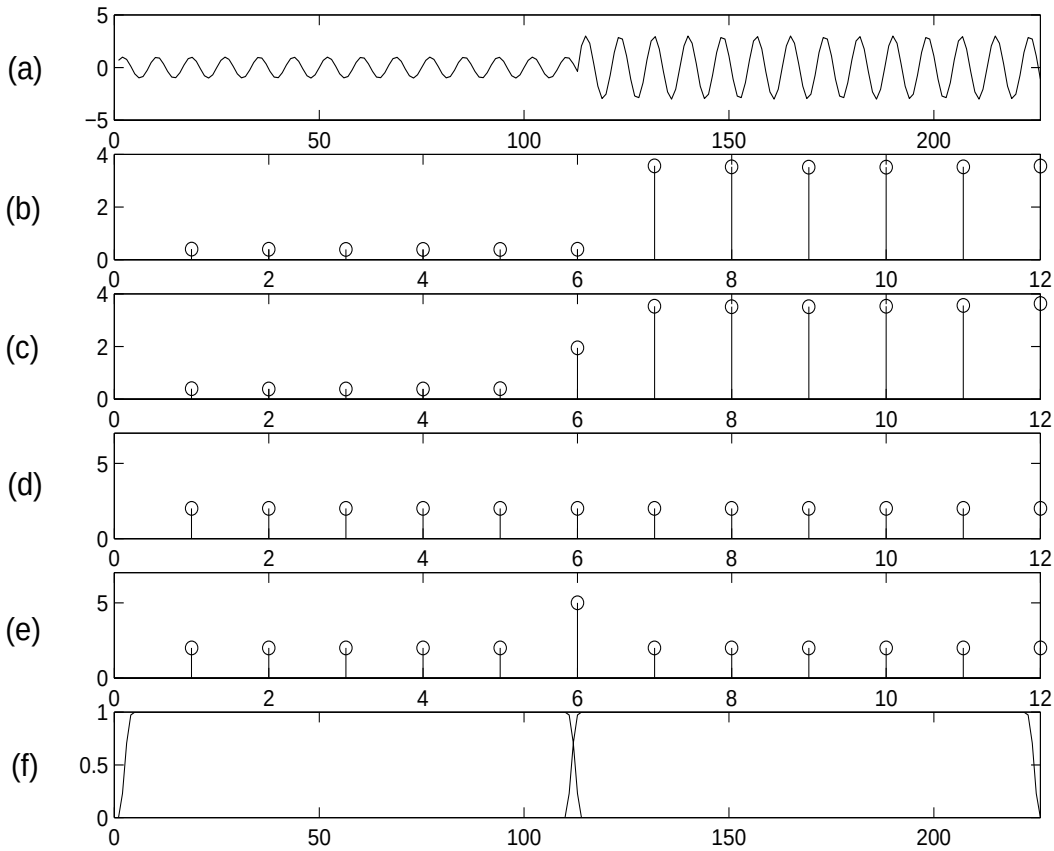

Figure 4 (a) The signal (b) Normalized energy in short window (c) Normalized energy in second short window (d) Number eigenvalues in first short window (e) Number of eigenvalues in long window (f) Segments.

Example 2: Contrary to example 1, in this example we keep the amplitude same during the whole signal but changed the frequency. Signal consists of two concatenated sinusoids as shown in Figure 5(a). It is given by

$$x(n) = \begin{cases} \sin(\omega_1 n) & 0 \leq n < 113 \\ \\ \sin(\omega_2 n) & 113 \leq n < 225 \end{cases}$$

where $\omega_1 = .24\pi$ and $\omega_2 = .7\pi$. As it is seen from Figure 5(b) and (c), energy between windows did not change much. On the other hand, if we compare the number of the eigenvalues between short and long window (Figure 5(d) and (e) respectively), we see a difference at 6th sample on x axis. The number of the eigenvalues are 2 in short window but it is 6 in longer window at that point. This difference corresponds to the change in the signal and final segments are shown in Figure 5(f). Since

we can compare the segments with the simulated signal,we can see that the segmentation is very accurate.

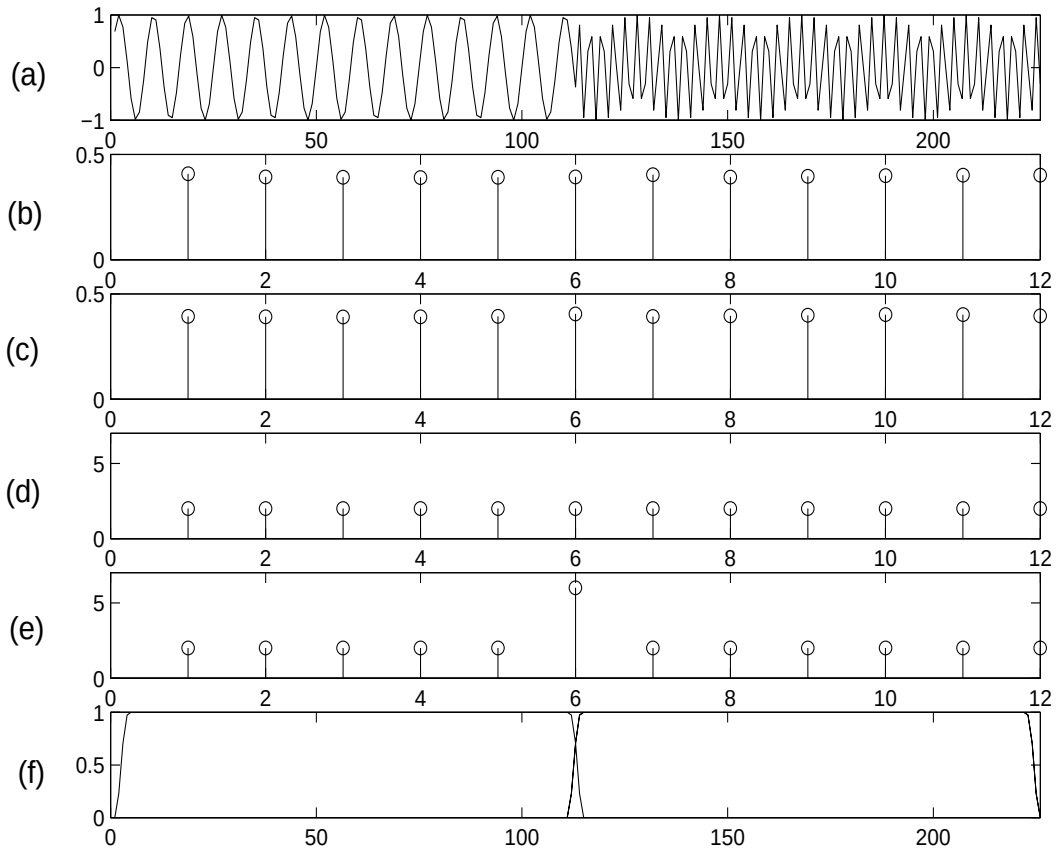

Figure 5 (a) The signal (b) Normalized energy in short window (c) Normalized energy in second short window (d) Number eigenvalues in first short window (e) Number of eigenvalues in long window (f) Segments.

Example 3: The signal consists of sinusoids, concatenated sinusoids, chirp and sinusoidal FM and is displayed in Figure 6(a). Amplitude of the signal also changes along time. The signal is given by

$$x(n) = \begin{cases} \sin(.7\pi n) & 0 \leq n < 56 \\ 3\sin(.7\pi n) & 57 \leq n < 79 \\ 2\cos(\frac{\pi n^2}{186}) & 80 \leq n < 173 \\ \sin(.24\pi n) & 174 \leq n < 211 \\ \sin(.24\pi n) + \sin(.7\pi n) & 212 \leq n < 256 \\ 3\sin(.54\pi n) & 257 \leq n < 329 \\ \cos(.5\pi n - 2.5\pi\cos(\frac{2\pi n}{64})) & 330 \leq n < 393 \\ 2\cos(.5\pi n - 2.5\pi\cos(\frac{2\pi n}{64})) & 394 \leq n < 457 \end{cases}$$

Although the signal is very complex, the method was able to separate the signal very accurately. We used the first method not the alternative one here. Three different window length (45, 33 and 22 points) were tried to see the effects of window length in segmentation. The shortest window gave the best segmentation, i.e., points where the signal changed (marked with thick solid lines in Figure 6(a)) were detected correctly except for the linear and sinusoidal FM signals where the method created some artificial boundaries. On the other hand, segments obtained using windows of length 45 and 33 did not always correspond to the original segments in the signal and furthermore there were still some artificial boundaries for linear and sinusoidal FM signals. The shorter the window the higher the resolution to recognize changes in the signal. But we cannot chose the window length too small either. One way to choose is to select the minimum window length as the max period which exists in the signal. Using longer windows resulted in fewer but longer segments. The longer the window the less sensitive the method gets towards the changes. As mentioned before, a long window is also used in segmentation and its length is twice the size of the short one. For sinusoidal signals, the method performed very well separating the different sinusoidals very accurately. On the other hand, as mentioned above, for signals like linear or sinusoidal FM, the method gave many small blocks

(smallest block can be the size of the short window) rather than one block for the whole signal. This is expected since the frequency of these signals change with time and number of the eigenvalues will be higher in longer window than short window. An alternative local segmentation algorithm was suggested in section 3.2.3 to obtain only one block for these kind of signals. Note that the alternative algorithm is not very usable for large data sets since it is computationally very expensive. Therefore it was not used for simulated and real signals in this thesis.

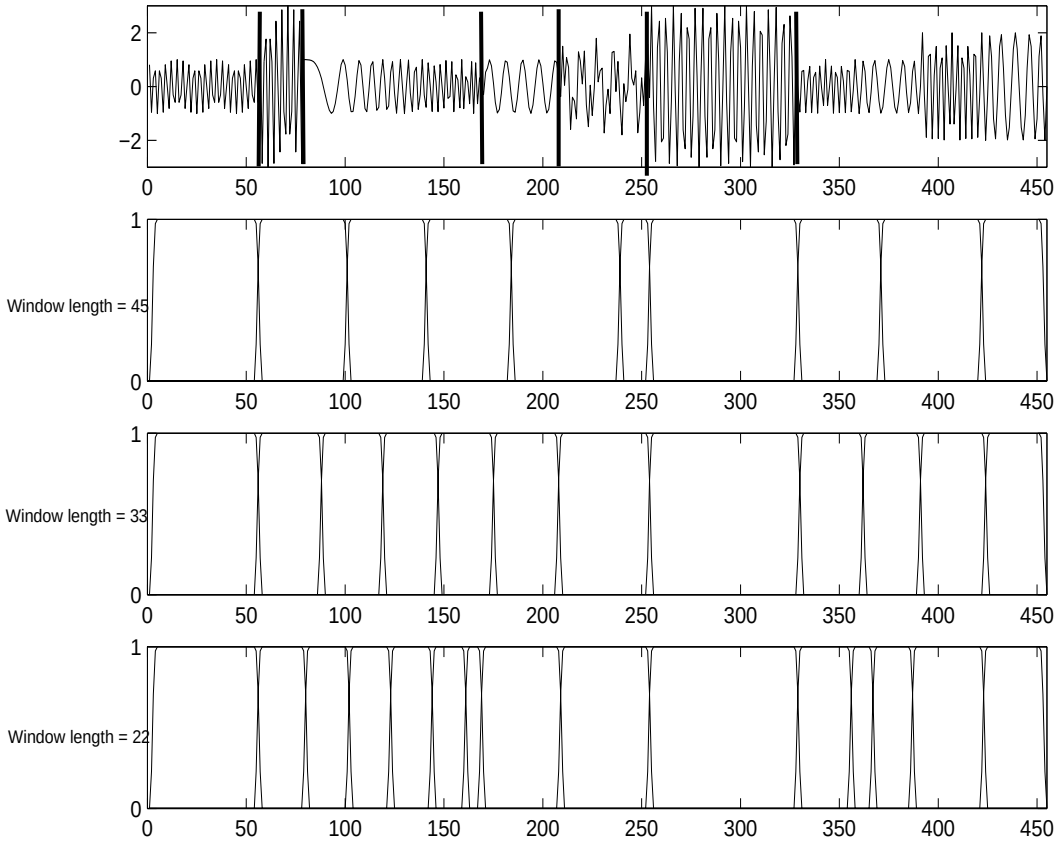

Figure 6 (a) Original Signal to be segmented (b) Segments obtained using 45 point window (c) Segments obtained using 33 point window (d) Segments obtained using 22 point window.

3.2.2.3 <u>Comparison With Other Techniques</u>. The local segmentation algorithm (algorithm I) has been compared with another segmentation algorithm (algorithm II) which is described by Andersson[52]. Andersson's algorithm builds AR or ARMA models assuming that the model parameters are piece-wise constant over time and splits the data record into segments over which the model remains constant. The model order and the noise variance need to be chosen a-priori.

Performance of these two segmentation algorithms is demonstrated using a simulated signal with two different SNRs (Figure 7 and 8). The signals consists of concatenated sinusoids with different amplitudes and frequencies embedded in white noise (SNR=10.2dB (Figure 7) and SNR=3.1 dB (Figure 8)). Solid vertical lines correspond to the actual segments. Figures 7(b) and 8(a) shows the segments (vertical dotted lines) obtained using the algorithm I. Figures 7(c) and 8(b) shows the results obtained from algorithm II. Algorithm I performed reasonably well, giving the segments that

were close to the original ones. Although the algorithm II produced similar results, it could not detect changes around sample 225 (Figure 8(b)) and sample 300 (Figure 7(c)).

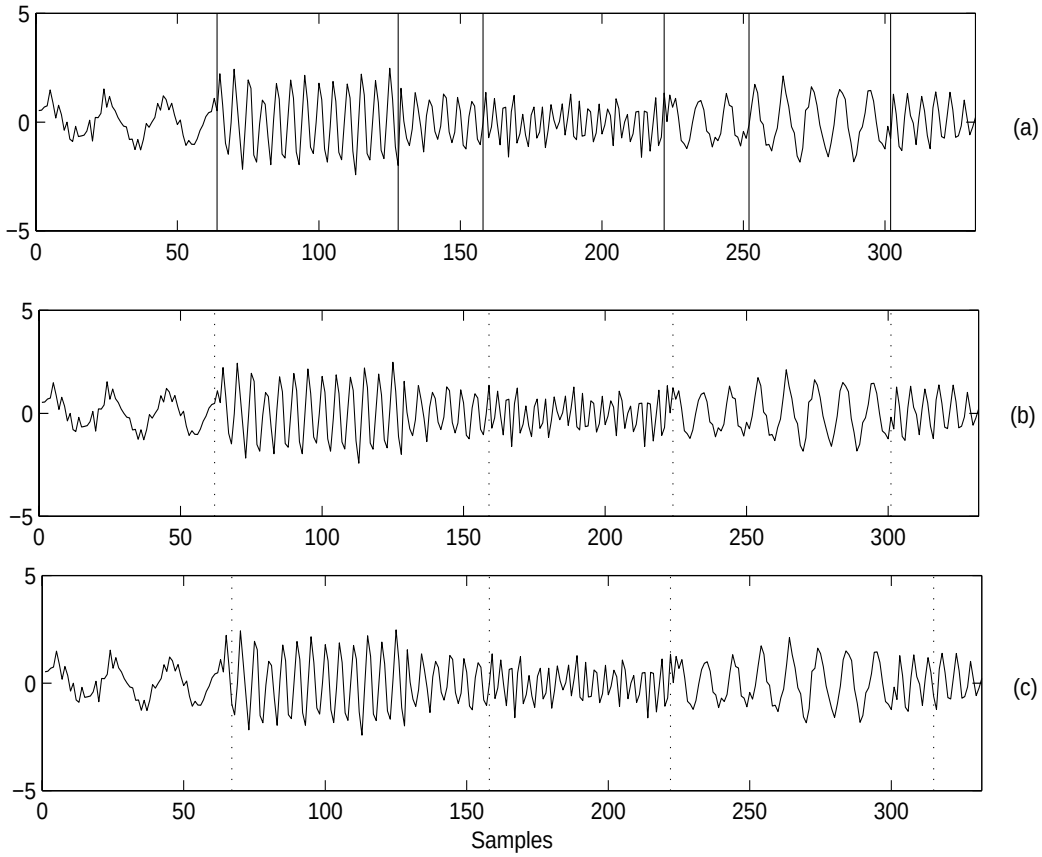

Figure 7 Performance of the two segmentation algorithms. The simulated signal (SNR=10.2 dB) (a). Solid vertical lines indicate the actual segments. Segments obtained by using Algorithm I (the segmentation window length is 16) (b) and Algorithm II (model order is 5) (c). Dotted lines represent the boundaries obtained by the corresponding algorithms.

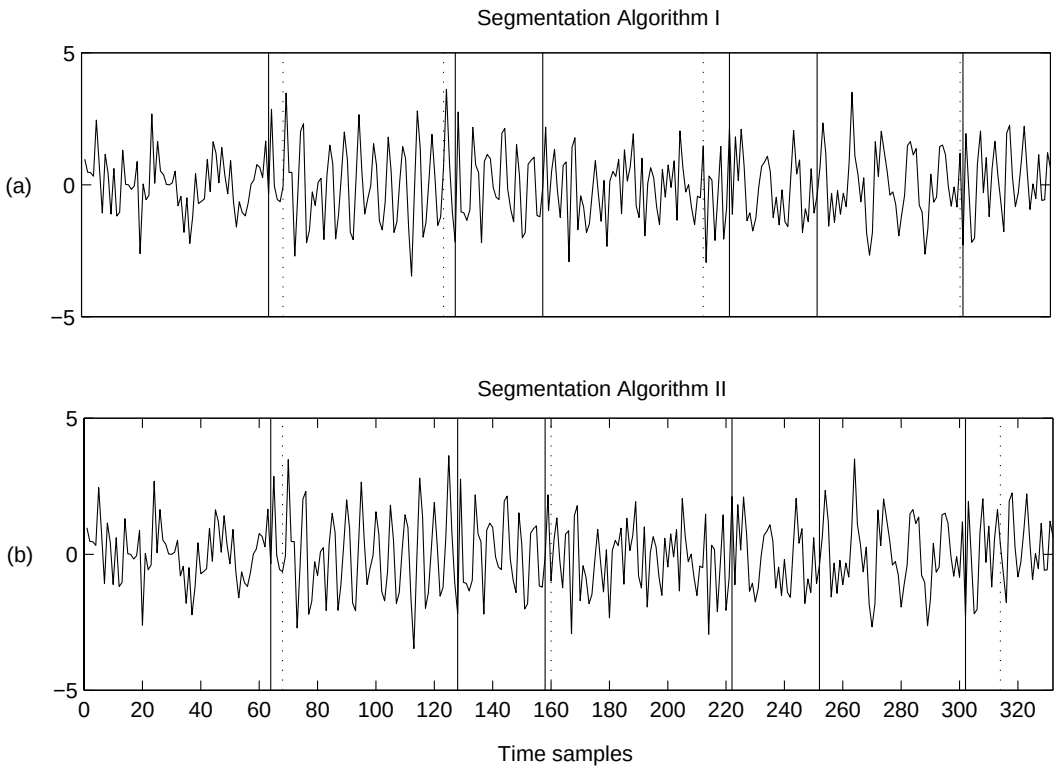

Figure 8 Performance of the two segmentation algorithms. Algorithm I (the segmentation window length is 16) (a), Algorithm II (model order is 7) (b) are compared by using a simulated signal (SNR=3.1 dB). Solid vertical lines indicate the actual segments. Dotted lines represent the boundaries obtained by the corresponding algorithms.

3.2.3 Alternative Local Segmentation Algorithm

This algorithm is an extension of the local segmentation algorithm described in Section 3.2.2. Note that this algorithm was not used in any studies of HRV data. The difference here is that we use only one segmentation window and shift the window by one point along the signal. The window used in segmentation is the same as in Figure 1. The reason that we propose this alternative algorithm is that the first algorithm (the one using multiple windows) gives very accurate segmentation for signals such as sinusoids. It separates a signal consisting of different sinusoids into blocks where each block corresponds to a different sinusoid. But in the case of signals such as linear or sinusoidal FM, the method breaks up the signal into many small blocks rather than one (Figure 9(c)). Although this is not wrong, we can still suggest another algorithm which will give only one block for these type of signals. Following are the steps of the algorithm:

Step 1 Window the signal starting from the beginning and find the covariance matrix of the windowed signal $x_j(n)$. Then calculate the eigenvalues of the covariance matrix R_{x_j} and order them from largest to smallest. Determine the number of the eigenvalues N_j required to include 90% of the total energy of $x_j(n)$.

Step 2 Once the number of the eigenvalues N_j is found in the current window, shift the window by one point and repeat the same procedure in step 1 to find the number of the eigenvalues N_{j+1} required in this new window. Then, compare the number of the eigenvalues and energy of the two windowed signal. Depending on the differences in N_j and N_{j+1} or E_j and E_{j+1}, windows will be combined or not.

The segmentation criterion is given by:

1. If $N_{j+1} < N_j^l$ or $N_{j+1} > N_j^u$ do not combine windows and go to next window, otherwise check 2
2. If $E_{j+1} < E_j^l$ or $E_{j+1} > E_j^u$ do not combine windows and go to next window
3. Otherwise combine windows

where

N_j^l : Lower threshold for the number of the eigenvalues

N_j^u : Upper threshold for the number of the eigenvalues

E_j^l : Lower threshold for energy

E_j^u : Upper threshold for energy

Example: In this example, we compared the alternative algorithm with the the local segmentation algorithm described in Section 3.4. The signal is shown on Figure 9(a) and is given by

$$x(n) = \begin{cases} \sin(.24\pi n) & 0 \leq n < 50 \\ \sin(.4\pi n) & 51 \leq n < 93 \\ \cos(\frac{\pi n^2}{186}) & 93 \leq n < 236 \end{cases}$$

The segments shown in Figure 9(b) is obtained with alternative algorithm described above. One sliding window is used. As it can be seen from the picture that we have one block for the chirp signal. On the other hand, the local segmentation algorithm gives one block for sinusoids but many small blocks for the chirp signal.

Actually the second result shown in Figure 9(c) is useful for the time-frequency representation which will be described in the next section. Each block nicely corresponds to changing frequencies in the signal. Furthermore, alternative algorithm is computationally very expensive compared the local segmentation algorithm and therefore it is not suitable for large data sets.

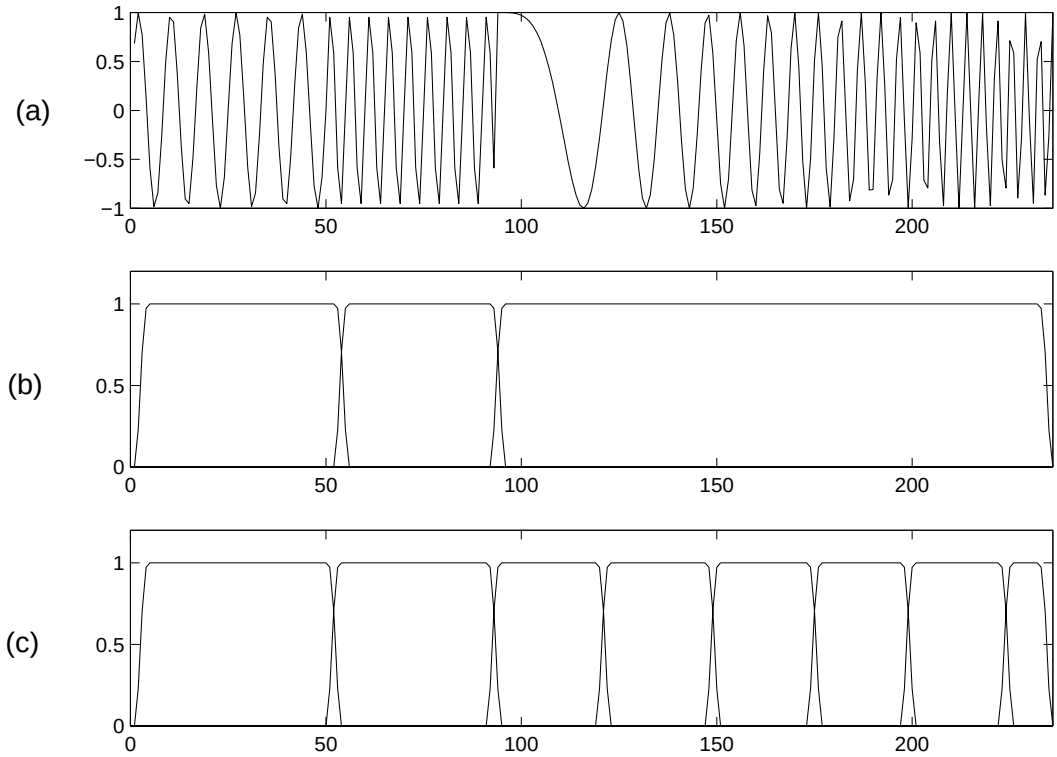

Figure 9 (a) The signal (b) Segments obtained using alternative algorithm (c) Segments obtained using the local segmentation algorithm.

So far we explained how to obtain optimal segments, in the next section we will now utilize those optimal segments to estimate the evolutionary spectrum of a non-stationary signal.

4.0 PARTITIONED TIME-FREQUENCY REPRESENTATION

The spectrum allows us to determine which frequencies exist but it does not say anything about when those frequencies occur. Time-frequency analysis allows us to determine which frequencies exist at a particular time.

One of the most common time-frequency analysis method is the spectrogram. It is ideal in many respects. The spectrogram is well defined and for many signals and situations it gives excellent time-frequency structure. However, if we want a good time localization we have to pick a narrow window in time domain, if we want a good frequency localization we need to pick a narrow window in the frequency domain. But both cannot be made arbitrarily narrow; therefore there is a trade-off between time and frequency localization in the spectrogram. For certain situations it may not be the best method available in the sense that it does not give us the clearest possible picture of what is going on. Thus other methods have been developed. One advantage of the spectrogram is that it is a proper distribution in the sense that it is positive [1].

Wigner distribution [8] is another method for time-frequency analysis. One of the advantages of the Wigner distribution over the spectrogram is that we do not have to bother with the choosing the window. The Wigner distribution gives a clear picture of the instantaneous frequency for single chirp. This is not the case with spectrogram. On the other hand, the Wigner distribution is not always positive which sometimes leads to results that cannot be interpreted. Furthermore it suffers from the fact that for multicomponent signals we get confusing artifacts which are called as cross terms.

There are also other approaches called Kernel methods for time-frequency analysis. These approaches characterize time-frequency distribution by the kernel functions. The properties of a distribution are reflected by simple constraints on the kernel, and by examining the kernel one

readily can ascertain the properties of the distribution [1]. We used the Choi-Williams distribution here as one of the Kernel methods to compare with our method.

Here, we propose a new method which we will call orthonormal-basis partitioning and time-frequency representation (OPTR). OPTR is a general name of the method which is the combination of the segmentation algorithm described in Chapter 3 and evolutionary spectrum which will be described in this chapter. The proposed algorithm provides the signal representation along with its time-varying spectrum [41].

One very important advantage of this method over the other methods is that its ability to detect most dominant components of a complex signal without dealing with less important ones. Since most of the physiological signals are very complex, direct time-frequency representations exhibit simultaneous, wide range changes in multiple frequency elements producing smeared time-frequency representations. Our method can be applied directly to relatively simple signals. But for complex signals, the method allows us to extract the most important components and obtain time-frequency representation of those components.

4.1 Orthonormal Expansion of the Partitioned Signal

Let us assume that we have a non-stationary signal $x(n)$ and it is already partitioned into I overlapping segments $\{x_j(n)\}$ by using the segmentation method introduced in the previous chapter. Then $x(n)$ can be written as

$$x(n) = \sum_{i=0}^{I-1} x_i(n) \tag{4-1}$$

If $x_i(n)$ is represented as a linear combination of some basis functions $u_{il}(n)$, i.e.,

$$x_i(n) = \sum_{l=0}^{l_i-1} c_{il} u_{il}(n) \tag{4-2}$$

then Equation (4-1) becomes

$$x(n) = \sum_{i=0}^{I-1} \sum_{l=0}^{l_i-1} c_{il} u_{il}(n) \qquad 0 \leq n \leq N-1 \tag{4-3}$$

where c_{il} are uncorrelated random KL expansion coefficients, $u_{il}(n)$ are the basis functions, and l_i corresponds to the length of the ith segment. Equation (4-3) is a time varying Karhunen-Loeve expansion since basis functions $u_{il}(n)$ are derived from different basis functions in each segment.

The functions $\{u_{il}(n)\}$ are the product of $\{\tilde{\phi}_{il}(n)\}$ (which are the extension of some orthonormal functions $\{\phi_{il}(n)\}$ defined on the ith time interval $(a_i, a_{i+1}])$ and a smooth window $\mathrm{w}_i(n)$ shown in the Figure 1. Properties of the window are given in the previous chapter. Orthonormal basis functions $\{\phi_{il}(n)\}$ are the KL basis functions of the signal $x_i(n)$ defined on $n \in (a_i, a_{i+1}]$. If we pad zeros to $\{\phi_{il}(n)\}$ when $n \notin (a_i, a_{i+1}]$, it is obvious that $\{\phi_{il}(n)\}$ $i \in \mathbf{Z}, 0 \leq l \leq l_i - 1$ form orthonormal bases. $\mathbf{Z}$ corresponds to integer numbers. However, since there are no overlaps between adjacent time intervals $(a_i, a_{i+1}]$, a blocking effect may occur in signal reconstructions [46]. Lapped orthogonal transform is used[53–56] to eliminate these blocking effect. The basic idea is to allow overlaps between adjacent time intervals. A method has been introduced by Xia [57] to extend basis functions. Extension is done by constructing the even reflection at a_i on $[a_i - \varepsilon_i, a_i]$ and the odd reflection at a_{i+1} on $[a_{i+1}, a_{i+1} + \varepsilon_{i+1}]$ in the following way

$$\tilde{\phi}_{il}(n) = \begin{cases} 0 & -\infty < n \leq a_i - \varepsilon_i & \text{(4-4a)} \\ \phi_{il}(2a_i - n + 1) & a_i - \varepsilon_i < n \leq a_i & \text{(4-4b)} \\ \phi_{il}(n) & a_i < n \leq a_{i+1} & \text{(4-4c)} \\ -\phi_{il}(2a_{i+1} - n + 1) & a_{i+1} < n \leq a_{i+1} + \varepsilon_{i+1} & \text{(4-4d)} \\ 0 & a_{i+1} + \varepsilon_{i+1} < n \leq \infty & \text{(4-4e)} \end{cases}$$

Then, $u_{il}(n)$ is formed as

$$u_{il}(n) \equiv \mathrm{w}_i(n)\tilde{\phi}_{il}(n) \qquad i \in \mathbf{Z}, 0 \leq l \leq l_i - 1 \tag{4-5}$$

The window $\mathrm{w}(n)$ is a Malvar window and shown in Figure 1. Because arbitrary partitioning of a signal introduces artifacts at the boundaries, here we consider techniques to eliminate these blocking effects and achieve an accurate signal representation. Malvar windows are used to remove

the blocking effects caused by non-overlapping adjacent time intervals in the signal reconstruction. The Malvar window is given by

$$\mathrm{w}_j(n) = \begin{cases} \mathrm{w}(\dfrac{n-a_j}{\varepsilon_j}) & n \in [a_j - \varepsilon_j, a_j + \epsilon_j] \quad \text{(4-6a)} \\ 1 & n \in [a_j + \varepsilon_j, a_{j+1} + \varepsilon_{j+1}] \quad \text{(4-6b)} \\ \mathrm{w}(\dfrac{a_{j+1}-n}{\varepsilon_{j+1}}) & n \in [a_{j+1} - \varepsilon_{j+1}, a_{j+1} + \varepsilon_{j+1}] \quad \text{(4-6c)} \\ 0 & n \in (\infty, a_j - \varepsilon_j] \bigcup [a_{j+1} + \varepsilon_{j+1}, \infty) \quad \text{(4-6d)} \end{cases}$$

where $\mathrm{w}(n) = \sin(\frac{\pi}{4}(1 + \sin(\frac{\pi n}{2})))$ and it has the following properties [46, 53–55]:

1. $0 \leq \mathrm{w}_j(n) \leq 1 \qquad$ for all $n \in \mathbf{Z}$
2. $\mathrm{w}_j(n) = 1 \qquad n \in (a_j + \varepsilon_j, a_{j+1} - \varepsilon_{j+1}]$
3. $\mathrm{w}_j(n) = 0 \qquad n \notin (a_j - \varepsilon_j, a_{j+1} + \varepsilon_{j+1}]$
4. $\mathrm{w}_j(a_j + \tau) = \mathrm{w}_{j-1}(a_j - \tau + 1) \qquad \tau \in (-\varepsilon_j, \varepsilon_j]$
5. $\mathrm{w}_j^2(n) + \mathrm{w}_{j-1}^2(n) = 1 \qquad n \in (a_j - \varepsilon_j, a_j + \varepsilon_j]$

where $\mathbf{Z}$ corresponds to the integer numbers. The fourth condition permits adjacent windows to have symmetric overlaps at a_j for any j. Furthermore, 1-3 and 5 result in $\sum_j \mathrm{w}_j^2(n) = 1$ for all n.

Expansion coefficients c_{il} are obtained as follows. If we compare Equation (4-1) and (4-3), we can write that

$$x_i(n) = \sum_{l=0}^{l_i - 1} c_{il} u_{il}(n) \tag{4-7}$$

The last equation in matrix form can be given by

$$x_i = U_i c_i \tag{4-8}$$

where

$$x_i = \begin{bmatrix} x_i(0) \\ x_i(1) \\ \vdots \\ x_i(N-1) \end{bmatrix} \tag{4-9}$$

and

$$U_i = \begin{bmatrix} u_{i0}(0) & u_{i1}(0) & \dots & u_{i(l_i-1)}(0) \\ u_{i0}(1) & u_{i1}(1) & \dots & u_{i(l_i-1)}(0) \\ \vdots & \vdots & \ddots & \vdots \\ u_{i0}(N-1) & u_{i1}(N-1) & \dots & u_{i(l_i-1)}(N-1) \end{bmatrix} \tag{4-10}$$

and

$$c_i = \begin{bmatrix} c_{i0} \\ c_{i1} \\ \vdots \\ c_{i(l_i-1)} \end{bmatrix} \tag{4-11}$$

Since basis functions $\{u_{il}(n)\}$ are orthonormal (see Appendix), we have

$$U_i^T U_i = I \tag{4-12}$$

where T stands for transpose. Then, multiplying both sides of Equation (4-8) by U_i^T, we get

$$c_i = U_i^T x_i \tag{4-13}$$

The last equation is given in open form as

$$c_{il} = \sum_{n=0}^{N-1} x_i(n) u_{il}(n) \qquad i \in \mathbf{Z}, 0 \leq l \leq l_i - 1 \tag{4-14}$$

Since $\{u_{il}(n)\}$ is zero when $n \notin (a_i - \varepsilon_i, a_{i+1} + \varepsilon_{i+1}]$, the last equation can also be given by

$$\begin{aligned} c_{il} &= \sum_{n=0}^{N-1} x(n) u_{il}(n) \\ &= \sum_{n=a_i-\varepsilon_i+1}^{a_{i+1}+\varepsilon_{i+1}} x(n) u_{il}(n) \end{aligned} \tag{4-15}$$

4.2 Time-Frequency Representation of the Partitioned Signal

Contrary to other orthogonal representations, where the basis functions are fixed and ordered such as Fourier or discrete cosine transformation, the basis functions used in our representation are not fixed and ordered according to their frequency content. They do not have a standard form

and are signal dependent. For example, the first basis function does not necessarily correspond to the lowest frequencies present in the signal. The basis functions in a KL expansion are ordered according to their corresponding eigenvalues. As a result, the expansion coefficients c_{jl} do not carry any information about frequency. But if basis functions are represented by Fourier bases, one can obtain the coefficients giving the frequency information we need.

Let us represent $\{\tilde{\phi}_{il}(n)\}$ in terms of exponentials

$$\tilde{\phi}_{il}(n) = \sum_{k=0}^{N-1} d_{il}(k) e^{j\omega_k n} \tag{4-16}$$

where $\omega_k = \frac{2\pi k}{N}$. By substituting the last equation in Equation (4-5), we get

$$u_{il}(n) = \mathrm{w}_i(n) \sum_{k=0}^{N-1} d_{il}(k) e^{jw_k n} \tag{4-17}$$

Then replacing $u_{il}(n)$ in Equation (4-3) results in the following representation of $x(n)$

$$\begin{aligned} x(n) &= \sum_{i=0}^{I-1} \sum_{l=0}^{l_i-1} c_{il} \mathrm{w}_i(n) \sum_{k=0}^{N-1} d_{il}(k) e^{jw_k n} \\ &= \sum_{k=0}^{N-1} \left\{ \sum_{i=0}^{I-1} \sum_{l=0}^{l_i-1} c_{il} \mathrm{w}_i(n) d_{il}(k) \right\} e^{jw_k n} \end{aligned} \tag{4-18}$$

Equation (4-18) is similar to the Wold-Cramer representation[19]. According to the Wold-Cramer representation , a non-stationary signal $x(n)$ can be expressed as

$$x(n) = \int_{-\pi}^{\pi} A(n,\omega) e^{j\omega n} dZ(\omega) \tag{4-19}$$

$Z(\omega)$ is an orthogonal process with $E\{dZ(\omega\} = 0 \ \forall\omega$ and

$$E\{dZ(\omega_1) dZ(\omega_2)\} = \frac{1}{2\pi} \delta(\omega_1 - \omega_2) d\omega_1 d\omega_2$$

where E is the expected value operator. The evolutionary spectrum is then defined as

$$S(n,\omega) = |A(n,\omega)|^2 \tag{4-20}$$

For a non-stationary deterministic signal an analogous Wold-Cramer representation of $x(n)$ is possible and can be given in its discrete form as

$$x(n) = \sum_{k=0}^{K} X(n,k) e^{j\omega_k n} \tag{4-21}$$

A discrete evolutionary transformation (DET) is obtained by expressing the kernel $X(n,k)$ directly from the signal [58]. In the next section, we will show how orthonormal extension of partitioned signal can be used to obtain the kernel. The evolutionary spectrum is then defined in terms of the kernel. Unlike STFT, the windows turn out to be dependent on time and frequency and the KL bases functions. We will give the definition of the DET which uses sinusoidal basis.

Then, in the discrete frequency case shown in Equation (4-18), the time-frequency kernel can be defined as

$$X(n,k) = \sum_{i=0}^{I-1} \sum_{l=0}^{l_i-1} c_{il} \mathrm{w}_i(n) d_{il}(k) \tag{4-22}$$

Thus, the evolutionary spectrum of $x(n)$ will be given as

$$S(n,k) = |X(n,k)|^2 \tag{4-23}$$

where n corresponds to time and k corresponds to frequency.

The method takes advantage of the local characteristics of the KL bases and uses partitioning to find an optimal representation of the signal. The proposed method has better time and frequency resolution compared to spectrogram and Choi-Williams distribution as demonstrated by the examples at the end of this chapter. Furthermore it does not suffer from cross terms as Wigner and Choi-Williams distributions do.

4.3 Sinusoidal DET

In this case, we wish to associate the sinusoidal representation in Equation (4-21) with an inverse discrete form that provides the evolutionary kernel $X(n,k)$ in terms of signal, more specifically in a form such as

$$X(n,k) = \sum_{m=0}^{N-1} x(m) \mathrm{W}_m(n,k) e^{-j\omega_k m} \tag{4-24}$$

where $\mathrm{W}_m(n,k)$ is in general a time and frequency dependent window. The sinusoidal DET and its inverse will then be given by Equation (4-21)and (4-24). The evolutionary spectrum will then be

defined as

$$S(n,k) = |X(n,k)|^2 \tag{4-25}$$

The DET is a generalization of the STFT and $S(n,k)$ is a generalization of the spectrogram. Equation (4-24) corresponds to the STFT of $x(n)$ when window $\mathrm{W}_m(n,k)$ is a function of m.

4.4 KL Based Sinusoidal DET

Let $x(n)$ can be represented as

$$x(n) = \sum_{i=0}^{I-1} x_i(n) \tag{4-26}$$

The discrete evolutionary transform (DET) $X(n,k)$ can be derived from the KL representation of the segmented signal $x_i(n)$ given by

$$x_i(n) = \sum_{l=0}^{l_i-1} c_{il} u_{il}(n) \tag{4-27}$$

Replacing Equation (4-5) in the last equation gives

$$x_i(n) = \sum_{l=0}^{l_i-1} c_{il} \mathrm{w}_i(n) \tilde{\phi}_{il}(n) \tag{4-28}$$

Then, replacing Equation (4-16) in Equation (4-28) results in

$$\begin{aligned} x_i(n) &= \sum_{l=0}^{l_i-1} c_{il} \mathrm{w}_i(n) \sum_{k=0}^{N-1} d_{il}(k) e^{j\omega_k n} \\ &= \sum_{k=0}^{N-1} \sum_{l=0}^{l_i-1} c_{il} \mathrm{w}_i(n) d_{il}(k) e^{j\omega_k n} \end{aligned} \tag{4-29}$$

By replacing the coefficients (Equation (4-15)) in the last equation, we obtain the segmented signal representation from the whole signal

$$\begin{aligned} x_i(n) &= \sum_{k=0}^{N-1} \sum_{l=0}^{l_i-1} \sum_{m=0}^{N-1} x(m) u_{il}(m) \mathrm{w}_i(n) d_{il}(k) e^{j\omega_k n} \\ &= \sum_{k=0}^{N-1} \left[\sum_{m=0}^{N-1} x(m) \mathrm{W}_m^i(n,k) e^{-j\omega_k m} \right] e^{j\omega_k n} \end{aligned} \tag{4-30}$$

where window $\mathrm{W}_m^i(n,k)$ is defined as

$$\mathrm{W}_m^i(n,k) = \sum_{l=0}^{l_i-1} u_{il}(m)\mathrm{w}_i(n)d_{il}(k)e^{j\omega_k m} \tag{4-31}$$

Comparing Equation (4-30) with Equation (4-21) yields the evolutionary kernel $X_i(n,k)$ of $x_i(n)$ as

$$X_i(n,k) = \sum_{m=0}^{N-1} x(m)\mathrm{W}_m^i(n,k)e^{-j\omega_k m} \tag{4-32}$$

The KL based discrete evolutionary transform $X(n,k)$ of $x(n)$ is then given by

$$\begin{aligned} X(n,k) &= \sum_{i=0}^{I-1} X_i(n,k) \\ &= \sum_{m=0}^{N-1} x(m) \sum_{i=0}^{I-1} \mathrm{W}_m^i(n,k)e^{-j\omega_k m} \end{aligned} \tag{4-33}$$

Then defining $\mathrm{W}_m(n,k) = \sum_{i=0}^{I-1} \mathrm{W}_m^i(n,k)$, we have

$$X(n,k) = \sum_{m=0}^{N-1} x(m)\mathrm{W}_m(n,k)e^{-j\omega_k m} \tag{4-34}$$

Then, evolutionary spectrum is given by

$$S(n,k) = |X(n,k)|^2 \tag{4-35}$$

The evolutionary kernel $X(n,k)$ is a generalization of the STFT with a window $\mathrm{W}_m(n,k)$ varying in time and frequency. If the window has the property that $\sum_k \mathrm{W}_m(n,k)e^{j\omega_k(n-m)} = \delta(n-m)$, the original signal can be recovered as

$$\begin{aligned} \sum_k X(n,k)e^{j\omega_k n} &= \sum_k \left[\sum_{m=0}^{N-1} x(m)\mathrm{W}_m(n,k)e^{-j\omega_k m}\right] e^{j\omega_k n} \\ &= \sum_{m=0}^{N-1} x(m) \sum_k \mathrm{W}_m(n,k)e^{j\omega_k(n-m)} \\ &= \sum_{m=0}^{N-1} x(m)\delta(n-m) \\ &= x(n) \end{aligned} \tag{4-36}$$

Once the windows $\{\mathrm{W}_m(n,k)\}$ are obtained and satisfy the above condition, the DET and its inverse are obtained as

$$X(n,k) = \sum_{m=0}^{N-1} x(m)\mathrm{W}_m(n,k)e^{-j\omega_k m} \tag{4-37}$$

$$x(n) = \sum_k X(n,k)e^{j\omega_k n} \tag{4-38}$$

4.5 Properties of The Evolutionary Spectrum

4.5.1 Energy

According to Parseval's theorem, the energy of a signal is the same whether it is calculated in time domain or in the frequency domain. We need to show that $S(n,k)$ is an energy density. Energy of the signal is given by

$$\sum_{n=0}^{N-1} |x(n)|^2 = \sum_{n=0}^{N-1} x(n)x^*(n) \tag{4-39}$$

Replacing Equation (4-3) in the last equation we get

$$\begin{aligned}
\sum_{n=0}^{N-1} |x(n)|^2 &= \sum_{n=0}^{N-1}\sum_{l=0}^{l_i-1}\sum_{i=0}^{I-1} c_{il}u_{il}(n) \sum_{p=0}^{l_i-1}\sum_{r=0}^{I-1} c_{pr}^* u_{pr}^*(n) \\
&= \sum_{l=0}^{l_i-1}\sum_{i=0}^{I-1} c_{il} \sum_{p=0}^{l_i-1}\sum_{r=0}^{I-1} c_{pr}^* \sum_{n=0}^{N-1} u_{il}(n)u_{pr}^*(n) \\
&= \sum_{l=0}^{l_i-1}\sum_{i=0}^{I-1} c_{il} \sum_{p=0}^{l_i-1}\sum_{r=0}^{I-1} c_{pr}^* \delta_{iplr} \\
&= \sum_{l=0}^{l_i-1}\sum_{i=0}^{I-1} |c_{il}|^2
\end{aligned} \tag{4-40}$$

Energy can also obtained from $S(n,k)$, i.e.,

$$\begin{aligned}
\sum_n\sum_k S(n,k) &= \sum_n\sum_k |x(n,k)|^2 \\
&= \sum_n\sum_k \sum_{m=0}^{N-1} x(m)\mathrm{W}_m(n,k)e^{-j\omega_k m} \sum_{p=0}^{N-1} x^*(p)\mathrm{W}_p^*(n,k)e^{j\omega_k p} \\
&= \sum_{m=0}^{N-1} x(m) \sum_{p=0}^{N-1} x^*(p) \sum_n\sum_k \mathrm{W}_m(n,k)\mathrm{W}_p^*(n,k)e^{j\omega_k(p-m)}
\end{aligned} \tag{4-41}$$

If

$$\mathrm{W}_m(n,k)\mathrm{W}_p^*(n,k)e^{j\omega_k(p-m)} = \delta(p-m) \qquad 0 \le m,p \le N-1 \tag{4-42}$$

we have that

$$\sum_n \sum_k S(n,k) = \sum_{n=0}^{N-1} |x(n)|^2 \tag{4-43}$$

The energy is the same in both time and frequency domain.

4.5.2 Time Marginal

Time marginal is satisfied if $TM(n) = \sum_k S(n,k) = |x(n)|^2$. Similarly, by imposing a condition on windows, one can satisfy the time marginal.

$$\begin{aligned} TM(n) = &= \sum_k S(n,k) \\ &= \sum_k \sum_{m=0}^{N-1} x(m) \mathrm{W}_m(n,k) e^{-j\omega_k m} \sum_{p=0}^{N-1} x^*(p) \mathrm{W}_p^*(n,k) e^{j\omega_k p} \\ &= \sum_{m=0}^{N-1} x(m) \sum_{p=0}^{N-1} x^*(p) \sum_k \mathrm{W}_m(n,k) \mathrm{W}_p^*(n,k) e^{j\omega_k (p-m)} \end{aligned} \tag{4-44}$$

If $\sum_k \mathrm{W}_m(n,k)\mathrm{W}_p^*(n,k)e^{j\omega_k(p-m)} = \delta(m-p)\delta(m-n)$ for $0 \le m,n,p \le N-1$, then the time marginal will be satisfied.

4.5.3 Frequency Marginal

Frequency marginal of the evolutionary spectrum is satisfied if

$$|X(e^{jw_k})|^2 = \sum_n S(n,k) = FM(k) \tag{4-45}$$

where $X(e^{jw_k})$ is the discrete Fourier transform of $x(n)$.

Frequency marginal of the evolutionary spectrum can be calculated as

$$\begin{aligned} FM(k) &= \sum_{n=0}^{N-1} S(n,k) \\ &= \sum_{n=0}^{N-1} A(n,k) A^*(n,k) \\ &= \sum_{n=0}^{N-1} \sum_{m=0}^{N-1} x(m) \mathrm{W}_m(n,k) e^{-j\omega_k m} \sum_{p=0}^{N-1} x^*(p) \mathrm{W}_p^*(n,k) e^{j\omega_k p} \\ &= \sum_{m=0}^{N-1} x(m) e^{-j\omega_k m} \sum_{p=0}^{N-1} x^*(p) e^{j\omega_k p} \sum_{n=0}^{N-1} \mathrm{W}_m(n,k) \mathrm{W}_p^*(n,k) \end{aligned} \tag{4-46}$$

If $\sum_{n=0}^{N-1} \mathrm{W}_m(n,k)\mathrm{W}_p^*(n,k)$ in Equation (4-46) is equal to a constant for $0 \leq m, p \leq N-1$ then the frequency marginal is satisfied.

Example 1: The signal used in this example is given by

$$x = \begin{cases} \sin(.6\pi n) & 0 \leq n < 74 \\ \sin(.2\pi n) + \sin(.4\pi n) & 75 \leq n < 115 \\ \sin(.2\pi n) & 115 \leq n < 174 \end{cases}$$

and shown in Figure 10(a). Reconstructed signal and magnitude squared reconstruction error displayed in Figures 10(b) and (c). It is clear that we have a very small reconstruction error which exists between different segments. The error at the beginning and at the end of the signal also comes from using windows. Time-frequency representations of the signal using OPTR, spectrogram, Wigner-Ville and Choi-Williams ($\sigma = 1$) distribution are shown in Figures 11(a)-(d). It is clear from the figure that OPTR showed a better time frequency resolution compared to all other methods. Furthermore the sudden changes in the frequency of the signal detected clearly in OPTR while in the other representations it was blurred. OPTR and Spectrogram did not suffer from cross terms in contrast to Choi-Williams and Wigner distributions. Time and frequency marginals of the same signal obtained from OPTR are displayed in Figures 12 and 13. The length of the segmentation window is 16. 64-point Hanning window was used for spectrogram analysis. All representations are given in logarithmic scale.

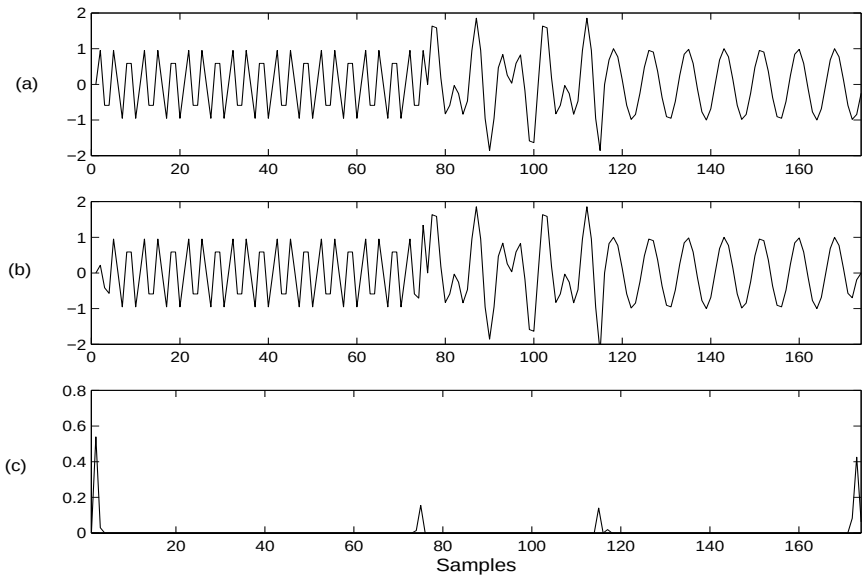

Figure 10 (a) Original signal (b) Reconstructed signal (c) Mean squared reconstruction error.

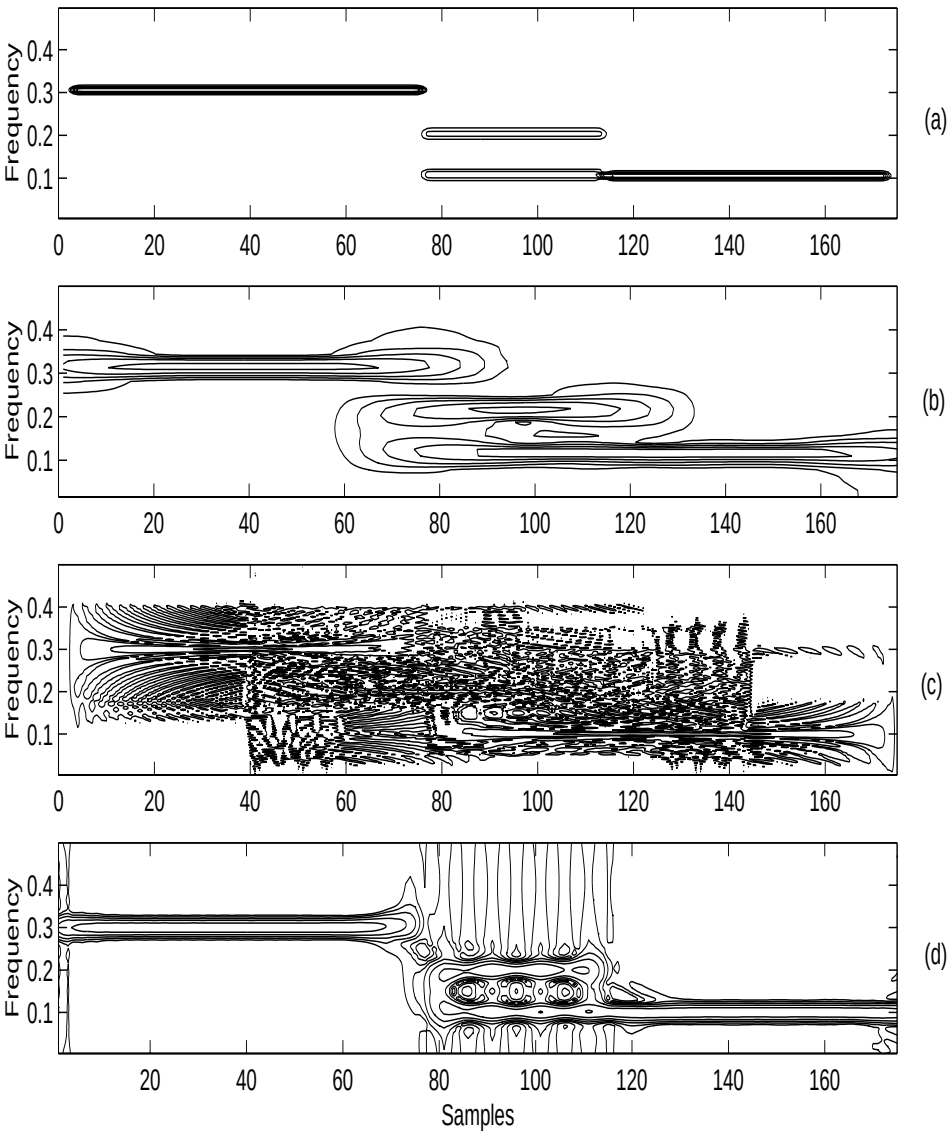

Figure 11 Power spectra of the simulated signal obtained using OPTR (segmentation window length L is 16 points) (a), Spectrogram using a 64-point Hanning window (b), the Wigner-Ville distribution (c) and the Choi-Williams distribution ($\sigma = 1$) (d). All power spectra are shown on a logarithmic scale.

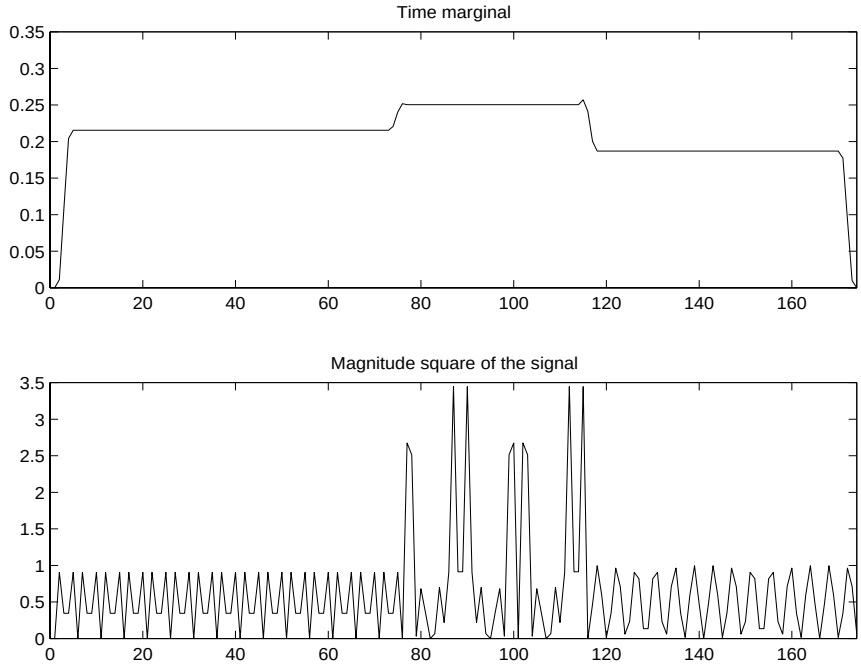

Figure 12 (a) Time-marginal (b) Magnitude square of x(n).

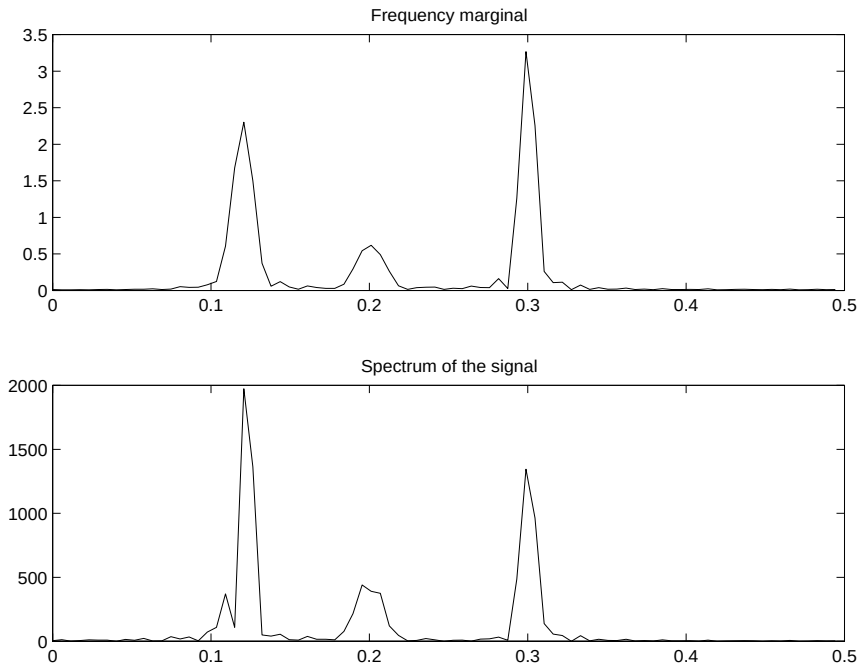

Figure 13 (a) Frequency marginal (b) Power spectrum of x(n).

Example 2: The OPTR is tested on a chirp signal in this example. The signal, reconstructed signal and reconstruction error are shown in Figures 14(a)-(c). Time-frequency representations of the signal using OPTR, spectrogram, Wigner-Ville and Choi-Williams ($\sigma = 1$) distribution are shown in Figures 15(a)-(d). Although OPTR was able to follow the changing frequencies in the signal correctly, it did put some artificial boundaries which was not the case with other methods. On the other hand resolution of OPTR was better than spectrograms and it did not suffer from the cross terms in contrast to Wigner-Ville and Choi-Williams distributions. Time and frequency marginals of OPTR are displayed in Figures 16 and 17. The length of the segmentation window is 16. A 32-point Hanning window was used for spectrogram analysis. All representations are given in logarithmic scale.

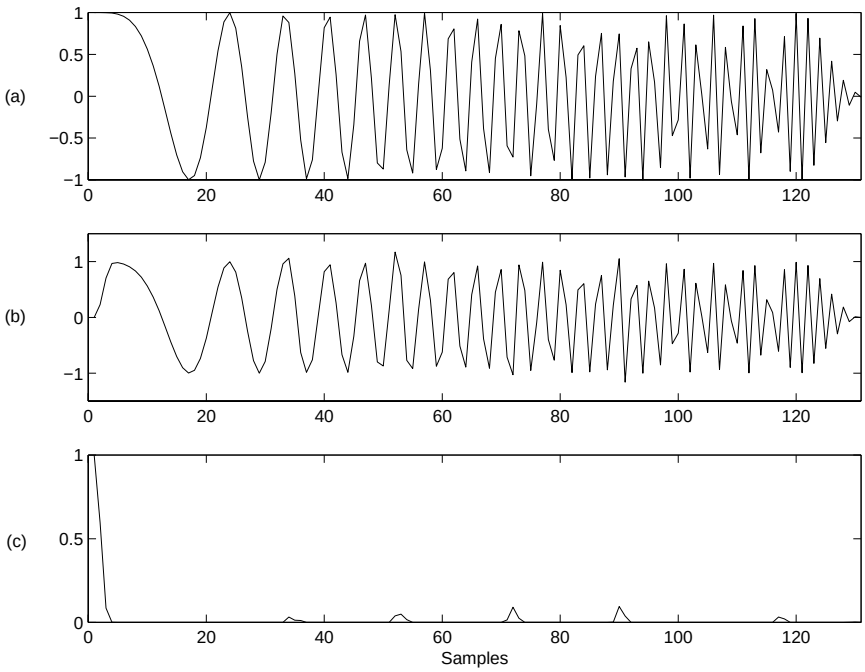

Figure 14 (a) Original signal (b) Reconstructed signal (c) Mean squared reconstruction error.

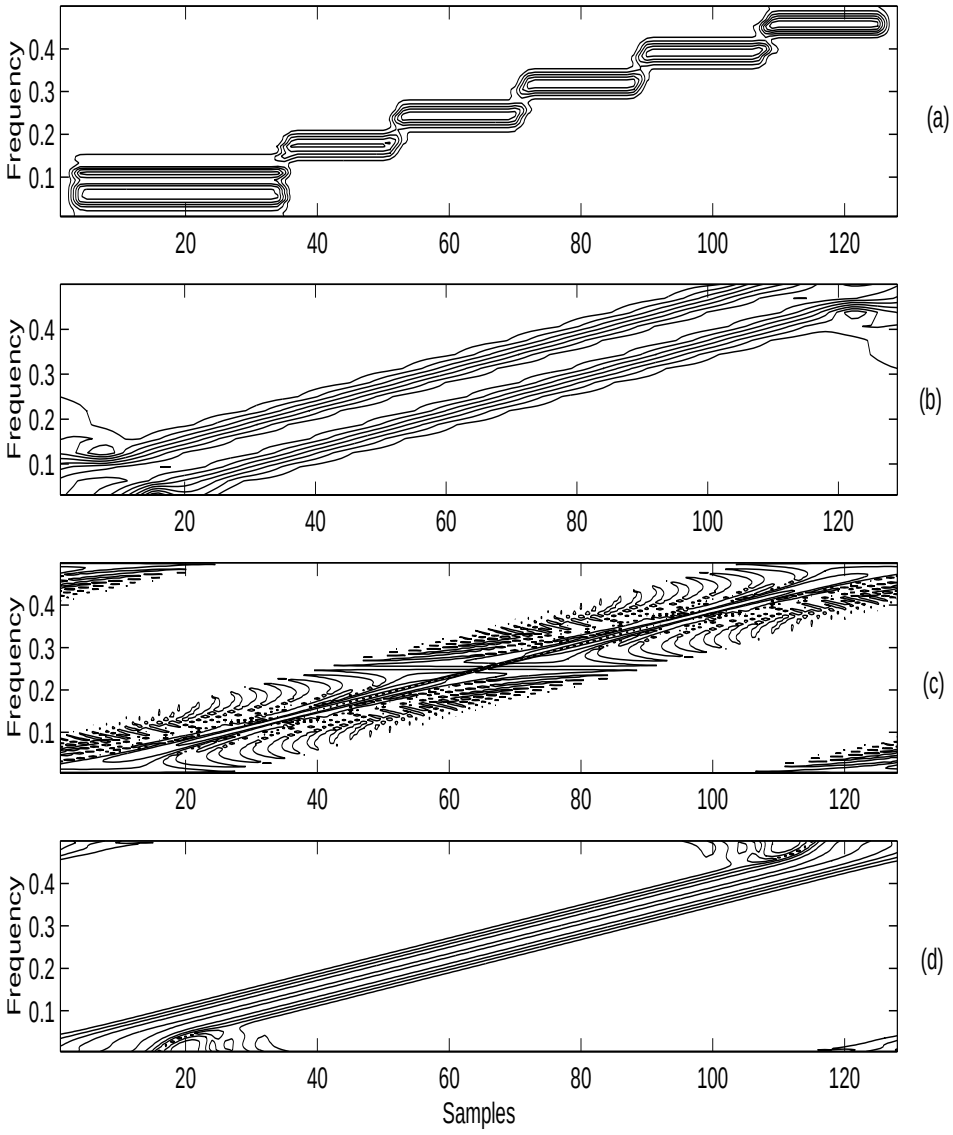

Figure 15 Power spectra of the chirp signal obtained using OPTR (segmentation window length L is 16 points) (a), Spectrogram using a 32-point Hanning window (b), the Wigner-Ville distribution (c) and the Choi-Williams distribution ($\sigma = 1$) (d). All power spectra are shown on a logarithmic scale.

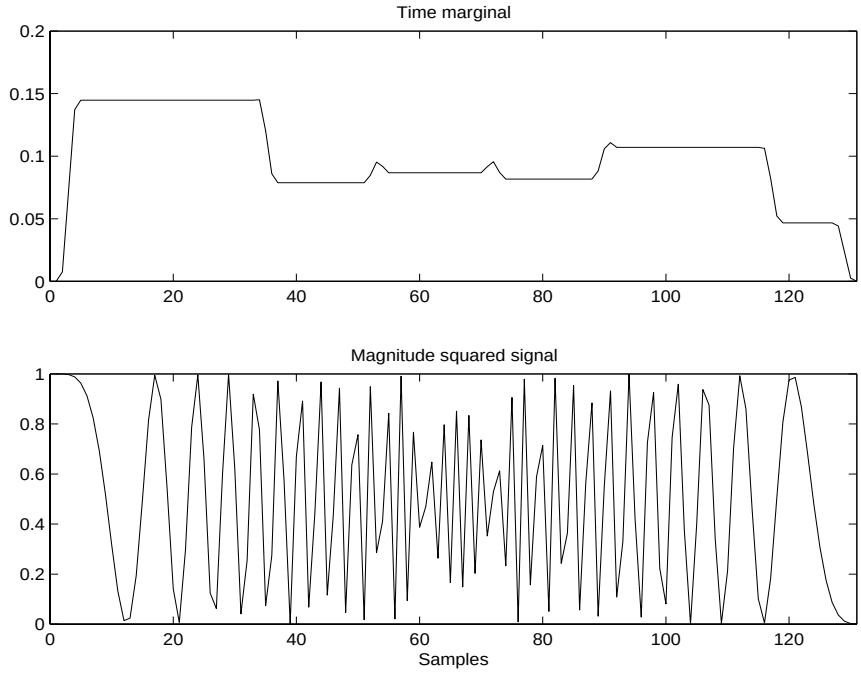

Figure 16 (a) Time-marginal (b) Magnitude square of x(n).

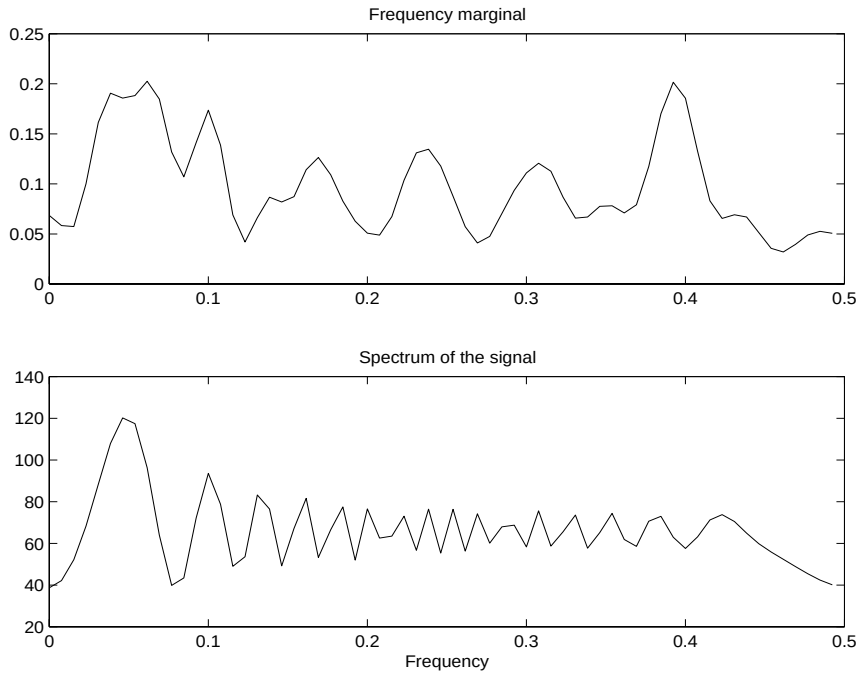

Figure 17 (a) Frequency marginal (b) Power spectrum of x(n).

Example 3: In this example the method is tested on a more complex signal comprised of sinusoidal and linear FM signals and sinusoids of different frequencies. The signal, reconstructed signal and reconstruction error are shown in Figures 18(a)-(c).The power spectrum obtained using OPTR (Figure 19(b)) is compared with the one obtained using spectrogram, Wigner-Ville and Choi-Williams distributions. (Figures 19(c)-(e)).

The time-frequency representation of this simulated signal is sufficiently clear obviating the need for time-frequency analysis of the most significant basis vectors. However, this "direct" time-frequency approach may not be effective when applied to the actual multicomponent physiological signals as will be shown later. OPTR has a higher time and frequency resolution than the spectrogram and Choi-Williams distribution. OPTR produces sharp inter-segment boundaries that coincide with the boundaries of the time segments, whereas in the other two methods, the boundaries between adjacent time segments are blurred. On the other hand, OPTR gives artificial boundaries for linear and sinusoidal FM signals which was not the case with other methods. The frequency resolution of OPTR reveals the sharp dominant frequency content of each time segment better than the other methods. Choi-Williams and Wigner-Ville distributions also suffered from cross terms in contrast to OPTR and spectrogram.

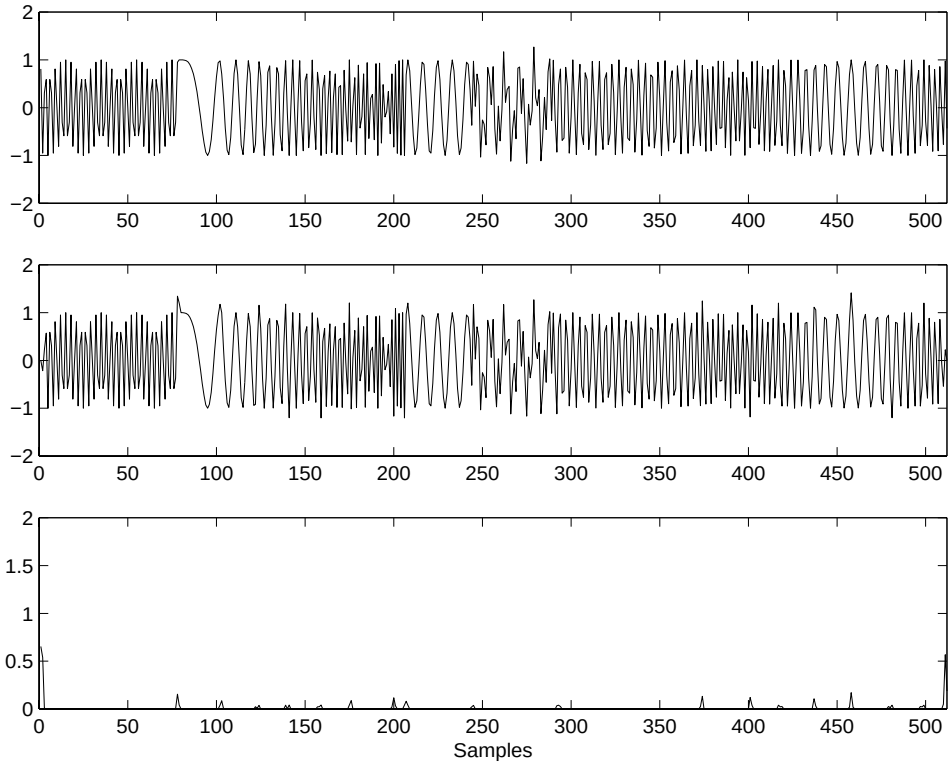

Figure 18 (a) Original signal (b) Reconstructed signal (c) Mean squared reconstruction error.

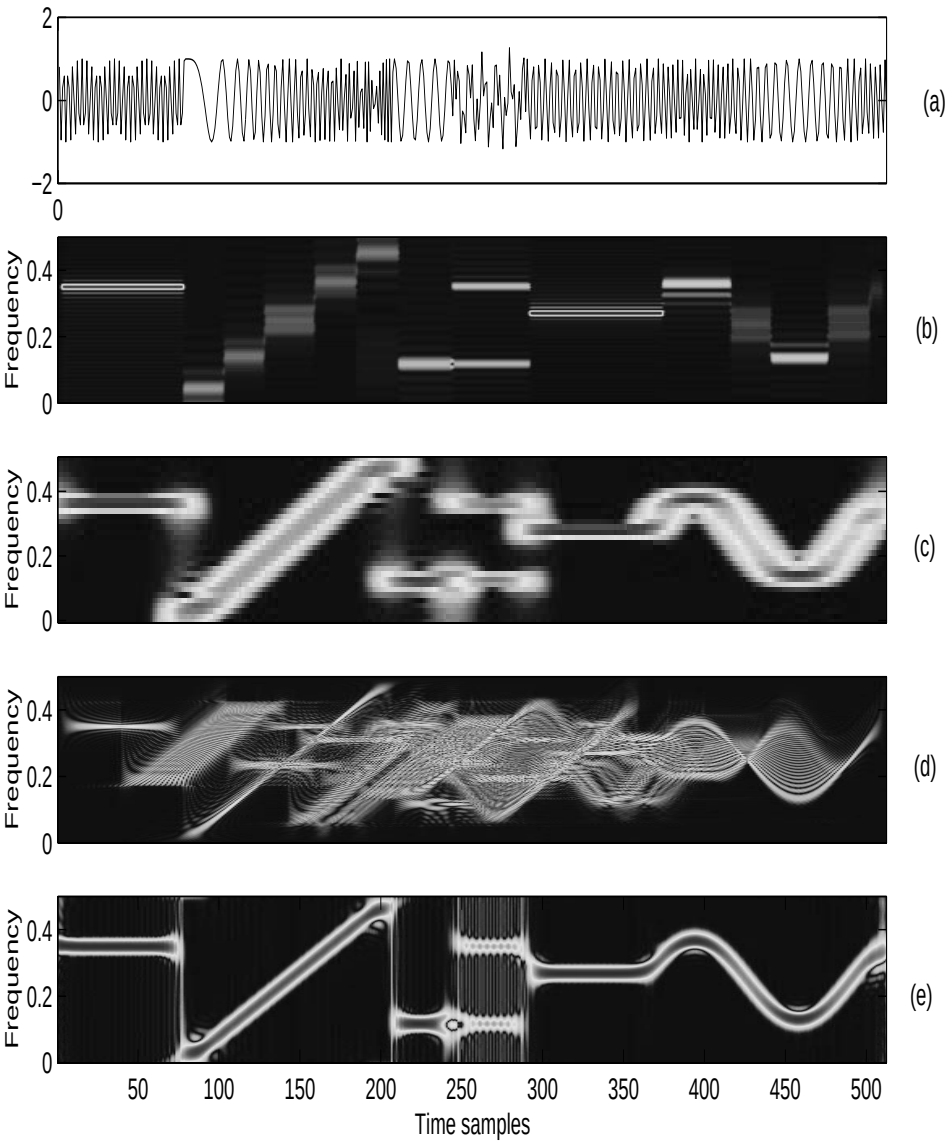

Figure 19 A simulated signal obtained by concatenating segments with different properties (a), and its power spectra obtained using OPTR (segmentation window length L is 30 points) (b), Spectrogram using a 64-point Hanning window (c), the Wigner-Ville distribution (d) and the Choi-Williams distribution ($\sigma = 1$) (e). All power spectra are shown on a logarithmic scale.

For relatively simple signals that exhibit few changes in a few frequency components, such as the simulated signals used in above examples, direct time-frequency representation without pre-processing is applied (i.e., the method is applied directly to the signal). However, for the complex signals, to avoid the smearing caused by direct time-frequency representation, pre-processing and exposure of the most significant features is required in each time segment. Although partitioning facilitates the analysis of the time-dependent variations in the structure of multicomponent signals, direct representation of signals that exhibit simultaneous, wide-range (complex) changes in multiple

frequency elements produces smeared time-frequency representations. This is usually the case with real signals. Therefore, getting a clear picture of changes in time-frequency plane for real signals is achieved by 1) extracting the most significant eigenvectors in each time segment, 2) representing each eigenvector in each time segment in the time-frequency plane (decomposed time-frequency representation), and 3) constructing the time series of the corresponding representations by concatenating all segments together. This will be illustrated in the next chapter.

5.0 APPLICATION TO HEART RATE VARIABILITY DATA

The relationship between autonomic nervous system and cardiovascular mortality caused the development of quantitative markers of the autonomic nervous system. Heart rate variability (HRV) became one of the most widely used indicators to describe variations of both instantaneous heart rate and RR intervals. An RR interval is shown in Figure 20 and it is described as the time distance between two consecutive heart beats. To describe oscillation in consecutive cardiac cycles, other terms such as cycle length variability, RR variability, heart period variability have been used in literature but none of them has been accepted as widely as HRV.

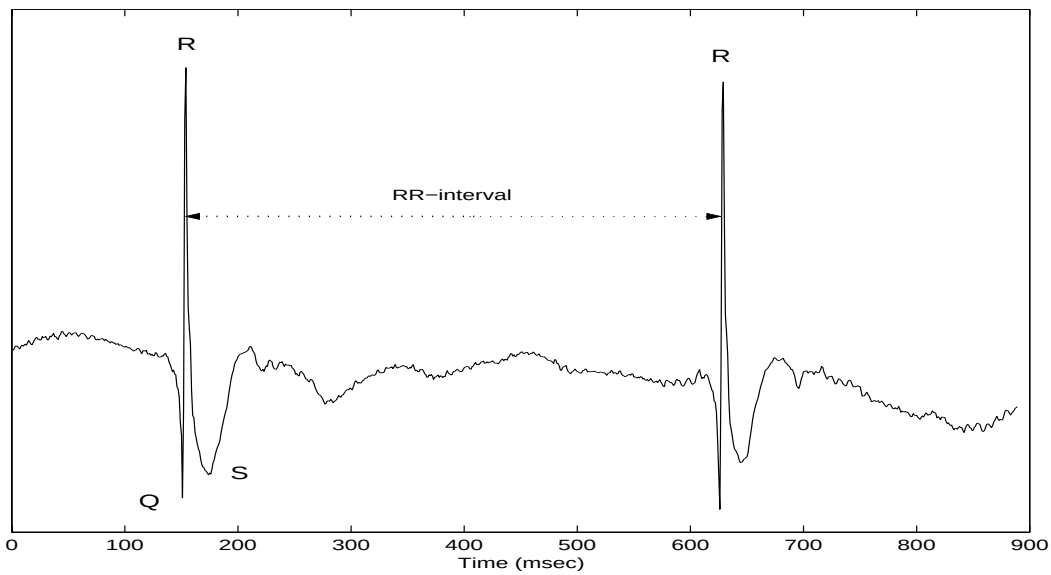

Figure 20 A typical ECG signal and RR-interval.

5.1 Extraction of HRV Data

HRV signals used here are obtained as follows: Electrocardiographic signals were recorded continuously using ambulatory (Holter) recorders. ECG data were digitized at 400 Hz, and QRS complexes were detected using a commercial scanning system and custom software, and verified by a cardiologist. The RR-intervals between normal QRS complexes were extracted, and a regularly spaced time series was sampled at 1 Hz using a boxcar low-pass filter [59]. Gaps in the time series

resulting from noise or ectopic beats were filled in with linear splines, which can cause a small reduction in high-frequency power but do not affect other components of the power spectrum.

5.2 Frequency Domain Analysis

Spectral analysis of HRV represents a major challenge because the structure of the signal includes multiple periodic, pseudo-periodic, and a-periodic components [42]. Frequency domain analysis contributed to the understanding of autonomic background of RR interval fluctuations [12]. Spectral analysis of HRV signals is a non-invasive method to study autonomic influences. In many cases, [59, 60] this analysis is carried out using standard Fourier analysis, which allows the decomposition of a signal into individual frequency components and establishes the relative intensity of each component. Alternatively, to provide average spectral estimates, long-term (24-hour or longer) recordings accumulating multiple cycles of the studied periodicities are used [61]. The power spectrum indicates what frequencies exist in the signal, and their intensity, but it does not reveal when these frequencies occur. In other words, the analysis is carried out assuming that the HRV signal is stationary. The HRV signal considered for such studies is typically in the range of a few minutes. However, there can be physiological phenomena such as physical stress, emotional stress and response to postural changes that can occur in this span of time [62] causing the statistics of the HRV signal to change. In such cases, the study of HRV signal density jointly in time and frequency is of great interest.

Time-frequency analysis of HRV signals has been performed with methods such as the spectrogram [63], the Wigner distribution [6] and the evolutionary periodogram [64]. While the time-frequency resolution of the spectrogram is badly affected by the windowing, the Wigner distribution cannot guarantee positivity of the estimates and shows cross terms. On the other hand, time-frequency analysis of multicomponent physiological signals such as cardiac rhythm is complicated by the presence of numerous overlapping frequency elements.

5.2.1 Physiological Experiments

The proposed method was tested on the heart rate variability (HRV) signals obtained in humans during physiological experiments and ambulatory conditions. Series of RR-intervals were separated into 15-min intervals, and a mean value in each interval was subtracted from the data. The starting window length was 60 sec for the short window and 120 sec for the long window. Threshold values are estimated as described in the boundary detection algorithm in Chapter 3 and α_1, α_2, α_3 were 1, .75, .75 respectively.

5.2.1.1 Controlled Respiration. HRV is modulated by respiration, and the HRV power spectrum exhibits a clear peak at the frequency of respiration [5]. Temporal variations in the frequency of breathing shift the location of the respiratory peak in HRV. Thus, respiration whose frequency is synchronized with external stimuli provides an "input" physiological signal with known time-frequency characteristics, and changes in HRV give the respective "output" signal whose time-frequency representation is being investigated. In our experiments, the frequency of respiration was controlled using computer-generated audio-signals. After 10 min of rest in a sitting position, the subjects were asked to breath synchronously with the sequence of audio-stimuli, whose frequency increased in 0.05 Hz increments from 0.015 to 0.4 Hz.

As shown in Figure 21, controlled respiration markedly changes the structure of the HRV signal. Using the variance of the most significant KL coefficients as the basis for a reliable and computationally efficient low-resolution partitioning, the onset and offset of the controlled respiration are readily identified. Figure 21(b) through 21(d) displays the first, second and third KL coefficients time series respectively. By selecting the section of the time series with low variance (section between two vertical lines in Figure 21) the segment corresponding to controlled respiration is determined. Next, the time-frequency representation obtained using OPTR (which includes the high-resolution partitioning), short-time Fourier transform, and evolutionary periodogram during the selected segment of

controlled respiration is shown in Figure 22. In these controlled conditions, the frequency content of the signal is relatively simple. Therefore, direct time-frequency representation of the raw signal and representations of the most significant eigenvectors would provide essentially the same information. This shows that the time-frequency representation of relatively simple physiological signals could be obtained directly and so that the time-frequency analysis of the basis vectors would be redundant.

OPTR accurately reproduced the incremental increase in the frequency of HRV, which followed the changes in the respiratory frequency. By contrast, STFT and EP representations required post processing (such as taking power of the spectrum) to reveal the dominant frequency content.

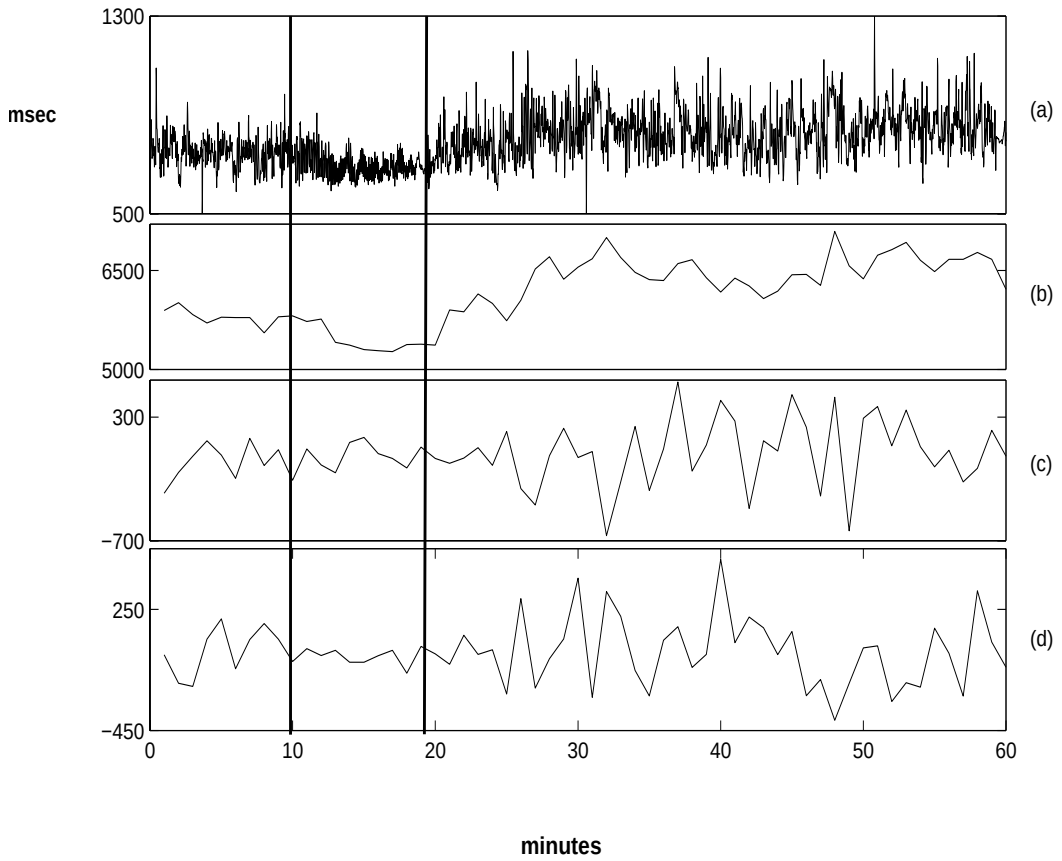

Figure 21 A representative example of a 1-hr long HRV signal (a), Time series of the first (b) the second (c) and the third (d) KL coefficients. The segment between two vertical lines represents a period of controlled respiration (see section 4.2.1 for details).

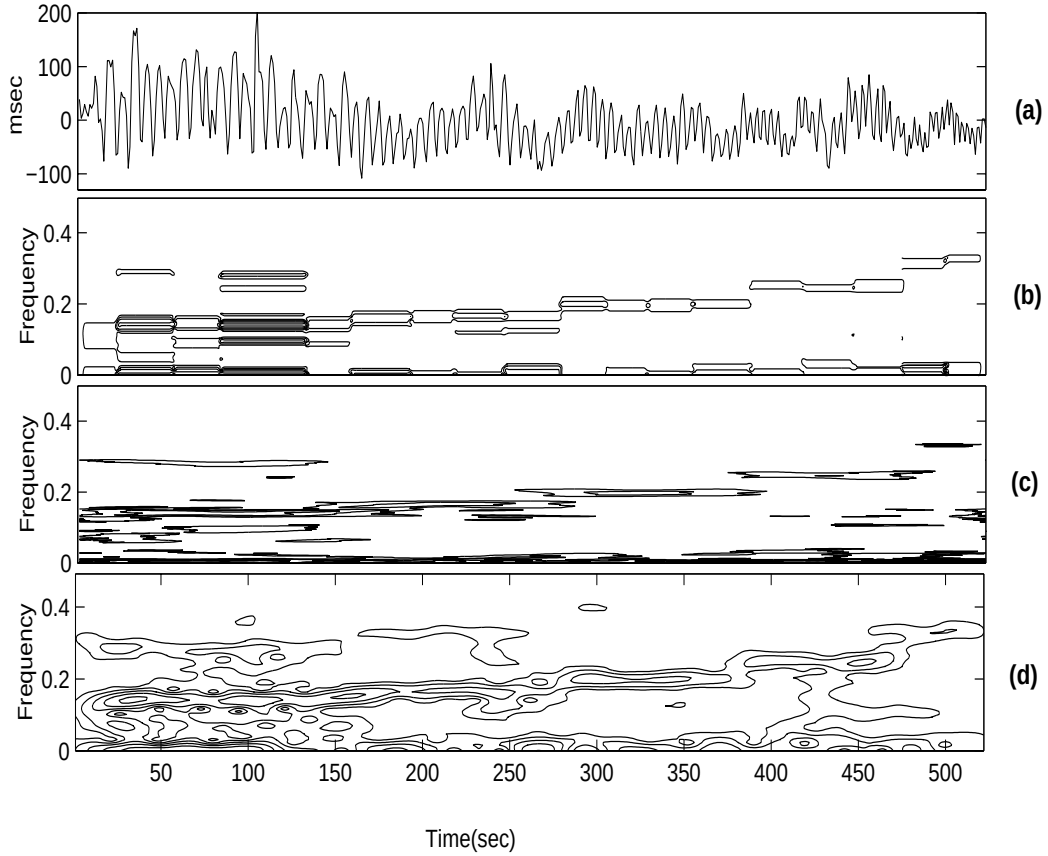

Figure 22 The HRV signal (mean was subtracted) that corresponds to the selected segment of controlled respiration (a), and its time-frequency representation obtained using OPTR (b), EP (c), and STFT (d).

5.2.1.2 Valsalva Maneuver. After sitting quietly for 10 min, subjects were asked to blow against pneumatic resistance during 30 sec, while maintaining a predetermined pressure [65]. Changes in the venous return to the heart and the stroke volume lead to changes in autonomic nervous system activity reflected in the modifications of cardiac rhythm. Initial short-time HR decrease is usually followed by a HR increase reflecting an increase in sympathetic activity [65]. Changes in the autonomic nervous system activity also produce changes in the spectral energy distribution during the test [63].

In agreement with previous reports [63], changes in the cardiac rhythm during Valsalva maneuver included several stages. A short period of faster, sympathetically mediated HR response was followed by a longer period of slower HR (Figure 23(a)). Changes in the frequency content of the signal were also similar to the previous observations by Pola et al [63]. An initial increase in the low frequency

power was followed by an increase in the higher frequency power, and then again by an increase in the low frequency power. These distinct spectral energy variations were clearly exposed by OPTR but blurred by the other studied time-frequency representations (Figure 23(b)-(d)).

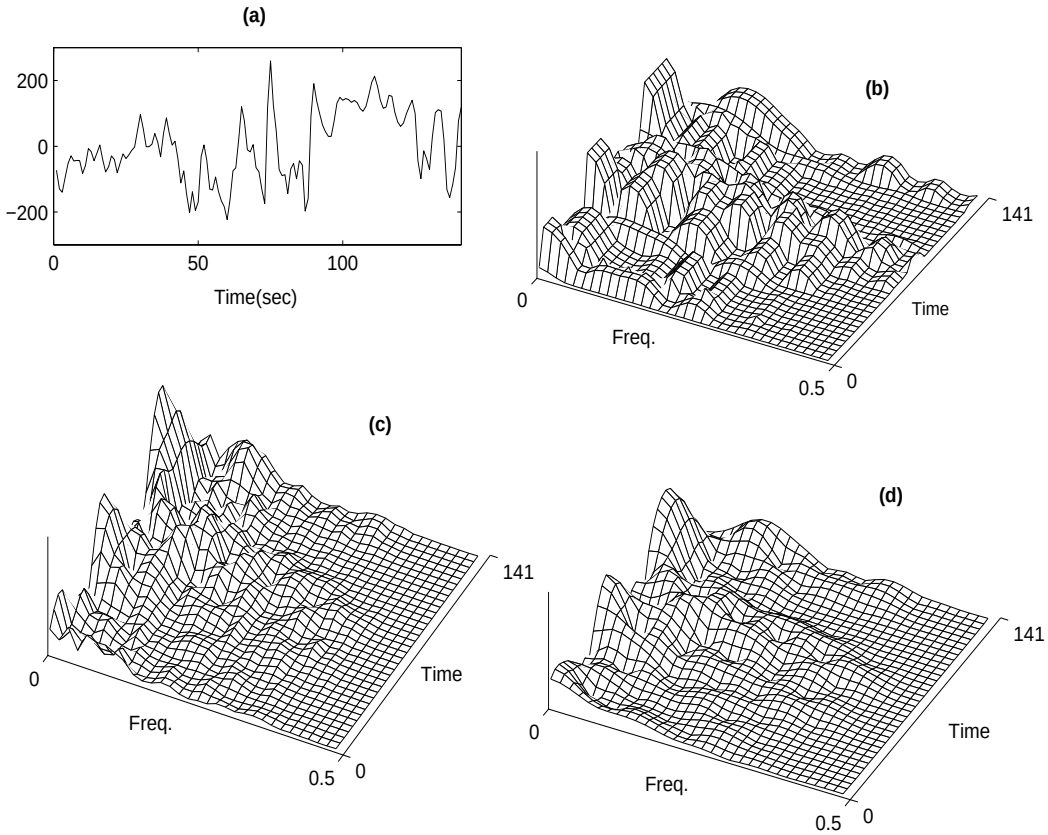

Figure 23 An example of the HRV signal obtained during Valsalva maneuver (a), and its time-frequency representations obtained using OPTR (b),EP (c), and STFT (d).

5.2.1.3 <u>Headup Tilt</u>. Fast change from supine to vertical body position causes an increase in blood volume below the diaphragm and a decrease in the blood flow in the organs above the level of the heart [5]. Because steady blood flow is critical for normal brain functioning, changes in body position cause an immediate increase in the sympathetic nervous system activity, which maintains normal level of blood flow to the brain by contracting peripheral blood vessels and increasing cardiac output. A typical response to headup tilt includes an increase in heart rate and a decrease in the high frequency spectral power of HRV.

The experiment consisted of 3 phases, baseline in a supine position during 10 min, passive,

headup 70 tilt during approximately 45 min followed by 10-min rest in a supine position. The protocol was approved by the Institutional Review Board of the University of Pittsburgh. Each subject was asked to sign an informed consent prior to the study. OPTR was applied to the HRV signals obtained from 34 subjects undergoing headup tilt. The subjects were divided into asymptomatic (Group 1: 20 subjects, age: 50.1±19.5 years, 9 male) and symptomatic (Group 2: 14 subjects, age: 45.1±20.4 years, 4 male). The symptoms included dizziness, lightheadedness, nausea and vomiting. None of the subjects had structural heart disease.

Note, that due to the multicomponent structure of this signal, a direct time-frequency representation is obscured and difficult to comprehend (Figure 24 (c),(d),(e)). For such signals, the time-frequency representation of the most significant basis vectors provides effective filtering of the information from the least significant eigenvectors to reveal the dominant changes in the signal properties (Figure 25).

To analyze the differences in the time-varying energy distributions between the two groups, we used the low-order conditional time-frequency moments, which effectively compress the information by tracking the changes in important physical properties of the signal. Energy distribution is compared by looking at the frequency band where most of the energy (70% of the total energy) is concentrated. Frequency band is estimated at each time in time-frequency plane before, during and after the tilt. Then taking the average of all frequency bands, we came up with a single number before, during and after tilt for every single subject. Then the frequency band is compared between two groups using nonparametric Mann-Whitney U-test.

At the beginning of the tilt, RR-intervals decrease in most patients and remain short until return to the supine position (Figure 24(a)). In asymptomatic patients (Figures 25-31, right column), the spectral energy is stable during the tilt and concentrated near 0.1 Hz, the frequency of the sympathetically modulated vasomotor tone. It has long been known that efficient adjustment to the vertical body position is accompanied by an increase in vascular activity [5]. However, due to

the multicomponent structure of the HRV signal, it has been difficult to detect the above-described pattern of the energy concentration without applying OPTR to the basis vectors. OPTR has also showed that symptomatic subjects had unstable and widely spread energy distribution (Figure 25-31, left column).

The frequency band where most of the energy is concantrated is compared in symptomatic and asymptomatic subjects for the five most significant basis vectors. Frequency band was smaller for asymptomatic patients compared to symptomatic ones for all eigenvectors (Figure 32).

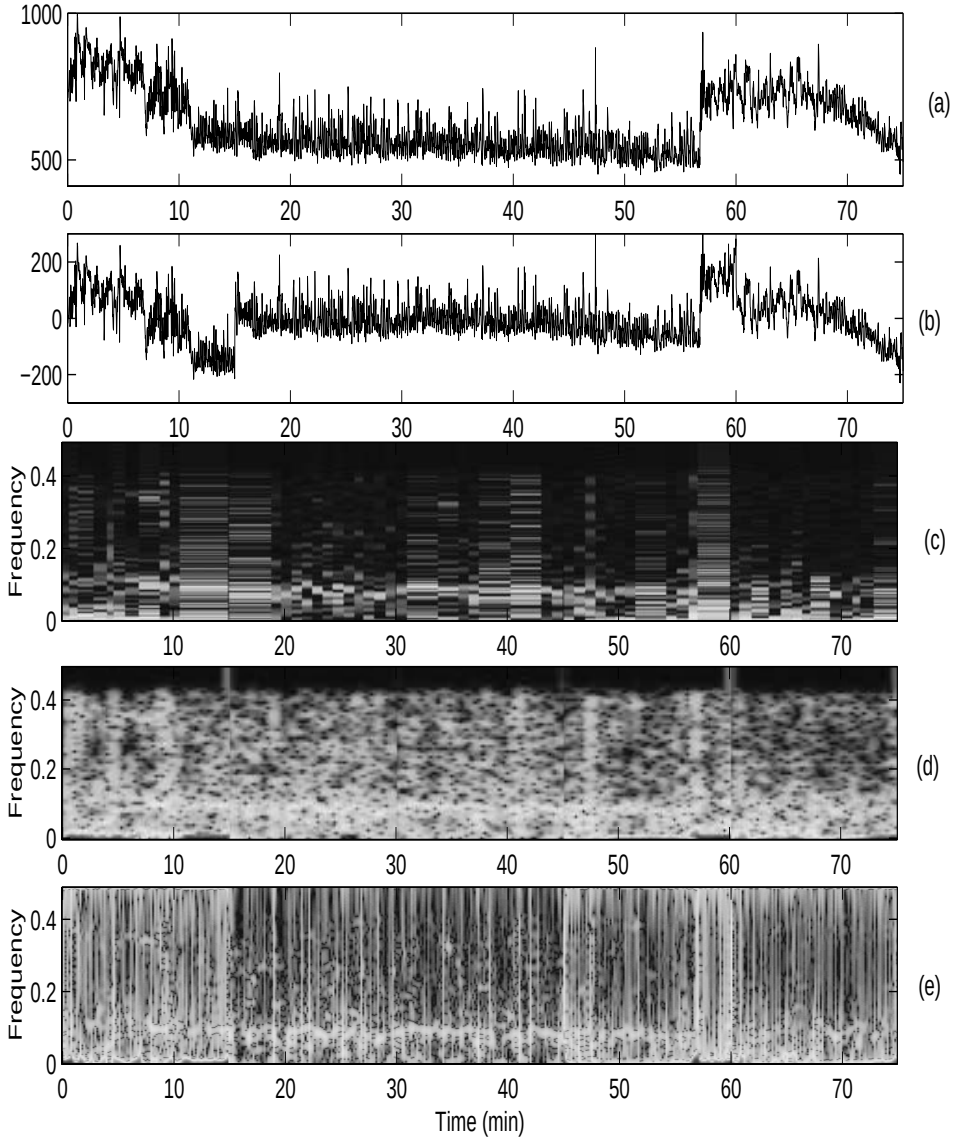

Figure 24 A representative example of the HRV signal obtained from asymptomatic subject during head up tilt (a), mean subtracted signal (mean is subtracted in each 15-min interval) (b), time-frequency representations of mean subtracted signal obtained using OPTR (c), Spectrogram using a 128-point Hanning window (d)), the Choi-Williams distribution ($\sigma = 1$) (e).

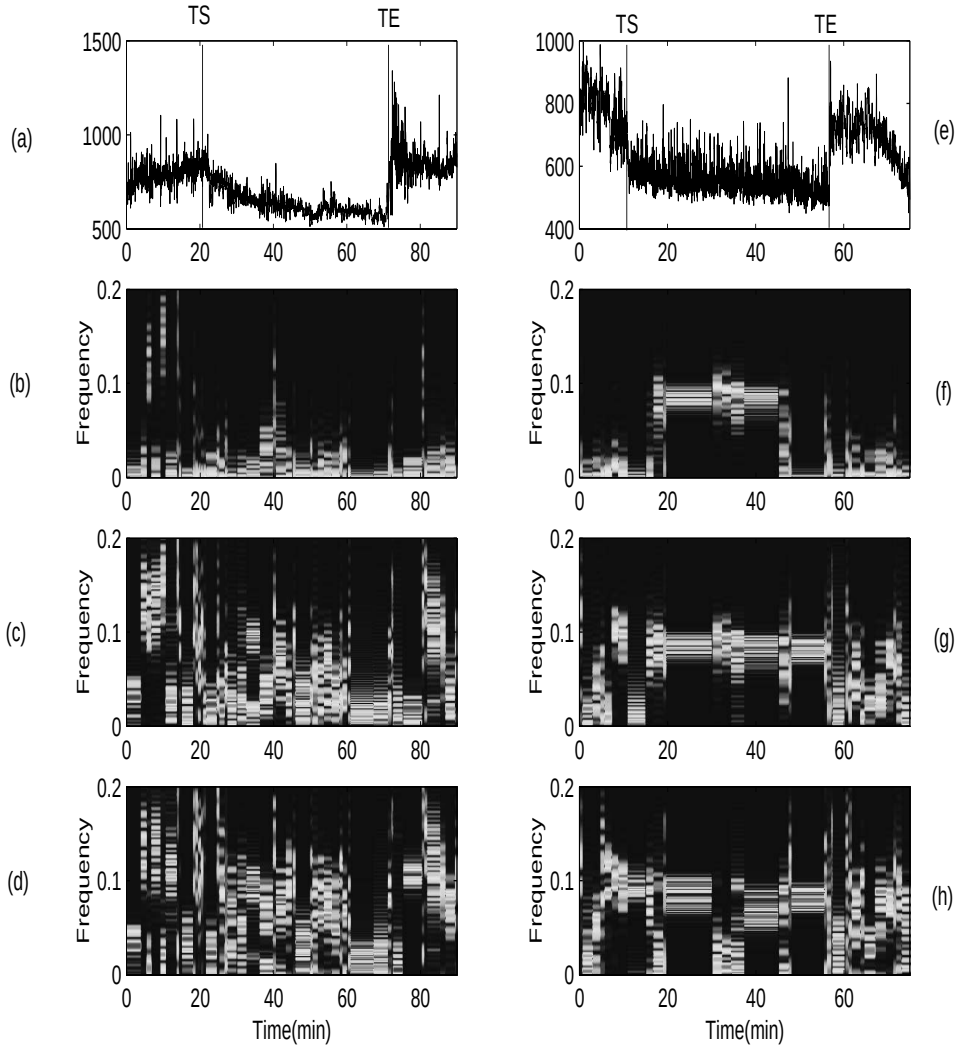

Figure 25 Time-frequency representations of the HRV basis vectors during head-up tilt in a symptomatic subjects (left column) and an asymptomatic subjects (right column).TS stands for tilt start and TE stands for tilt end.

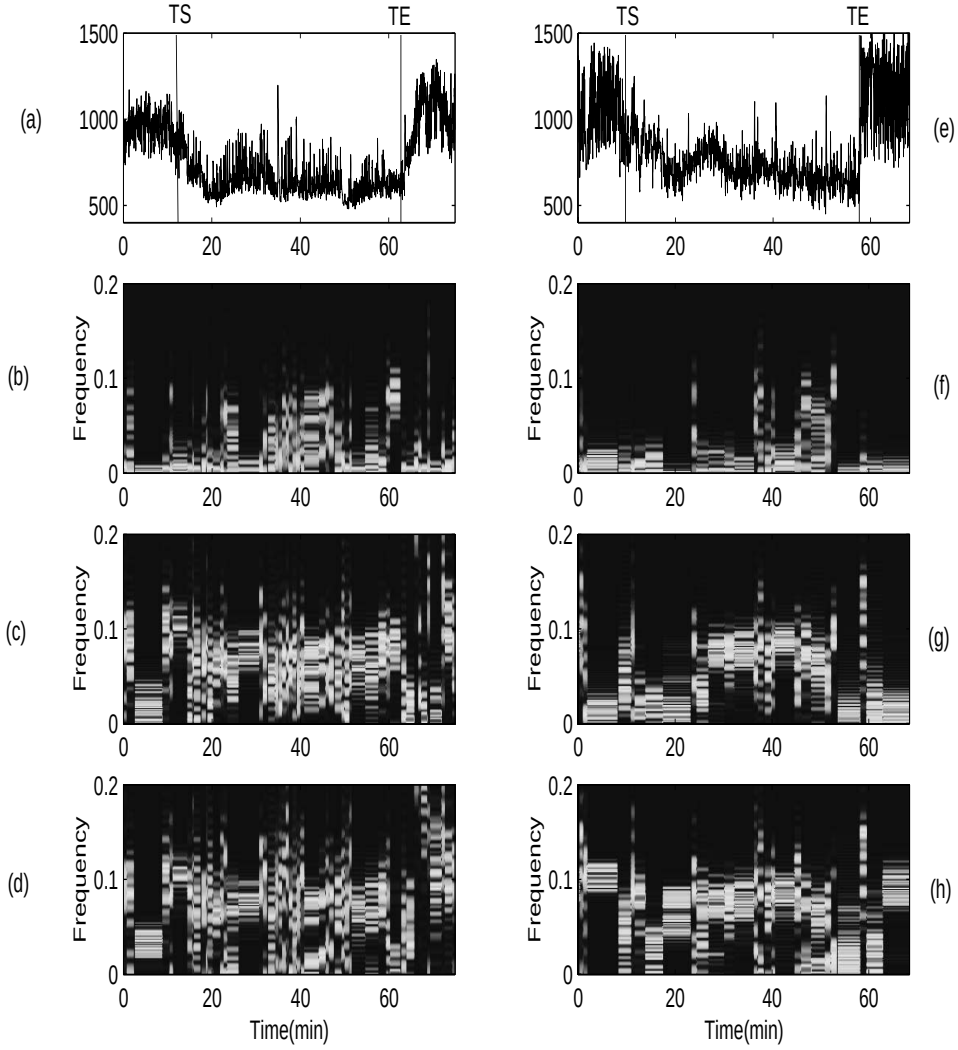

Figure 26 Time-frequency representations of the HRV basis vectors during head-up tilt in a symptomatic subjects (left column) and an asymptomatic subjects (right column).TS stands for tilt start and TE stands for tilt end.

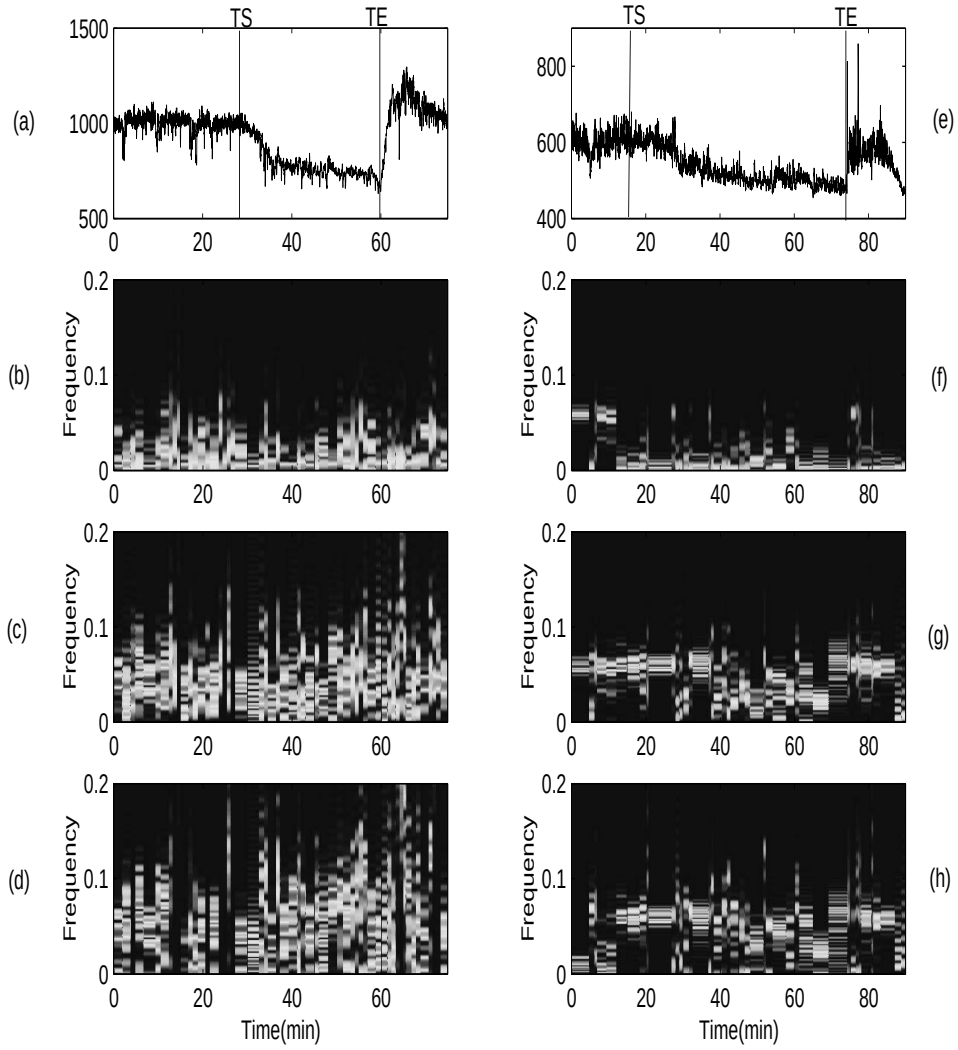

Figure 27 Time-frequency representations of the HRV basis vectors during head-up tilt in a symptomatic subjects (left column) and an asymptomatic subjects (right column).TS stands for tilt start and TE stands for tilt end.

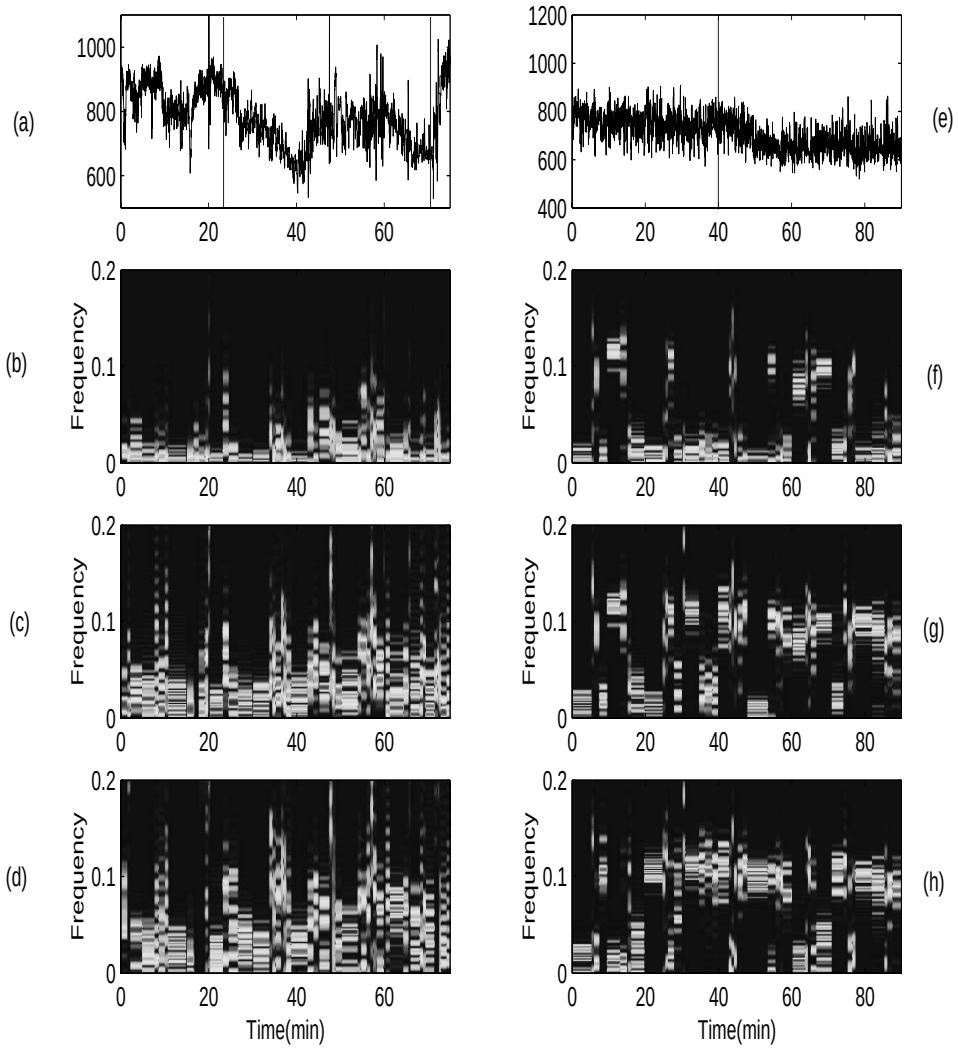

Figure 28 Time-frequency representations of the HRV basis vectors during head-up tilt in a symptomatic subjects (left column) and an asymptomatic subjects (right column).TS stands for tilt start and TE stands for tilt end.

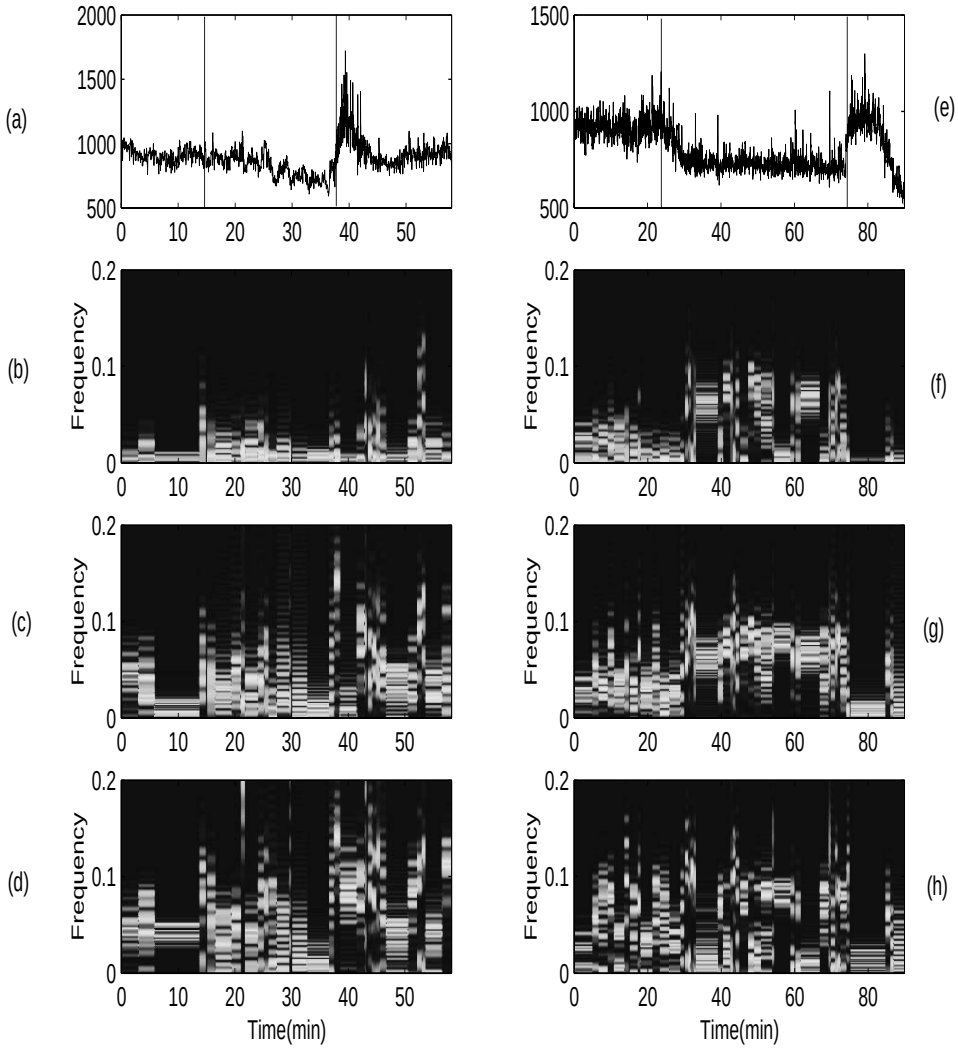

Figure 29 Time-frequency representations of the HRV basis vectors during head-up tilt in a symptomatic subjects (left column) and an asymptomatic subjects (right column).TS stands for tilt start and TE stands for tilt end.

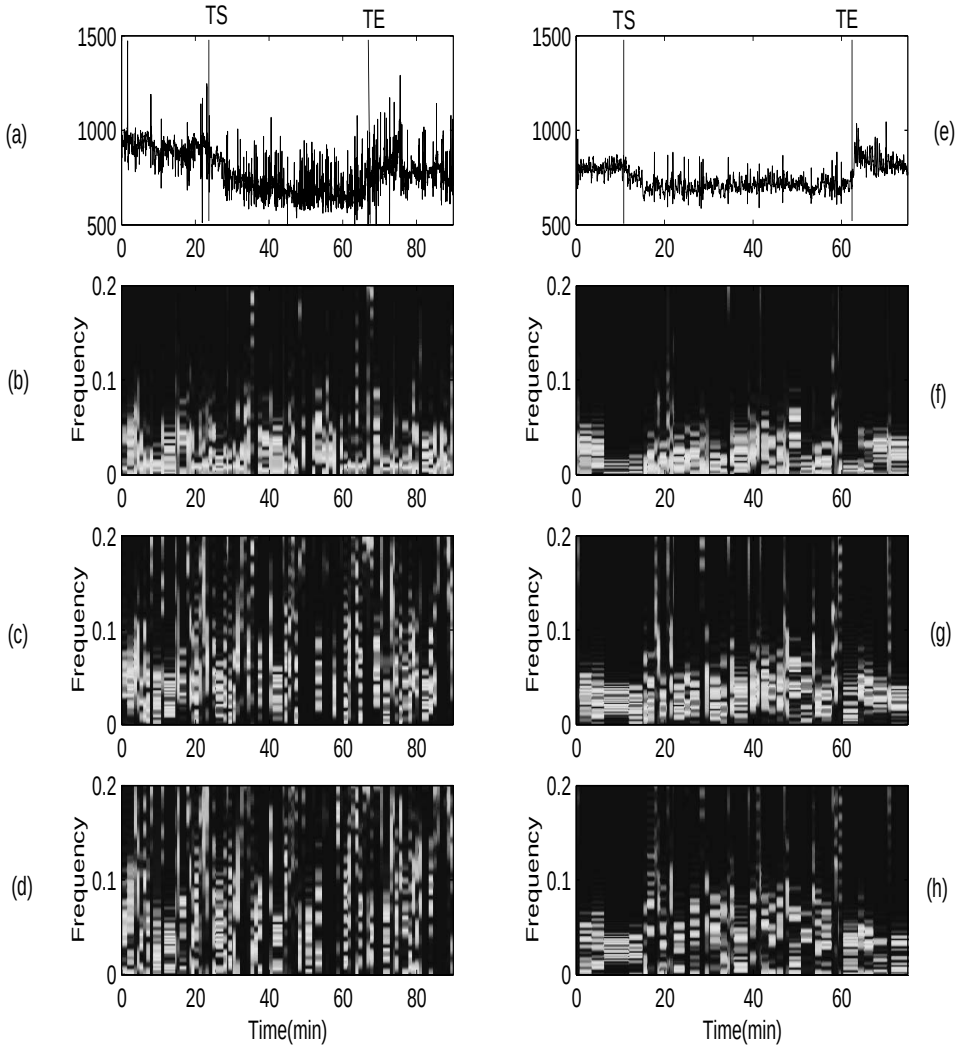

Figure 30 Time-frequency representations of the HRV basis vectors during head-up tilt in a symptomatic subjects (left column) and an asymptomatic subjects (right column).TS stands for tilt start and TE stands for tilt end.

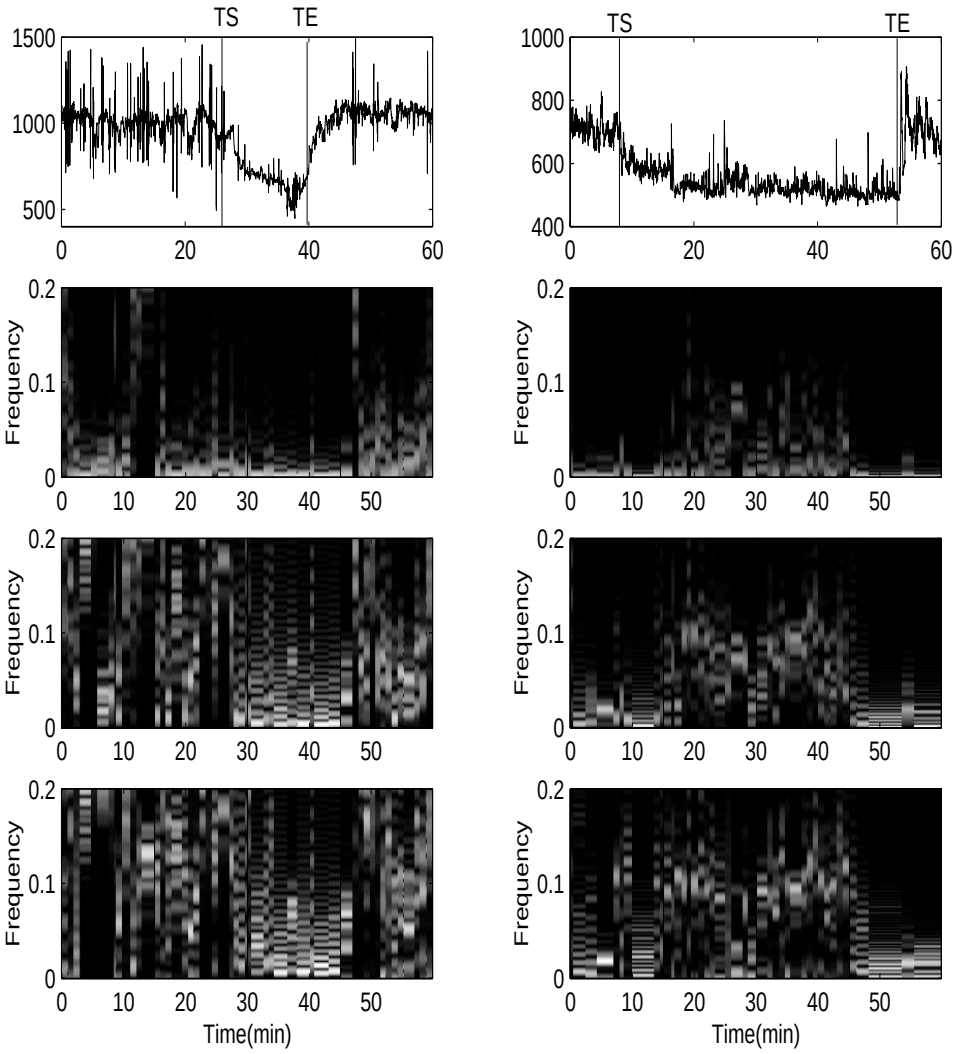

Figure 31 Time-frequency representations of the HRV basis vectors during head-up tilt in a symptomatic subjects (left column) and an asymptomatic subjects (right column).TS stands for tilt start and TE stands for tilt end.

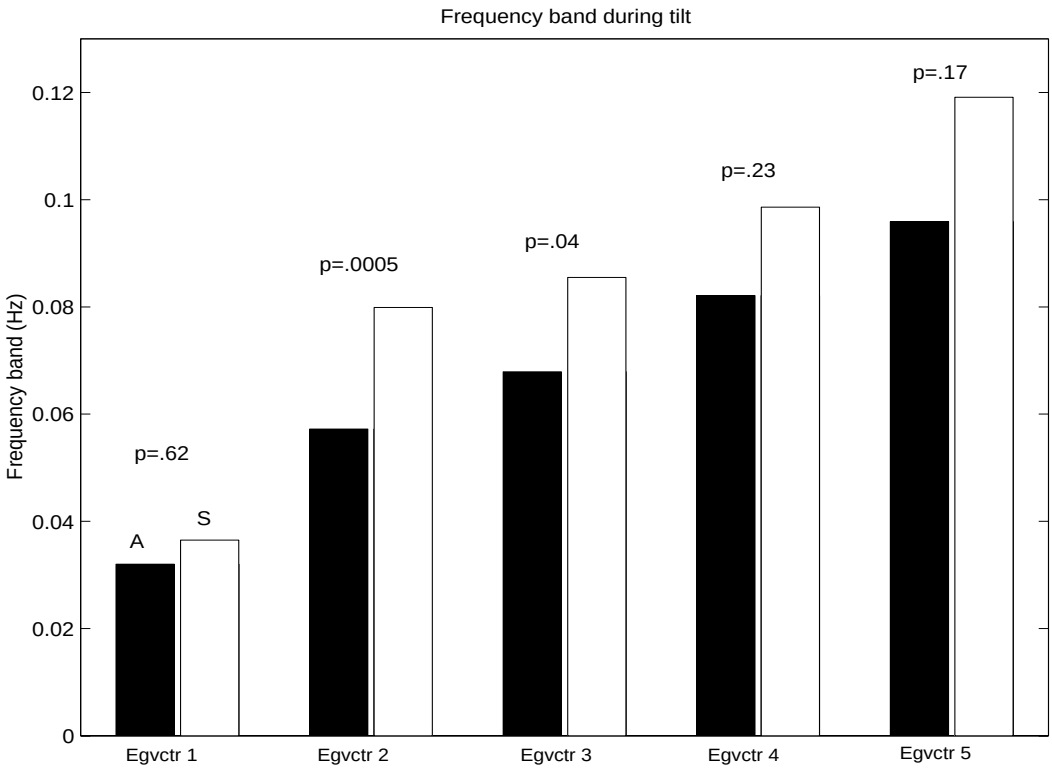

Figure 32 Frequency bands obtained from OPTR of five eigenvectors during tilt for symptomatic and asymptomatic subjects. p numbers were obtained using Mann-Whitney U test. ($p < .05$ indicates the significant differences between groups).

Since the tilt data is relatively long (approximately 1.5 hour) estimation of the T-F representation by using OPTR takes some time. To make the process faster we suggest another way of analyzing the tilt data. In here, we first perform low resolution partitioning on tilt data then we select segments of the tilt data according to low resolution partitioning. By doing so we reduce the amount of data dramatically. Now instead of performing OPTR on the whole tilt data, we only perform on the section of the data which is selected with the help of low resolution partitioning. This kind of an application is illustrated in the following two examples. Please note that this is just an illustration of using low resolution partitioning and OPTR together to reduce the computational cost.

Figure 33(a) shows the tilt data of an asymptomatic subject. Figures 33(a)-(b) correspond to global KL coefficient time series of the same data. As we can see the standard deviation(SD) of the coefficients increase around 130 sample indicating a change in the structure of the tilt data. Actually

the time of the increase in SD of coefficients correspond to approximate time of tilt ending and start of the supine position. Then we selected two 5 min intervals of the tilt data before and after that time. Since signal structure changed at that time, choosing short intervals of the data before and after the change and performing OPTR on those intervals can give us an idea of how the signal properties changed. Selected short intervals and their corresponding T-F representations are shown in Figures 34(b)-(e). It is clear from the Figures 34(c) and (e) that signal energy concentrated in a small frequency band in prior short interval. On the other hand, signal energy was spread wide in time-frequency plane in posterior short interval.

We performed the same procedure in another tilt data shown in Figure 35(a). This time the data came from a symptomatic subject. Similarly to previous example, KL coefficients indicated the approximate time of tilt ending. In this case the energy of signals in both short intervals did not differ much (Figures 36(c),(e))indicating that contrary to asymptomatic patients, symptomatic patients may not react to changes in the body position appropriately.

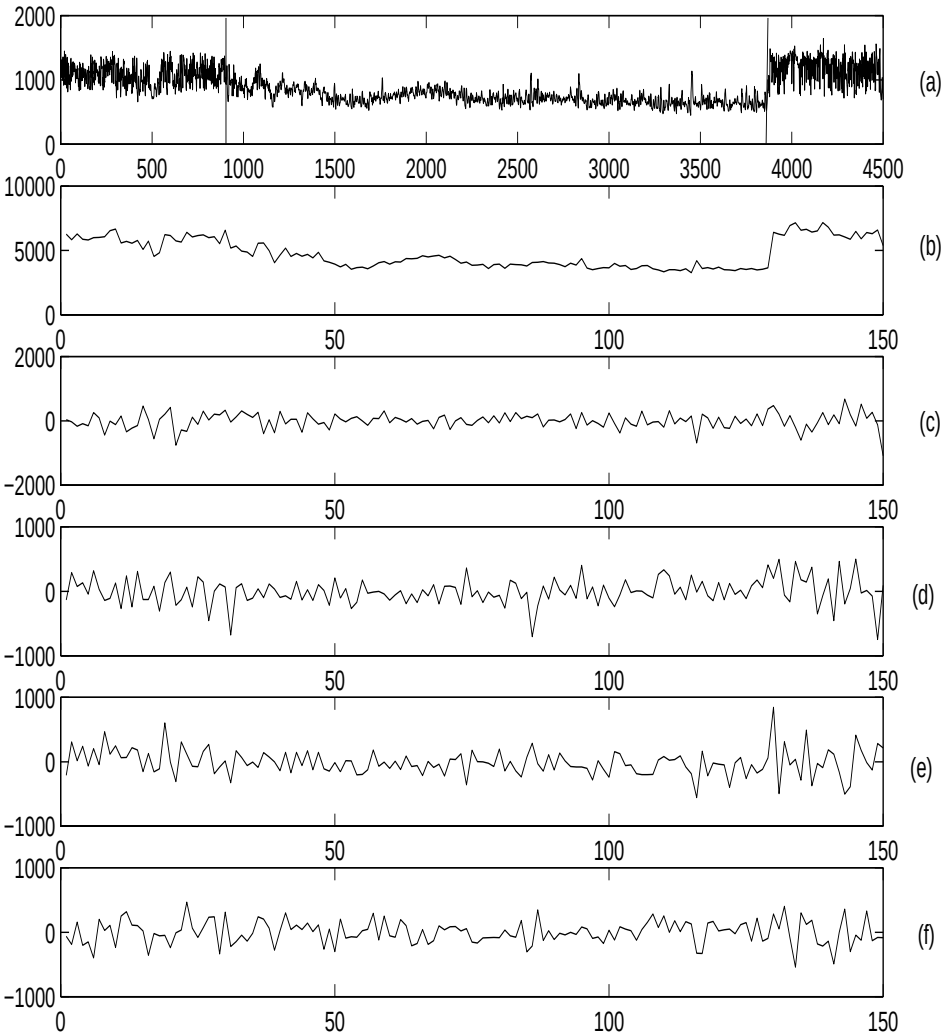

Figure 33 HRV data of an asymptomatic subject during tilt test (a). First (b), second (c), third (d), fourth (e), fifth (f) global KL expansion coefficients series.

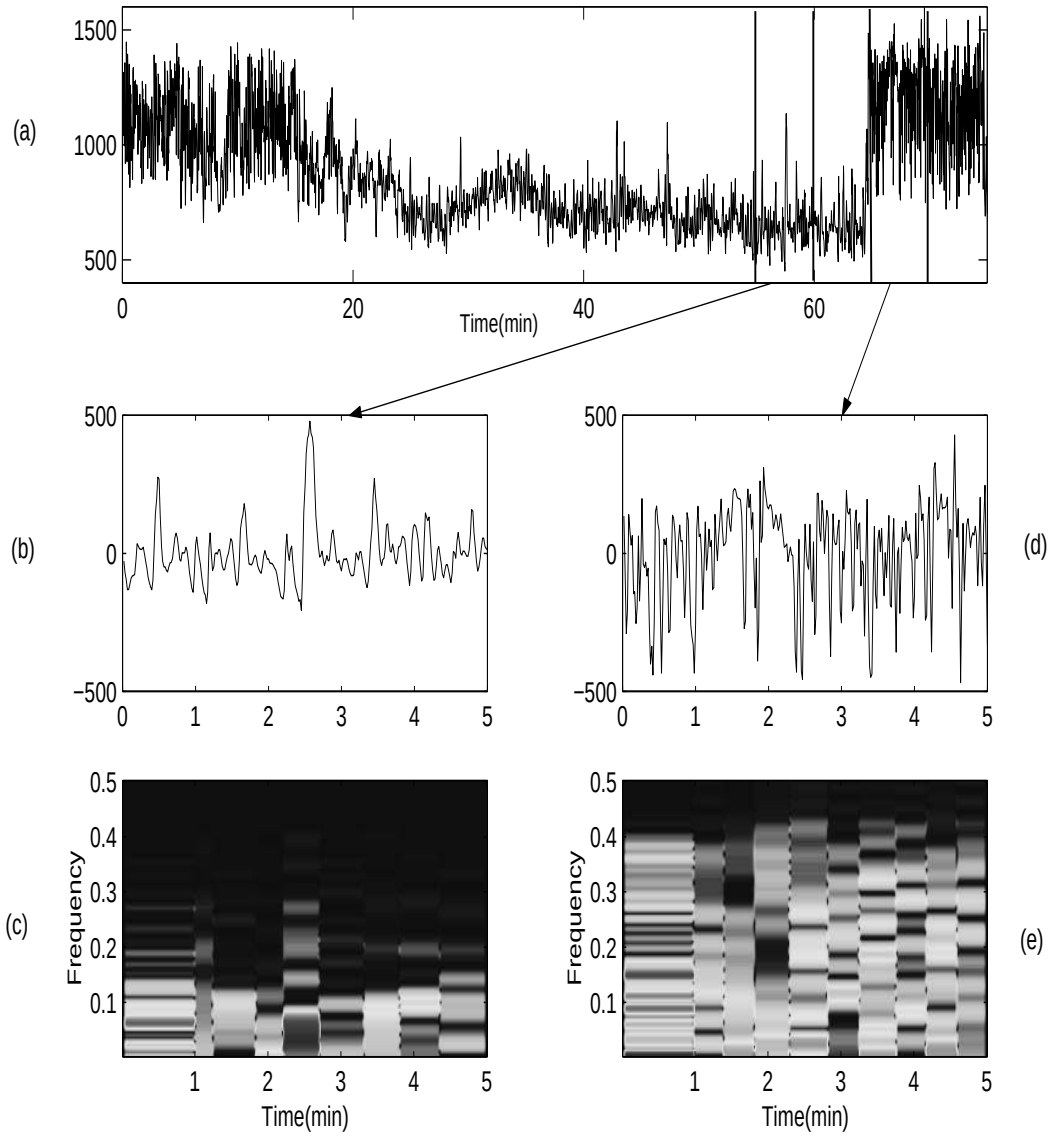

Figure 34 HRV data (a), a section of HRV data during tilt (b) and its time-frequency representation using OPTR (c), a section of HRV data after tilt (d) and its time-frequency representation using OPTR (e).

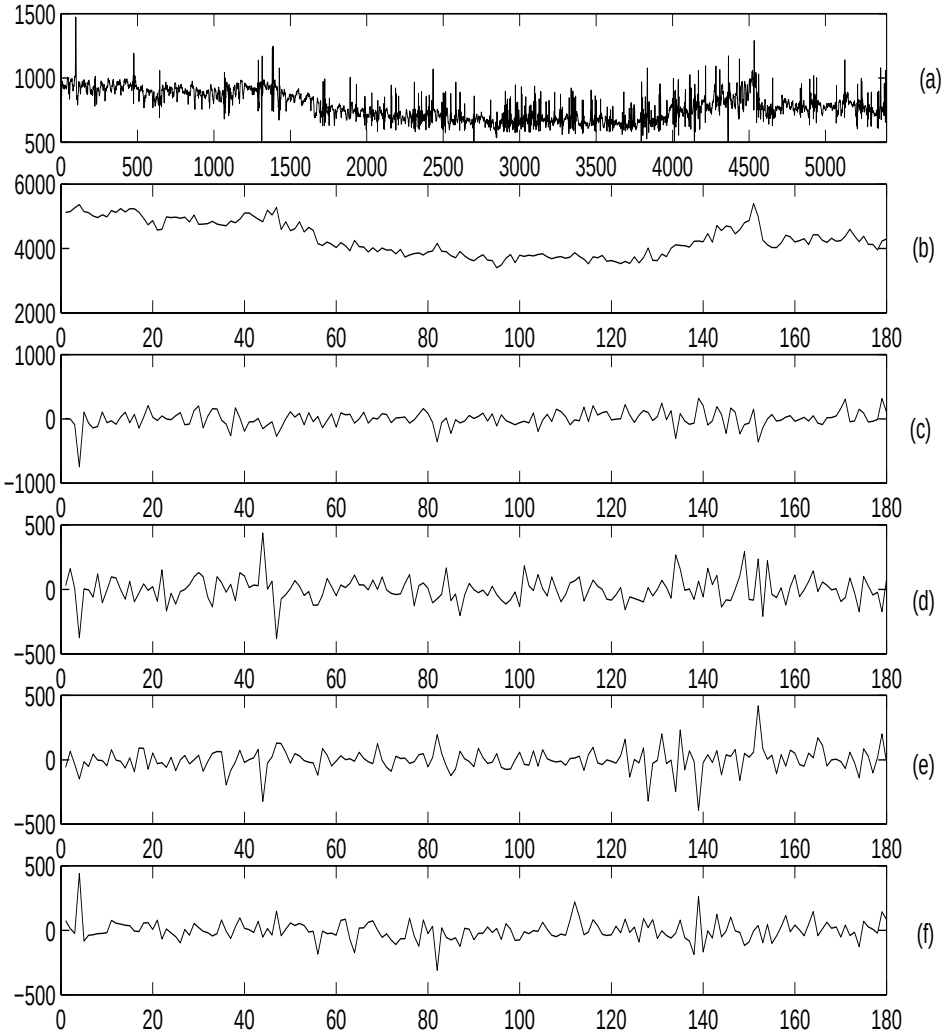

Figure 35 HRV data of a symptomatic subject during tilt test (a). First (b), second (c), third (d), fourth (e), fifth (f) global KL expansion coefficients series.

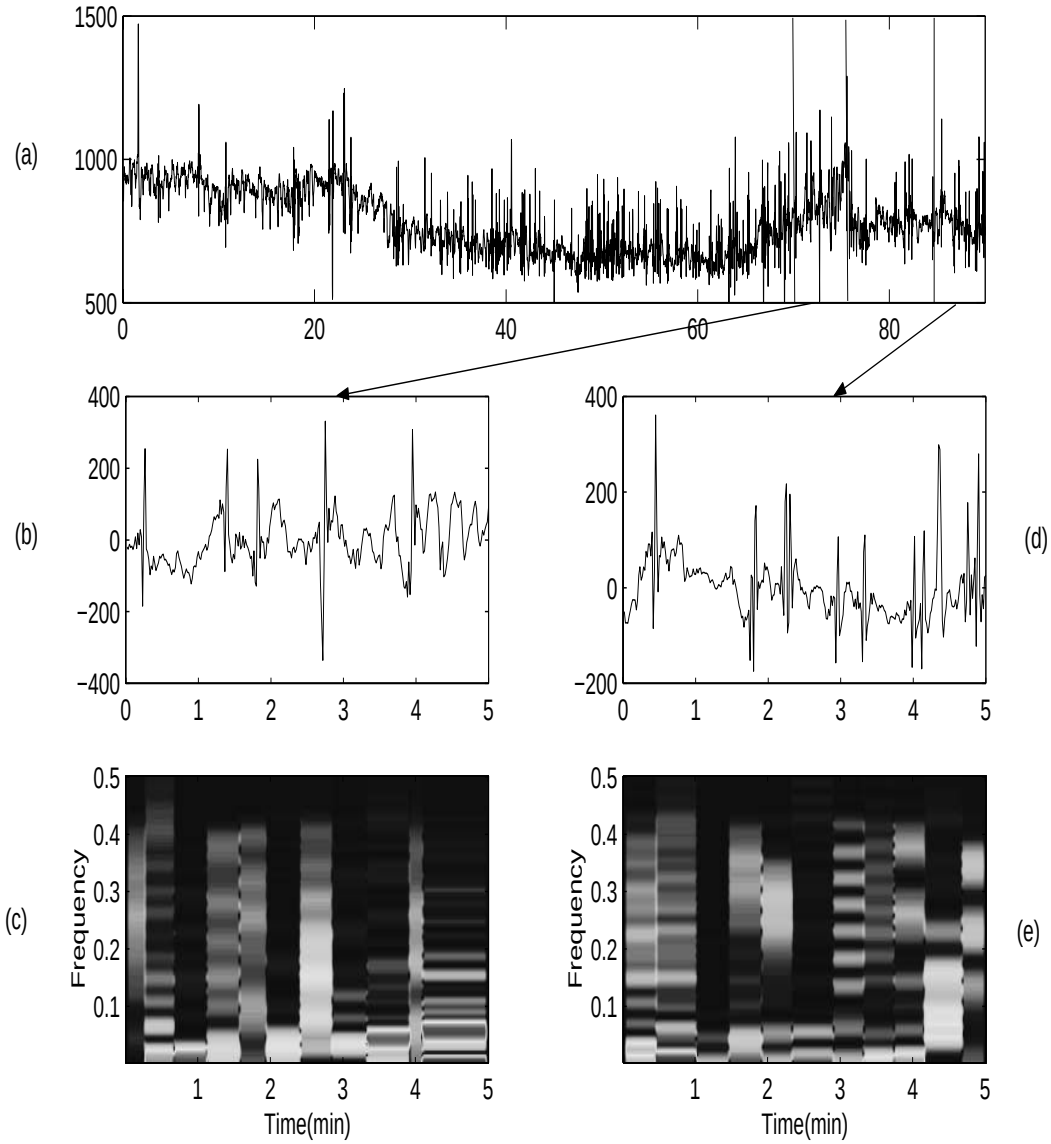

Figure 36 HRV data (a), a section of HRV data during tilt (b) and its time-frequency representation using OPTR (c), a section of HRV data after tilt (d) and its time-frequency representation using OPTR (e).

5.2.2 24-Hour Ambulatory Recording

The 24-hour ambulatory ECG was recorded from a 62 year-old man without a prior history of structural heart disease. The data were obtained in sinus rhythm, but at the end of the recording, the patient suffered an episode of paroxymal atrial fibrillation.

The 24-hour HRV signal (Figure 37(a)) has been processed using GKL expansion to obtain time series of the projection coefficients (Figures 37(b-g)). An increase in the variance of the time series allows selecting a 1-hr segment at the end of the recording, in which the signal becomes unstable (Figure 37(h)). In this segment, changes in the structure of the signal were further investigated using OPTR (Fig. 28(i)), spectrogram with a 128 point Hanning window (Figure 37(j)) and the Choi-Williams (Figure 37(k)) TFR. OPTR of the 1-hr signal shows transients at 30-40 and 50-60 min more clearly than the other TFR. However, because the structure of the signal is complex, the "direct" TFR is difficult to comprehend. OPTR of the 3 most significant eigenvectors (Figure 37(l-h)) reveals the underlying patterns of changes in the signal.

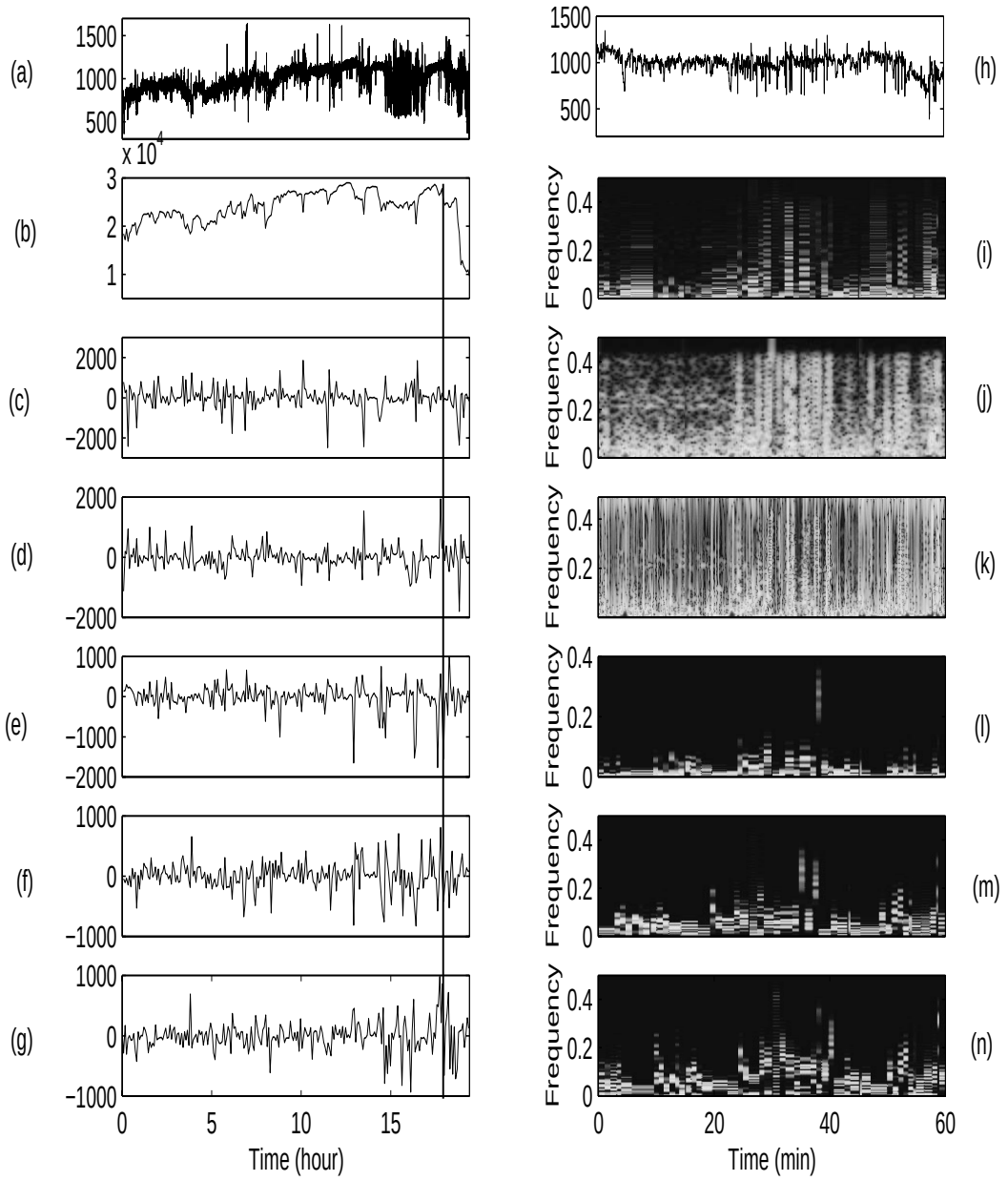

Figure 37 The 24-hour HRV signal obtained from an ambulatory Holter recording (a), time series of the GKL coefficients (b-g), a 1-hour segment of the HRV signal selected by using the changes in variance of the time series of the GKL coefficients (h), OPTR (i), Spectrogram using a 128-point Hanning window (j) and the Choi-Williams (k) TFR of 1-hour data. OPTR of the 3 most significant basis functions of the 1 hour data (l-n).

6.0 CONCLUSIONS

In this study, we first developed a new segmentation algorithm for nonstationary signals. The algorithm consists of two parts which can be applied together or independently: a low resolution algorithm which uses global features of the signal and high resolution algorithm which uses local features of the signal for partitioning. The low resolution partitioning is based on the projection of time series onto a small set of global basis vectors, compressing the information into a few projection coefficients. In the high resolution partitioning, the basis vectors are local. Changes in the structure of a signal may be detected by comparing the number of the eigenvalues of a covariance matrix of short intervals in the signal.

Then, we came up with a new TF representation which uses high resolution partitioning and local KL bases. The method is compared with other TF representations such as spectrogram, Wigner-Ville and Choi-Williams distributions. Proposed method accurately tracked the time-varying frequency content of the signals and showed better time and frequency resolution than the other methods. Unlike other time-frequency analysis methods, it also provides simultaneously a representation of the signal and its time-varying spectrum. Furthermore, the proposed method did not suffer from the cross terms as Choi-Williams and Wigner-Ville distributions did. On the other, it generated some artificial boundaries for signals such as linear and sinusoidal FM. The method is referred to as orthonormal basis partitioning and time-frequency representation (OPTR) and applied to HRV signals.

Time-frequency representations of nonstationary HRV signals have been extensively studied previously, and several alternative approaches have been proposed [4, 5, 63]. The traditional time-frequency representations, including the short-time Fourier transform, the exponential and the Wigner distributions have been used to demonstrate HRV changes during controlled physiological and pharmacological experiments. In these controlled conditions, changes in the signal structure usually involve a

few, distinct frequency elements, which could be readily detected by visual inspection and quantified by the spectral energy integration over the range of interest [63]. In uncontrolled, real-life conditions, however, the number of overlapping frequency elements that exhibit simultaneous changes often makes "direct" time-frequency representations incomprehensible.

OPTR obviates this problem and can be applied to all types of the HRV signals both in controlled and in ambulatory conditions. First, the signal is partitioned into the segments with distinct properties and then each segment is represented in the time-frequency plane using the basis functions that are derived from the signal itself.

We also describe different applications of this approach for various types of HRV signals. For hours-long signals with multicomponent structure, first we apply an efficient low-resolution partitioning to select the transients and short segments of interest. For short segments, we apply a more computationally demanding high-resolution partitioning with subsequent time-frequency representation. Finally, for such "content-rich" multicomponent signals, we use the time-frequency representation of the most significant basis vectors, which provides an effective compression of the information and reveals the underlying dominant pattern. This was the case for HRV data obtained during a tilt test. OPTR allowed us to differ a symptomatic subject from an asymptomatic subjects during a tilt test therefore it can be used as a tool for diagnosis.

The effects of the window size on the time and frequency resolution have been described previously [5]. Note, that although the window lengths in OPTR are determined adaptively, by tracking the changes in the signal structure, the size of the initial window used in partitioning can affect the results. In particular, if the initial window size is too small, some of the frequency content of the signal could be lost. On the other hand, long initial windows can diminish the time resolution and lead to inaccurate partition. Thus, care and some a-priori knowledge are required for choosing the

initial window length. In general, shorter physiological maneuvers, such as Valsalva maneuver, require higher time resolution and shorter window length than more gradual orthostatic or pharmacological tests.

APPENDIX A

APPENDIX A

Orthonormality of the basis functions $\mathbf{u_{il}(n)}$

Since $\sum_n u_{ik}(n)u_{jl}(n) = 0$ if $|i-j| \geq 2$ for all $i, j \in \mathbf{Z}$; therefore to have orthonormality we need to prove that [46]

1. $\sum_n u_{ik}(n)u_{il}(n) = \delta_{kl}$ for $0 \leq k, l \leq (l_i - 1)$

2. $\sum_n u_{(i-1)k}(n)u_{il}(n) = 0$ for $0 \leq k \leq (l_{(i-1)} - 1), 0 \leq l \leq (l_i - 1)$

under the condition the Malvar windows have symmetric overlaps at the partition points.

Case 1 For $i = j$

$$\begin{aligned}
\sum_n u_{jk}(n)u_{jl}(n) &= \sum_{n=a_j-\varepsilon_j+1}^{a_{j+1}+\varepsilon_{j+1}} \mathrm{w}_j^2(n)\tilde{\phi}_{jk}(n)\tilde{\phi}_{jl}(n) \\
&= \sum_{n=a_j-\varepsilon_j+1}^{a_j} \mathrm{w}_j^2(n)\phi_{jk}(2a_j - n + 1)\phi_{jl}(2a_j - n + 1) \\
&+ \sum_{n=a_j+1}^{a_j+\varepsilon_j} (\mathrm{w}_j^2(n) - 1)\phi_{jk}(n)\phi_{jl}(n) \\
&+ \sum_{n=a_j+1}^{a_{j+1}} \phi_{jk}(n)\phi_{jl}(n) \\
&+ \sum_{n=a_{j+1}-\varepsilon_{j+1}+1}^{a_j+1} (\mathrm{w}_j^2(n) - 1)\phi_{jk}(n)\phi_{jl}(n) \\
&+ \sum_{n=a_{j+1}+1}^{a_{j+1}+\varepsilon_{j+1}} \mathrm{w}_j^2\phi_{jk}(2a_{j+1} - n + 1)\phi_{jl}(2a_{j+1} - n + 1)
\end{aligned}$$

Since $\mathrm{w}_j^2(n) + \mathrm{w}_{j-1}^2(n) = 1$ which is the property of the Malvar windows, we get

$$
\begin{aligned}
\sum_n u_{jk}(n)u_{jl}(n) &= \sum_{n=a_j-\varepsilon_j+1}^{a_j} \mathrm{w}_j^2(n)\phi_{jk}(2a_j-n+1)\phi_{jl}(2a_j-n+1) && (1)\\
&+ \sum_{n=a_j+1}^{a_j+\varepsilon_j} -\mathrm{w}_{j-1}^2(n)\phi_{jk}(n)\phi_{jl}(n) && (2)\\
&+ \sum_{n=a_j+1}^{a_{j+1}} \phi_{jk}(n)\phi_{jl}(n) && (3)\\
&+ \sum_{n=a_{j+1}-\varepsilon_{j+1}+1}^{a_j+1} -\mathrm{w}_{j+1}^2(n)\phi_{jk}(n)\phi_{jl}(n) && (4)\\
&+ \sum_{n=a_{j+1}+1}^{a_{j+1}+\varepsilon_{j+1}} \mathrm{w}_j^2\phi_{jk}(2a_{j+1}-n+1)\phi_{jl}(2a_{j+1}-n+1) && (5)
\end{aligned}
$$

Equation 1 cancels Equation 2 and Equation 4 cancels Equation 5 due to property that $\mathrm{w}_j(a_j+\tau) = \mathrm{w}_{j-1}(a_j-\tau+1)$ for $\tau \in (-\varepsilon_j, \varepsilon_j]$. Then, the fact that $\sum_n \phi_{jk}(n)\phi_{jl}(n) = \delta_{kl}$ from Equation 3 so $\sum_n u_{jk}(n)u_{jl}(n) = \delta_{kl}$.

Case 2 For $i = j-1$

$$
\begin{aligned}
\sum_n u_{ik}(n)u_{jl}(n) &= \sum_{n=a_j-\varepsilon_j+1}^{a_j+\varepsilon_j} \mathrm{w}_{j-1}(n)\mathrm{w}_j(n)\tilde{\phi}_{(j-1)k}(n)\tilde{\phi}_{jl}(n)\\
&= \sum_{n=a_j-\varepsilon_j+1}^{a_j} \mathrm{w}_{j-1}(n)\mathrm{w}_j(n)\phi_{(j-1)k}(n)\phi_{jl}(2a_j-n+1) && (6)\\
&- \sum_{n=a_j+1}^{a_j+\varepsilon_j} \mathrm{w}_{j-1}(n)\mathrm{w}_j(n)\phi_{(j-1)k}(2a_j-n+1)\phi_{jl}(n) && (7)
\end{aligned}
$$

The difference is cancelled for the same reason as case 1, so $\sum_n u_{(j-1)k}(n)u_{jl}(n) = 0$. This is also true for the case $i = j+1$. Therefore, the basis functions $\{u_{jk}(n) | j \in \mathbf{Z}, 0 \le k \le l_j-1\}$ are orthonormal set.

APPENDIX B

APPENDIX B

The 90% energy threshold

As we mentioned Chapter 3, we are looking at the differences in the number of the eigenvalues of the covariance matrices of the windowed signals $x_j^s(n) = x(n)\mathrm{w}_j^s(n)$ $a_j - \varepsilon \leq n \leq a_{j+1} + \varepsilon$ and $x_j^l(n) = x(n)\mathrm{w}_j^l(n)$, $a_j - \varepsilon \leq n \leq a_{j+2} + \varepsilon$. Eigenvalues correspond to the eigenvectors which are used to represent the local signals $x_j^s(n)$ and $x_j^l(n)$. The number of the eigenvectors used in signal representation determines how good the representation is. Having a good representation without using all the eigenvectors will allow us to distinguish between $x_j^s(n)$ and $x_j^l(n)$. In our algorithm we chose the representation which will correspond to 90% of the energy of the local signal which results in only 10% representation error. Since the eigenvalues are ordered from largest to smallest, 90% will correspond to most significant ones. Least significant ones will be ignored. We could not use the 100% threshold (which is perfect representation) since, in this case, the number of the eigenvalues N_j^s and N_j^l would be equal to length of the local signals. Since the length of the x_j^s and x_j^l are always different, N_j^s and N_j^l would also be different all the time. Therefore the algorithm would give many small segments even though the signal does not change. On the other hand, choosing a lower threshold would results in a poor representation of the local signal and therefore the algorithm may not detect the changes in the signal correctly.

We tested different threshold values and an example is shown in the following figure. Figure 38(a) shows the simulated signal needs to be segmented. The signal consists of two concatenated sinusoids with different frequencies. Figure 38(b) through (d) displays the segments obtained by using the local segmentation algorithm when 90%, 100% and 75% thresholds are chosen. It is clear

from the figure that 90% threshold gave the best segmentation. On the other hand 100% threshold gave so many small segments as expected. Although 75% threshold was good enough identify the second sinusoid as one segment, it did not give one block for the first sinusoid.

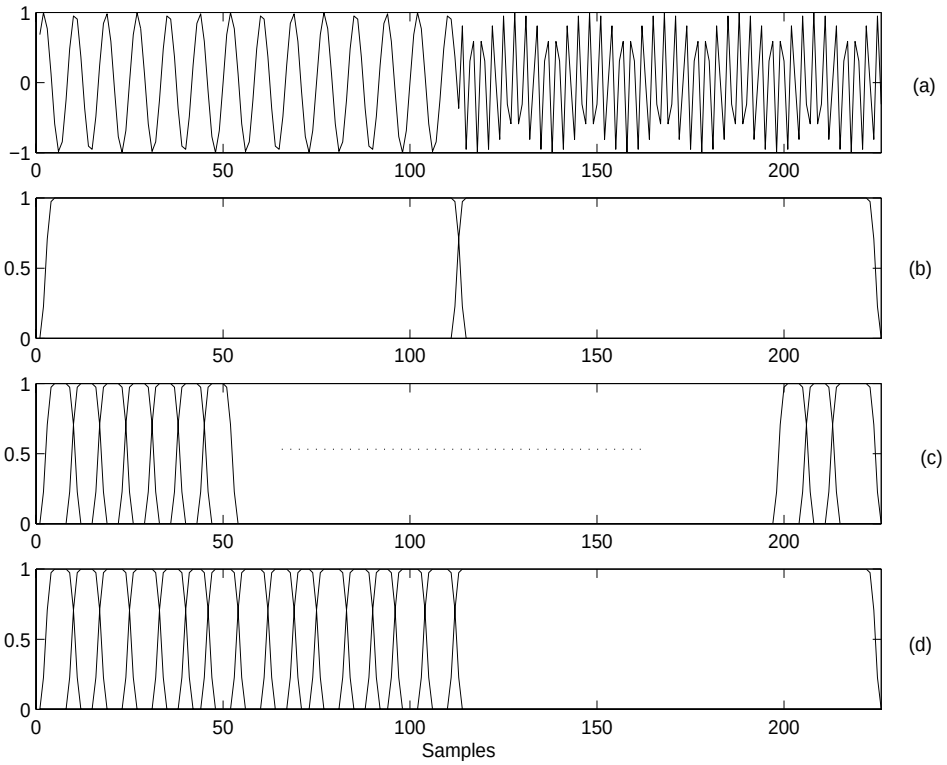

Figure 38 The simulated signal (a) Segments obtained by using the local segmentation algorithm when thresholds were 90% (b), 100% (c) and 75% (d).

BIBLIOGRAPHY

BIBLIOGRAPHY

[1] Cohen, L., *Time-Frequency Analysis.* Prentice Hall, NJ, 1995.

[2] Qian, S. and Chen, D. *Joint Time-Frequency Analysis: Methods and Applications.* Prentice Hall, NJ, 1996.

[3] Boashash, B. *Time-Frequency Analysis: Methods and Applications.* Halsted Press, NY, 1992.

[4] Akselrod, S., Gordon, D., Ubel, F.A., Shannon, D.C., Barger, A.C., Cohen, R.J. "Power spectrum analysis of heart rate fluctuation: a quantitative probe of beat to beat cardiovascular control," *Science*, vol.213, pp.220-222, 1981.

[5] Keselbrener, L. and Akselrod, S., "Selective Discrete Fourier Transform Algorithm for Time-Frequency Analysis: Method and Application on Simulated and Cardiovascular Signals," *IEEE Trans. Biom. Eng.*, vol.43, No.8, pp.789-803, 1996.

[6] Novak, P. and Novak, V., "Time-frequency mapping of the heart rate, blood pressure and respiratory signals," *Med. Biol. Eng. Comp.*, vol.31, pp.103-10, 1993.

[7] Marchesi, C., Venturi, M., Pola, S., Conforti, F., Macerata, A., Varanini, M., Emdin, M., "Sequential estimation of the power spectrum for the analysis of variability of non stationary cardiovascular signals," *Proc. IEEE*, vol.13, pp.578-79, 1991.

[8] T. A. C. M. Claasen and W. F. G. Mecklenbrauker, "The Wigner Distribution - A Tool for Time-Frequency Signal Analysis," *Philips J. Res.*, vol.35, pp.276-300, 1980.

[9] Kayhan A. S., El-Jaroudi A. and Chaparro L. F., "Evolutionary Periodogram for Non-stationary Signals," *IEEE Trans. Signal Processing*, Vol.42, No.6, pp.1527-1536, June 1994.

[10] Porges, S. W., Vagal mediation of respiratory sinus arrythmia: Implications for drug delivery. In J.M. Hrushesky, R. LangerF. Theeuwes (Eds.), *Temporal delivery of drugs*, pp.57-66, New York: New York Academy of Sciences.

[11] Hon, E.H. and Lee, S.T., "Electronic evaluations of the fetal heart rate patterns preceding fetal death: further observations," *Am. J. Obstet Gynecol.* vol.87, pp.814-826, 1965.

[12] Task Force of the European Society of Cardiology and the North American Society of Pacing and Electrophysiology., Heart Rate Variability: Standards of Measurement, Physilogical Interpretation and Clinical Use, *Circulation*, vol.93, pp.1043-1065, 1996.

[13] Sayers, B. M., Analysis of Heart Rate Variability. *Ergonomics*, vol.16, pp.17-32, 1973.

[14] Penaz, J., Roukenz, J., Van der Waal H.J. In: Drischel, H., Tiedt, N. eds. *Spectral Analysis of Some Spontaneous Rhythms in the Circulation.* Leipzig, Germany: Biokybernetik, Karl Marx University, pp.233-241, 1968.

[15] Luczak, H. and Lauring W. J., "An analysis of heart rate variability," *Ergonomics*, vol.16, pp.85-97, 1973.

[16] Hirsh, J. A. and Bishop, B. "Respiratory sinus arrhytmia in humans: how breathing pattern modulates heart rate," *Am. J. Physiol*, vol.241, pp.H620-H629, 1981.

[17] Pomeranz, M., Macaulay, R.J.B., Caudill, M.A., Kutz, I., Adam, D., Gordon, D., Kilborn, K.M., Barger A.C., Shannon, D.C., Cohen, R.J., Benson, M. "Assessment of autonomic function in humans by heart rate spectral analysis," *Am. J. Physiol*, vol.248, pp.H151-H153, 1985.

[18] Porges, S.W. and Byrne, E.A., Research methods for measurement of heart rate and respiration, *Biological Physchology*, vol.34, pp.93-130, 1992.

[19] Priestley, M. B., *Nonlinear and Non-stationary Time Series Analysis.* London: Academic Press, 1988.

[20] Tou, J. T. and Gonzales, R. C., *Pattern Recognition Principles.* Reading, MA: Addison-Wesley, 1979.

[21] Ahmed N. and Rao, K. R., *Orthogonal Transforms for Digital Signal Processing.* New York: Springer-Verlag, 1975.

[22] Jayant, N. S. and Noll, P., *Digital coding of Waveforms.* Englewood Cliffs, NJ: Prentice-Hall, 1978.

[23] Van Trees, H. L., *Detection, Estimation and Modulation Theory.* New York: John Wiley, 1968.

[24] Selin, I., *Detection Theory.* NJ: Princeton University Press, 1965.

[25] Chien, T. and Fu, K. S., "On the Generalized Karhunen-Loeve Expansion," *IEEE Trans. Inform. Theory*, IT-13, pp.518-520, 1968.

[26] Watanabe, S. "Karhunen-Loeve expansion and factor analysis-Theoretical remarks and applications," *Proc. 4th Prague Conf. on Information Theory*, 1965.

[27] Chien, T. and Fu, K. S., "Selection and Ordering of Features Observations in a Pattern Recognition System," *Information and Control*, vol.12, pp.395-414, 1968.

[28] Fukunaga, K., Koontz, W. L. G., "Application of the Karhunen-Loeve Expansion to Feature Selection and Ordering," *IEEE Trans. on Computers*, pp.311-18, April 1970.

[29] Andrews, H. C. "Multidimensional Rotations in Feature Selection," *IEEE Trans. on Computers*, pp. 1045-51, September 1971.

[30] Aysin B, Chaparro L.F., Shusterman V, Grave I., "Denoising of Nonstationary Signals by Using Optimized Karhunen-Loeve Transformation," *Proceedings of the IEEE-SP International Symposium on Time-Frequency and Time Scale Analysis*, pp.621-624, 1998 Pittsburgh, PA.

[31] Coifman, R. R. and Saito, N. "The local Karhunen-Loeve bases," *Proceedings of the IEEE-SP International Symposium on Time-Frequency and Time Scale Analysis*, pp. 129-132, 1996.

[32] I. Naohiri, I. Akira and N. Suzumura. "Segmentation of non-stationary time series," *Int. J. Systems Sci*, vol.10, No.8, pp.883-94, 1979.

[33] I. Naohiri, A. Iwata and N. Suzumura. "Detection of abrupt change and trend in time series," *Int. J. Systems Sci*, vol.11, No.5, pp.557-66, 1980.

[34] M. Basseville and A. Benveniste. "Sequential Detection of Abrupt Changes in Spectral Characteristics of Digital Signals," *IEEE Trans. on Inf. Theory*, vol.IT-29, No.5, Sep. 1983.

[35] B. Lovell and B. Boashash. "Segmentation of Non-Stationary Signals with Applications," in *Proc. ICASSP*, pp.2685-88, 1988.

[36] P. M. Djuric, S. M. Kay and G. F. Boudreaux-Bartels, "Segmentation of Nonstationary Signals," in *Proc. ICASSP*, pp.161-64, 1992.

[37] Coiffman R. R. and Wickerhauser M. V., "Entropy-Based Algorithms for Best Basis Selection," *IEEE Trans. on Inf. Theory*, vol.38, No.2, pp.731-8, March 92.

[38] Wickerhauser M. V., *Adapted Wavelet Analysis from Theory to Software.* pp.273-86, AK Peters, MA 1994.

[39] G. A. Tsihrintzis and C. L. Nikias, "Robust Change-Point Detection and Segmentation in Data Streams," *IEEE MILCOM'95*, pp.125-129, 1995.

[40] T. D. Popescu' "Change Point Detection in Signals Using Linear Regression Models," *Proc. of IEEE Int. Symp. on Computer Aided Control System Design*, pp.182-187, 1999.

[41] Aysin B., Chaparro, L. F., Grave, I. and Shusterman, V. "Orthonormal Basis-Partitioning and Time-Frequency Representation of Cardiac Rhythm Dynamics," submitted to *IEEE Trans. on Biomed. Eng.*, 2002.

[42] V. Shusterman, B. Aysin, K. P. Anderson, A. Beigel, "Multidimensional Rhythm Disturbances as a Precursor of Sustained Ventricular Tachyarrhythmias," *Circulation Research*, vol.88, pp.705-712, 2001.

[43] Aysin B, Chaparro L. F, Grave I, Shusterman V., "Detection of Transient Changes in Heart Rate Variability Signals Using a Time-Varying Karhunen-Loeve Expansion," *IEEE Int. Conf. On Acoustic, Speech and Signal Processing*, vol.6, pp:3586-89, Istanbul, Turkey, 2000.

[44] Basseville M, Benveniste A, Moustakides G. "Detection and diagnosis of abrupt changes in modal characteristics of nonstationary digital signals," *IEEE Trans. Information Theory.* Vol.32, No.3, pp.412-417,1986.

[45] M. Basseville and N. Nikiforov. *The Detection of Abrupt Changes - Theory and Applications.* Englewood Cliffs, NJ: Prentice Hall, 1993.

[46] X. G. Xia, B. W. Suter and M. E. Oxley, "Malvar Wavelets with Asymmetrical Overlapped Windows," *IEEE Trans. Signal Processing*, Vol.44, No.3, pp.723-28, March 1996.

[47] Malvar, H. S., "Lapped Transforms for Efficient Transform/Subband Coding," *IEEE Trans. Signal Processing*, Vol.38, pp.969-78, June 1990.

[48] Arfken, G., *Mathematical Methods for Physicists.* Academic Press, CA, 1985.

[49] Strang, G., *Linear Algebra and Its Applications.* 1988.

[50] Kayhan A. S., El-Jaroudi A. and Chaparro L. F., "Evolutionary Autocorrelation Estimation for Non-stationary Process," *Proc. Conf. Inform. Sci. and Syst.*, pp.1992, Princeton, NJ, March 1992.

[51] Kayhan A. S., El-Jaroudi A. and Chaparro L. F., "Data-Adaptive Evolutionary Spectral Estimation," *IEEE Trans. Signal Processing*, Vol.43, No.1, pp.204-13, Jan. 1995.

[52] P. Andersson, "Adaptive forgetting in recursive identification through multiple models," *Int. J. Control*,vol. 42, No.5, pp. 1175-1193, 1985

[53] Aharoni, G., Averbunch, A., Coifman, R. and Israeli, M., "Local Cosine Transform- A Method for the Reduction of the Blocking Effect in JPEG," *Journal of Mathematical Imaging and Vision*, Vol.3, No.1, pp.7-38, Mar. 1993.

[54] Meyer, Y., *Wavelets: Algorithms and Applications*, pp.75-85, SIAM, Philadelphia, 1993.

[55] Suter, B. W., "On Variable Overlapped Windows and Weighted Orthonormal Bases," *IEEE Trans. Signal Processing*, Vol.42, No.8, pp.1932-73, Aug. 1994.

[56] ——, *Signal Processing with Lapped Transforms*. Norwood, MA:Artech, 1992.

[57] Xia, X. G. and Suter B. W., "A Systematic Method for the Construction of Time Varying FIR Multirate Filter Banks with Perfect Reconstruction," *Proceedings of the IEEE-SP International Symposium on Time-Frequency and Time Scale Analysis*, pp. 120-123, 1994.

[58] Suleesathira, R., Chaparro, L. F. and Aydin, A., "Discrete Evolutionary Transform for Time-Frequency Signal Analysis," *Journal of Franklin Institute*, Vol.337, No.4, pp.347-64, Jul. 2000.

[59] Berger, R. D., Akselrod, S., Gordon, D and Cohen, R. J. "An Efficient Algorithm for Spectral Analysis of Heart Rate Variability," *IEEE Trans. on Biomed. Eng.*, vol.33, No.9, pp.900-904, 1986.

[60] DeBoer, R. W., Karemaker, J. M. and Strackee, J. "Computing spectra of a series of point events particularly for the heart rate variability data," *IEEE Trans. on Biomed. Eng.*, BME-31, pp.383-387, 1994.

[61] V. Shusterman, B. Aysin, R. Weiss, S. Fahrig, S. Brode, V. Gottipaty, D. Schwartzman, K. P. Anderson for the ESVEM investigators. "Autonomic Nervous System Activity and Spontaneous Initiation of Ventricular Tachycardia," *J Am Coll Cardiol* vol.32, pp.1891-1899, 1998.

[62] Appel, M., Berger, R. and *et al* Saul, J. "Beat to beat variability in cardiovascular variables: Noise or music," *J. Am. Coll. Cardiol.*,14, pp.1139-1147, 1989

[63] S. Pola, A. Macerata, M. Emdin and C. Marchesi, "Estimation of the Power Spectral Density in Nonstationary Cardiovascular Time Series: Assessing the Role of the Time-Frequency Representations (TFR)," *IEEE Trans. Biomed. Eng.*,vol.43,pp.46-58,1996.

[64] Niccolai, M., Varanini, M., Macerata, A., Pola, S., Emdin, M., Cipriani, M., Marchesi, C. "Analysis of non-stationary heart rate series by evolutionary periodogram," *IEEE Computers in Cardiology*, pp.449-52, 1995.

[65] E. E. Benarroch, P. Sandroni, P. A. Low, "The Valsalva maneuver," in *Clinical Autonomic Disorders: Evaluation and Management*. Ed. PA Low, Little, Brown and Company: Boston, Toronto, London, p.209-215, 1993.